Faculty of Engineering of the University of Porto

FEUP

Multifunctional Electrospun Fibre Membranes Associated to Bone Grafts for Bone Regeneration

Daniel Santos

DISSERTATION

Integrated Master in Bioengineering
Major in Biomedical Engineering

Supervisor: Prof. Dr. José Domingos Santos
Co-supervisor: Dr. Vitor Sencadas

June 2015

Resumo

Os procedimentos tradicionais no tratamento cirúrgico de problemas ósseos requerem frequentemente a implantação de autoenxertos e aloenxertos, métodos que têm revelado diversas limitações, como a necessidade de uma incisão extra para a colheita de tecido, a quantidade limitada de enxerto do doador ou mesmo a rejeição, algo altamente indesejável. Assim, o desafio atual da engenharia de tecidos passa pela produção de um enxerto ósseo bioartificial que se assemelhe à matriz extracelular (MEC) e seja capaz de uma mineralização óssea eficaz. Não obstante, tem existido um interesse considerável na produção de materiais nanofibrosos pela técnica de *electrospinning* para a área da regeneração de tecidos.

As fibras produzidas por *electrospinning* possuem uma gama alargada de aplicações, particularmente no campo da regeneração óssea. De facto, esta técnica de *electrospinning* permite a fabricação de membranas fibrosas com elevado rácio superfície-volume, com porosidade controlável e maleabilidade para se produzir fibras com uma grande variedade de tamanhos e formas, alargando desta forma sua aplicabilidade. Considerando que o osso é composto por nanocompósitos inorgânicos e orgânicos, este trabalho visa o desenvolvimento e caracterização de fibras multifuncionais produzidas por *electrospinning* para a regeneração óssea, baseadas num compósito de Poli (ácido lático) (PLA) e em Hidroxiapatite (HA) reforçada com vidro – *Bonelike*®. O PLA tem gerado grande interesse, visto ser um dos polímeros biodegradáveis mais promissores devido às suas propriedades mecânicas, à sua processabilidade termoplástica e biodegradabilidade. O *Bonelike*® é uma hidroxiapatite sintética sinterizada na presença de vidro do sistema $CaO\text{-}P_2O_5$, o que lhe confere propriedades mecânicas e bioatividade melhoradas, tornando-o ideal para a osteocondução e osteointegração como substituto ósseo.

Após a preparação das membranas e do *Bonelike*®, as suas propriedades morfológicas, térmicas e físico-químicas foram avaliadas com recurso a diversas técnicas. As membranas exibiram uma distribuição aleatória das fibras com um diâmetro médio de 0.51±0.15 μm e 0.44±0.17 μm no caso das membranas de Poli (L-ácido lático) (PLLA) e PLLA/*Bonelike*®, respetivamente. Ambas as membranas apresentaram igual comportamento hidrofóbico e a de PLLA/*Bonelike*® mostrou possuir maior porosidade do que a composta puramente por PLLA. Os padrões da difração de raios-X (DRX) demostraram que o *Bonelike*® é de facto composto por uma matriz de hidroxiapatite modificada com fases secundárias de α e β-fosfato tricálcio (α-TCP e β-TCP), e provaram ainda a efetiva incorporação deste cerâmico nas membranas de PLLA. Os resultados da análise térmica diferencial (ATM) mostraram que a incorporação das partículas de *Bonelike*® leva a uma translação para temperaturas mais baixas de transição

vítrea e de cristalização a frio do polímero, e com a temperatura de fusão a registar-se aproximadamente nos 150 ºC. A quantidade de *Bonelike*® presente nas membranas foi avaliada através de uma análise termogravimétrica (AT), através da qual foi obtido um intervalo de 62-80%. Ademais, a teoria de Kissinger revelou que a incorporação das partículas de *Bonelike*® leva a uma diminuição da energia de ativação do processo de degradação térmica. Além disto, estudos de citocompatibilidade e proliferação de células osteoblásticas MG-63 foram realizados através de ensaios de MTT e resazurina. A atividade da fosfatase alcalina (ALP) foi avaliada como um marcador de diferenciação dos osteoblastos. Em ambos os tipos de membranas, as células foram capazes de aderir e proliferar, mas as membranas de PLLA/*Bonelike*® provaram ter melhores propriedades biológicas, uma vez que exibiram favorável adesão e crescimento das células osteoblásticas, bem como mostraram um aumento na atividade funcional destas células ósseas.

Este trabalho deu origem a uma apresentação oral no ***"VII INTERNATIONAL MATERIALS SYMPOSIUM | XVII CONFERENCE OF SOCIEDADE PORTUGUESA DOS MATERIAIS"*** *(ver Anexo A).*

Abstract

Surgical bone standard treatments frequently require implantation of autografts and allografts, which are methods that have revealed several limitations ranging from the need of a separate incision for harvesting, donor site scarcity or even undesirable rejection. Thus, the current challenge in bone tissue engineering is to fabricate bioartificial bone graft mimicking the extracellular matrix (ECM) with effective bone mineralization. Though, considerable interest in nanofibrous materials fabricated by electrospinning technique for tissue regeneration has been evidenced.

Electrospun fibres have a widely range of applications, particularly in the bone regeneration field. In fact, the electrospinning technique allows the fabrication of fibre mats with high surface-to-volume ratio, tunable porosity and malleability to conform to a large variety of sizes and shapes, widening their applicability. Considering that bone is composed of organic-inorganic nanocomposites, this work aims at the development and characterization of multifunctional electrospun membranes for bone regeneration based on Poly (lactic acid) (PLA) and glass-reinforced hydroxyapatite (HA) composites - Bonelike®. PLA has generated great interest as one of the most promising biodegradable polymers due to its mechanical properties, thermoplastic processability and biodegradability. Bonelike® is a synthetic hydroxyapatite sintered in the presence of $CaO\text{-}P_2O_5$ based glass, which confers improved mechanical properties and enhanced bioactivity to the material, ideal for osteoconduction and osteointegration as a bone substitute.

Following the membranes and Bonelike® preparation, their morphological, thermal and physico-chemical properties were assessed using several techniques. Membranes exhibited random fibre distribution with a mean diameter of 0.51±0.15 μm and 0.44±0.17 μm for Poly (L-lactic acid) (PLLA) and PLLA/Bonelike®, respectively. Both membranes presented the same hydrophobic behavior and PLLA/Bonelike® showed higher porosity than neat PLLA membrane. X-Ray diffraction (XRD) patterns showed that Bonelike® was, in fact, composed of a modified HA matrix with α and β-tricalcium phosphate (α-TCP and β-TCP) secondary phases, and proved the effective incorporation of this ceramic in the PLLA mats. Differential scanning calorimetry (DSC) experiments showed that the incorporation of the Bonelike® particles leads to a shift towards lower temperatures of the polymer glass transition and cold crystallization, and the melting temperature occurred at ~150 ºC. The real amount of Bonelike® present in the membranes was assessed by thermogravimetric analysis (TGA), whereby a range of 62-80% was obtained. Moreover, Kissinger's theory revealed that the incorporation of the Bonelike® particles leads to a decrease of the activation energy of the thermal degradation process.

Furthermore, cytocompatibility and MG-63 osteoblastic cell proliferation studies were performed through MTT and resazurin assays. Alkaline phosphatase activity (ALP) was assessed as a marker of osteoblasts differentiation. On both types of membranes, cells were able to adhere and proliferate, but PLLA/Bonelike® fibre membranes proved to have improved biological properties since they exhibited favorable adhesion and growth of osteoblastic cells, as well as enhanced functional activity of bone-associated cells.

*This work gave rise to an oral presentation at the **VII INTERNATIONAL MATERIALS SYMPOSIUM | XVII CONFERENCE OF SOCIEDADE PORTUGUESA DOS MATERIAIS** (see Appendix A).*

Agradecimentos

Começo por agradecer ao Professor José Domingos Santos e ao Dr. Vitor Sencadas por me terem permitido fazer parte deste projeto. Agradeço o apoio constante e as inúmeras sugestões que me deram ao longo do trabalho. Não podia deixar de expressar ainda um agradecimento extra ao Vitor pela ajuda e paciência mesmo de longe, que o digam as dezenas de emails que recebeu! À Dina Silva, um grande obrigado pela disponibilidade que sempre demonstrou para me ajudar naquilo que precisasse.

Agradeço a todas as pessoas do departamento de Farmacologia da Faculdade de Medicina Dentária da Universidade do Porto pela forma acolhedora como me receberam. Destaco os conselhos e a contribuição preciosa da Professora Maria Helena Fernandes ao longo desta etapa. Um agradecimento especial à Cristina por toda a paciência ao longo de todo o trabalho. Pelo muito que aturaste e ajudaste, um muito obrigado!

Agradeço ainda a todos os meus Amigos que de uma ou de outra forma tornaram possível este meu percurso. Foi deveras gratificante e animadora esta longa caminhada convosco ao meu lado. Isto não teria sido a mesma coisa sem vocês!

Por último, um obrigado enorme à minha família, especialmente aos meus Pais, a quem dedico este trabalho.

Obrigado!

"HARD WORK BEATS TALENT WHEN TALENT DOESN'T WORK HARD"

Tim Notke

Contents

Resumo ..... **iii**

Abstract ..... **v**

Agradecimentos ..... **vii**

Contents ..... **xi**

List of Figures ..... **xiii**

List of Tables ..... **xvii**

Abbreviations and Symbols ..... **xix**

Chapter 1 ..... **1**

Introduction 1
1.1. Context and Motivation 1

Chapter 2 ..... **3**

State of the Art 3
2.1. Bone 3
2.2. Fibres 4
2.3. Electrospinning 5
2.3.1. Effects of Various Parameters on Electrospinning 6
2.3.1.1. Solution Parameters 6
2.3.1.1.1. Concentration and Viscosity 6
2.3.1.1.2. Molecular Weight 7
2.3.1.1.3. Surface Tension 8
2.3.1.1.4. Conductivity 9
2.3.1.2. Processing Parameters 10
2.3.1.2.1. Electric Field 10
2.3.1.2.2. Flow Rate/ Feed Rate 11
2.3.1.3. Ambient Parameters 12
2.3.1.3.1. Humidity 12
2.3.1.3.2. Pressure 12
2.3.1.3.3. Temperature 13
2.3.2. Fibre Alignment 14
2.3.2.1. Cylinder Collector and Thin Wheel with Sharp Edge 14
2.3.2.2. Parallel Conducting Collector 15
2.3.3. Polymers and Solvents Used in Electrospinning 15
2.3.4. Electrospinning Applications 16

2.4. Poly (lactic acid) (PLA) 18
2.4.1. PLA Applications 19
2.5. Piezoelectricity 20
2.6. Bonelike® 21
2.6.1. Bonelike® Applications 22
2.7. MG-63 Cell Line 22

Chapter 3 25

Materials and Methods 25
3.1. Materials Fabrication 25
3.1.1. Bonelike® 25
3.1.2. PLLA and PLLA/Bonelike® Solutions 26
3.1.3. Electrospun PLLA and PLLA/Bonelike® Membranes 26
3.2. Fibre Membranes Characterization 26
3.2.1. Morphology 26
3.2.2. Porosity 26
3.2.3. Wettability 27
3.2.4. Fourier Transform Infrared (FTIR) Spectroscopy 27
3.2.5. X-Ray Diffraction 27
3.2.6. Thermal Analysis 27
3.2.6.1. Differential Scanning Calorimetry (DSC) 27
3.2.6.2. Thermogravimetry 27
3.3. *In Vitro* Cell Studies 29
3.3.1. Cell Culture and Seeding 29
3.3.2. SEM 30
3.3.3. MTT Assay 30
3.3.4. Resazurin Assay 31
3.3.5. Alkaline Phosphatase (ALP) Activity and Total Protein Content 31
3.4. Statistical Analysis 32

Chapter 4 33

Results and Discussion 33
4.1. Bonelike® Morphology and Porosity 33
4.2. Fibre Membranes Characterization 34
4.2.1. Morphology 34
4.1.1. Porosity 36
4.1.2. Water Contact Angles 36
4.1.3. Fourier Transform Infrared Spectroscopy 37
4.1.4. X-Ray Diffraction 40
4.1.5. Thermal Properties 41
4.1.5.1. Differential Scanning Calorimetry 41
4.1.5.2. Thermogravimetric Analysis 43
4.2. *In Vitro* Cell Studies 47
4.2.1. MTT Assay 47
4.2.2. Resazurin Assay 48
4.2.3. SEM 49
4.2.4. ALP 49

Chapter 5 53

Conclusions 53

References 55

Appendix A 61

List of Figures

Figure 2.1. Schematic illustration of bone structure at cellular level 4

Figure 2.2. Electrospun fibres. [A] Fibres with circular cross section. [B] Flat fibres. [C] Branched fibres. [D] Split fibres 4

Figure 2.3. Schematic image of: [A] Fibre with spherical like beads; [B] Fibre with spindle like beads; [C] Bead-free fibre (uniform fibre).. 5

Figure 2.4. Schematic illustration of the basic setup for electrospinning – [A] and [B] show, respectively, the typical vertical and horizontal setup. The Taylor cone formed in the nozzle of the spinneret is also illustrated. 6

Figure 2.5. SEM photographs of the morphology of PEO beaded fibres, obtained by electrospinning, versus solution viscosity. The horizontal edge of each image represents 20 microns long.. 7

Figure 2.6. Effect of the surface tension on the solvent distribution. [A] High viscosity solution – the solvent molecules are completely distributed over the entangled polymer molecules. [B] Low viscosity solution - the solvent molecules have the tendency to congregate and adopt a spherical shape.. 8

Figure 2.7. TEM images of PVP electrospun nanofibres from [a] ethanol, [b] MC, and [c] DMF (PVP: 4 wt.%). The surface tension (in centipoise) of each one of the systems is (a) 29.3, (b) 38.7, (c) 47.1. Nanofibres from ethanol present a largely smooth distribution (100-625 nm). A lot of spindle-like beads are seen on the nanofibres from MC solution. Sphere-like beads are shown on the nanofibres from DMF solution 9

Figure 2.8. Electrospun nylon using different distances between the tip and the collector. [A] Deposited at 2.0 cm, resulting in round fibres. [B] Deposited at 0.5 cm, resulting in flat fibres 11

Figure 2.9. Polycaprolactone fibres with increasing beads size with increasing feed rate: [A] 0.5 mL/hour and [B] 2 mL/hour 12

Figure 2.10. Schematic electrospinning setups to obtain aligned fibres. [A] Cylinder collector. [B] Thin wheel with sharp edge collector. [C] Two parallel conducting collector and the profile of the electric field. 15

Figure 2.11. Current and potential applications of electrospun polymer nanofibres. 17

Figure 2.12. Main application fields targeted by US patents on electrospun nanofibres. 17

Figure 2.13. Optical isomers of lactic acid. 18

Figure 2.14. Piezoelectric constant, d, of three optically active polymers. 21

Figure 3.1. Illustration of the samples display (the inserts mentioned above are the white tubes) 7 days after cell seeding. Different colors are due to the resazurin solution where a change from blue to pink is observed in each of the growing cultures. 30

Figure 3.2. Principal stages of the osteoblast development in culture and respective temporal expression of genes characteristic of this process. H4, histone; COL I, type I collagen; ALP, alkaline phosphatase; OPN, osteopontin; OC, osteocalcin. 31

Figure 4.1. SEM images showing Bonelike® granules. The scale bar corresponds to 100 μm and 20 μm in [A] and [A'], respectively. 33

Figure 4.2. SEM images showing the PLLA ([A] and [A']) and PLLA/Bonelike® ([B] and [B']) microfibres electrospun at a traveling distance of 15 cm, a needle diameter of 0.5 mm, an electric field of 1.5 $kV.cm^{-1}$ and flow rate of 0.5 $mL.h^{-1}$. The scale bar corresponds to 100 μm in ([A]; [B]) and to 10 μm and 20 μm in [A'] and [B'], respectively. Inset in [B'] shows a higher magnification of a single fibre (scale bar corresponds to 2 μm). 35

Figure 4.3. Size distribution of fibres in SEM photographs of Figure 4.1 [A'] and Figure 4.1 [B']. Graph A corresponds to PLLA microfibres and graph B corresponds to PLLA/Bonelike® microfibres. Average diameter of the fibres was 0.51±0.15 μm in the PLLA membranes and 0.44±0.17 μm in the PLLA/Bonelike® membranes (data is expressed as mean ± standard deviation of 50 measurements). 35

Figure 4.4. SEM image showing the Bonelike® effect on maintaining a higher distance between the PLLA fibres. The scale bar corresponds to 20 μm. 36

Figure 4.5. Water sessile drop on [A] PLLA and [B] PLLA/Bonelike® membranes. 37

Figure 4.6. FTIR transmission spectra of Bonelike®, PLLA and PLLA/Bonelike® electrospun fibres. 37

Figure 4.7. FTIR transmission spectra of [A] PLLA and [B] Bonelike® with identified absorption bands. 39

Figure 4.8. XRD pattern of Bonelike®. 40

Figure 4.9. XRD pattern of Bonelike® and PLLA/Bonelike® composite fibre membranes. 41

Figure 4.10. [A] DSC normalized thermograms of electrospun PLLA (blue curve) and PLLA/Bonelike® (red curve) membranes. Both thermograms were recorded after heating the samples from 30 to 200 ºC at a heating rate of 10 $ºC.min^{-1}$. [B] PLLA/Bonelike® thermogram represented in detail with the used baseline (brown) for integration in ΔH_m calculation. [C] PLLA thermogram represented in detail with the used baseline (brown) for integration in ΔH_m calculation. 42

Figure 4.11. [A] TGA and [B] DTG results for PLLA electrospun mats at different heating rates. 43

Figure 4.12. [A] TGA and [B] DTG results for PLLA/Bonelike® electrospun composite membranes. In [A], when temperature exceeded 450 ºC, approximately 82, 71, 63 and 62% of the original weight remained for 40, 30, 20 and 10 ºC.min^{-1} heating rates, respectively. 44

Figure 4.13. TGA and DTG (inset) results for PLLA and PLLA/Bonelike® electrospun membranes at a heating rate of 30 ºC.min^{-1}. 45

Figure 4.14. Linear fittings obtained with Kissinger's method for PLLA and PLLA/Bonelike® membranes. 46

Figure 4.15. Cell proliferation of MG-63 cells cultured on PLLA (n=3) and PLLA/Bonelike® membranes (n=3) for 1, 3 and 7 days, estimated by MTT assay. Controls were performed on TCPS. Data plotted as mean ± standard. Statistical analysis was only performed between PLLA and PLLA/Bonelike® results; *p<0.05. 47

Figure 4.16. Cell proliferation of MG-63 cells cultured on PLLA (n=3) and PLLA/Bonelike® membranes (n=3) for 1, 3 and 7 days, estimated by Resazurin assay. Controls were performed on TCPS. Data plotted as mean ± standard. Statistical analysis was only performed between PLLA and PLLA/Bonelike® results (no significant differences were found). 49

Figure 4.17. SEM images of MG-63 cells cultured on PLLA ([A], [C] and [E] represent samples at day 1, 3 and 7, respectively] and on PLLA/Bonelike® ([B], [D] and [F] represent samples at day 1, 3 and 7, respectively]. [A'], [B'], [C'], [D'], [E'] and [F'] (scale bar corresponds to 20 μm) are higher magnifications images of [A], [B], [C], [D], [E] and [F] (scale bar corresponds to 100 μm). 51

Figure 4.18. ALP activity of MG-63 cells cultured on PLLA (n=3) and PLLA/Bonelike® membranes (n=3) for 3 and 7 days. Controls were performed on TCPS. Data plotted as mean ± standard. Statistical analysis was only performed between PLLA and PLLA/Bonelike® results; *p<0.05. 50

List of Tables

Table 2.1 — Electrospinning parameters and their respective effect on fibre morphology.. 13

Table 2.2 — Properties of different solvents used in electrospinning. 16

Table 2.3 — Properties of PLLA. 19

Table 4.1 — Physical properties (fibre diameter; porosity and water contact angle) of PLLA and PLLA/Bonelike® fibre membranes. 34

Table 4.2 — Wavenumbers (cm^{-1}) and vibrational assignments associated with different phases of PLLA. 38

Table 4.3 — Thermal parameters of the fibres of neat PLLA and PLLA/Bonelike® composite..... 43

Table 4.4 — Thermogravimetric characteristic temperatures ($T_{initial}$, T_{onset} and T_p) for PLLA and PLLA/Bonelike® membranes..... 46

Table 4.5 — Microscopic photographs of PLLA and PLLA/Bonelike® membranes taken before the addition of the DMSO during the MTT assay. Purple dots indicate the presence of cells. The scale bar corresponds to 0.5 cm. 48

Abbreviations and Symbols

3-D	Three Dimensional
AC	Alternating Current
ALP	Alkaline Phosphatase
ATR	Attenuated Total Reflectance
COL I	Type I Collagen
C_p	Heat Capacity
d	Piezoelectric Constant
DC	Direct Current
DMF	Dimethylformamide
DMSO	Dimethylsulphoxide
DSC	Differential Scanning Calorimetry
DTG	Differential Thermogravimetry
E_{act}	Activation Energy
ECM	Extracellular Matrix
FBS	Fetal Bovine Serum
FTIR	Fourier Transform Infrared Spectroscopy
HA	Hydroxyapatite
MC	Dichloromethane
MEM	Minimum Essential Medium
MSCs	Mesenchymal Stem Cells
MTT	3-(4,5-dimethyl-2-thiazolyl)-2,5-diphenyl tetrazolium bromide
Mv	Viscosity Average Molecular Weight
Mw	Molecular Weight
OPN	Osteopontin
OC	Osteocalcin
$P75^{NTR}$	P75 Neurotrophin Receptor
PCL	Poly (ε-caprolactone)
PDLA	Poly (D,L-lactic acid)
PEO	Polyethylene oxide
PGA	Poly (glycolic acid)

PLA	Poly (lactic acid)
PLLA	Poly (L-lactic acid)
P(LLA-CL)	Poly (L-lactide-co-ε-caprolactone)
pNPP	p-Nitrophenyl Phosphate
PU	Polyurethane
PVA	Polyvinyl Alcohol
PVP	Polyvinylpyrrolidone
RGD	Arginylglycylaspartic Acid
SEM	Scanning Electron Microscopy
T_{cc}	Cold Crystallization Temperature
T_g	Glass Transition Temperature
TGA	Thermogravimetric Analysis
TGF-β	Transforming Growth Factor beta
TCP	Tricalcium Phosphate
TCPS	Tissue Culture Polystyrene
T_m	Melting Temperature
UV	Ultraviolet
V_c	Critical Voltage
X_c	Degree of Crystallinity
XRD	X-Ray Diffraction
wt%	Weight-Weight Percentage
ΔH_m	Melting Enthalpy
ΔH_f	Heat of Fusion

Chapter 1

Introduction

1.1. Context and Motivation

People suffering from bone defects arising from trauma, tumor or bone diseases is effectively a reality in the present days [1]. In fact, every year are performed several million orthopedic procedures by surgeons. At present, the standard treatments for bone repair involve in general autografts, where bone is transplanted from another part of the recipient's body, and allografts, where bone is transplanted from genetically non-identical members of the same species. These grafting solutions present several limitations, namely donor site scarcity, rejection, diseases transfer, need of a separate incision for harvesting and post-operative morbidity [2, 3]. Therefore, there is a need to explore novel biomaterials in bone tissue engineering, so that the treatment strategy can be as quickly and efficient as possible.

In this context, tissue engineering, an emerging interdisciplinary field, has an important role to provide functional substitutes for the damaged tissues [4, 5]. This area aims to manufacture man-made substitutes (known as scaffolds) capable of mimicking the natural tissue environment in order to successfully meet or perhaps surpass the original mechanical, structural, and functional properties [4]. The conception of a scaffold with such features is a demanding task, bearing in mind that it should provide a transitional three dimensional support for cell migration, attachment and proliferation, as well as offer mechanical and biological influences to guide the cell behavior until the tissue is formed [5].

To satisfy all of these requirements, the electrospinning technique is a versatile technique to produce fibrous membranes. This is a flexible process in fabricating randomly or aligned fibres that are characteristic of the extracellular matrix (ECM) [4]. Besides, the electrospun fibres with diameters ranging from micro to nanometer scale offer several advantages such as an extremely high surface-to-volume ratio, tunable porosity, malleability to conform to a wide variety of sizes and shapes and the ability to control the nanofibre composition [6]. Furthermore, scaffolds consisting of electrospun fibres can be functionalized for enhanced cellular activities by incorporating important compounds like hydroxyapatite.

Doubtless, the current challenge in bone tissue engineering is to fabricate bioartificial bone graft mimicking the ECM, allowing, at the same time, an effective bone mineralization [1].

In the wake of the aforementioned ideas, different biomaterials, such as bioactive ceramics and degradable polymers, have been developed to mimic the mechanical and biological properties required by the tissues [7]. However, the electric properties of the materials, important to promote electrical stimulus to the cells, have been bleached in these advancements. More recently, conductive polymers have been used for tissue engineering applications, but some drawbacks exist concerning these materials, such as the need of an external power source to promote electrical stimuli to the cells and their inability to biodegradation, which may induce chronic inflammation and required surgical removal [8]. Therefore, the next generation of biomaterials must combine biological, chemical, mechanical and electrical stimulatory cues, being the last one without wires [9, 10].

In addition to conductive polymers, piezoelectric polymeric materials have also been considered for tissue and biomedical applications. Piezoelectric materials generate transient surface charges by tiny mechanical deformations of the material under mechanical solicitation and do not require additional energy sources or electrodes. Piezoelectricity is a property of many non-centrosymmetric ceramics, polymers and other biological systems and seems to have therefore prospective utility to promote cell growth and proliferation by its electromechanical stimulation [11, 12].

In 1953, Yasuda *et al.* [13] discovered that bone produces electricity by bending deformation, where the compressed and the elongated regions are respectively, negatively and positively polarized, being the callus formed in the negatively polarized regions. Since this work intends to achieve a better bone regeneration, it is crucial to have in mind the piezoelectric properties of the biomaterials.

This dissertation aims at the development and characterization of multifunctional electrospun membranes for bone regeneration, based on PLA and glass-reinforced HA - Bonelike®.

PLA has generated great interest as one of the most promising biodegradable polymers due to its mechanical properties, thermoplastic processability and biodegradability, becoming highly attractive for biological and medical applications [3, 14]. Furthermore, the degradation products of poly(lactides) are nontoxic, which is fundamental to its applications in biomedicine field. In addition, PLA is also known for the piezoelectric activity similar to the one found in human body [13, 15, 16].

Regarding Bonelike®, it is a synthetic HA which is sintered in the presence of $CaO\text{-}P_2O_5$ based glass using a patented process [owned by Biosckin SA (WO2000068164 A1) [17]]. Hydroxyapatite ($Ca_{10}(PO_4)_6(OH)_2$) is the major mineral constituent of the bone matrix but its fragile characteristic and its low reabsorption rate by the organism compromise the recovery of bone normal strength, causing the bone to remain brittle and easily prone to fractures [18, 19]. Bonelike® will be incorporated within the fibre membranes since it is a material with improved mechanical properties and enhanced bioactivity, when compared to the usual commercial HA [19]. Bonelike® particles have a highly controlled micro and macroporous structure, making it also ideal for osteoconduction and osteointegration as a bone substitute.

Considering that bone is composed of organic-inorganic nanocomposites and taking into account the properties of PLA and the Bonelike®, the ceramic-polymer approach of this work intends to achieve a bone regenerative matrix with improved biological, electrical, mechanical and electromechanical properties.

Chapter 2

State of the Art

2.1. Bone

First of all, it is important to understand the biomechanical and biological properties of bone in order to make the right decision on the choice of the materials that fit a potential bone regenerative matrix to reconstruct eventual bone damages.

Bone is a complex, highly organized and specialized connective tissue. When compared to soft tissues, bone is physically hard and rigid, and contains relatively few cells with abundant intercellular matrix in the form of collageneous fibres and stiffening inorganic substances [20]. Bone is responsible for different functions, such as structural support, protection and storage of healing cells, and mineral ions homeostasis [20, 21].

In an architectural viewpoint, bone is composed by the following three levels of structures, which define the organization of the bone tissue [21]:

- Nanostructure (non-collagenous organic proteins, fibrillar collagen, mineral crystals);
- Microstructure (lamellae, osteons, Haversian systems);
- Macrostructure (cancellous and cortical bone).

There are three types of cells comprising the bone: osteoblasts, osteocytes and osteoclasts (Figure 2.1). Acting in a synergetic way, they are responsible by the bone remodeling process.

Osteoblasts (bone forming-cells) are located on the surfaces of bone and regulate the formation and organization of the bone ECM and its subsequent mineralization. Osteoblasts are activated by growth factors (e.g. insulin-like growth factors I and II) secreted by osteoclasts and/or osteocytes to deposit calcium-containing minerals [21].

Osteoclasts (bone-resorbing cells) adhere to the bone surface through integrins, which are specialized cell surface receptors. Osteoclastic bone resorption takes places towards an initial mineral dissolution followed by the degradation of bone. Osteoblasts are activated by cytokines, proteins or growth factors of the bone matrix [20, 21].

Osteocytes (bone-maintaining cells) also regulate new bone formation due to their action in modulating the osteoblasts differentiation from noncalcium-depositing to calcium-depositing cells. This is only possible by the osteocytes secretion of growth factors (insulin-like growth factor I and transforming growth factor b) [20].

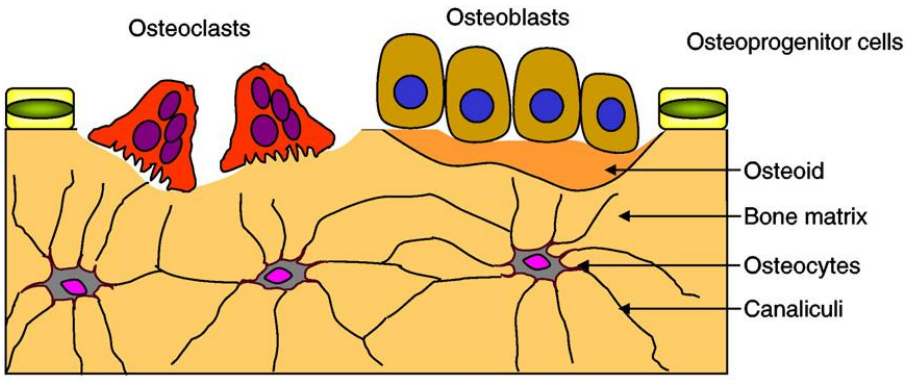

Figure 2.1. Schematic illustration of bone structure at cellular level [20].

2.2. Fibres

A fibre has several definitions, according different professional viewpoints. In a geometric perspective, a fibre can be defined as a slender, elongated threadlike object or structure [22]. The production of fibres with smaller diameters, in the micron to submicron range (10-100 μm) or even on the nanometer range (10–100 nm), confers unique properties to the fibres, such as very large surface area to volume ratio, flexibility in surface functionalities and superior mechanical performance (stiffness and strength) as compared to any other form of the materials [23]. The above mentioned characteristics provide a variety of important applications to the polymeric nanofibres.

Polymeric nanofibres can be processed by different techniques, such as electrospinning, drawing, template synthesis, phase separation and self-assembly [22, 23]. Nevertheless, electrospinning seems to be the ideal method since it is cost effective and allows the production of one-by-one continuous nanofibres from various polymers. In addition, the process can be scaled to a mass production [22, 23]. Depending on the spinning conditions, electrospinning can be used to produce novel fibres with diameters ranging from micro to nanometer scale [23].

Fibrous structures of diverse arrangements and morphologies may be obtained from different parameters used in the electrospinning process, as it will be further discussed. This can lead to the formation of fibres with a variety of cross-sectional shapes. Round fibres, flat fibres, branched fibres and split fibres are shown in Figure 2.2.

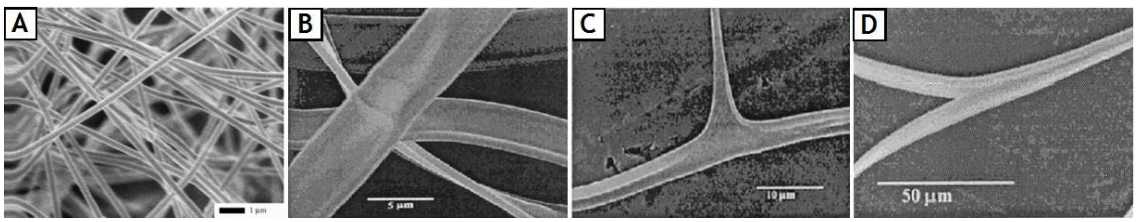

Figure 2.2. Electrospun fibres. [A] Fibres with circular cross section. [B] Flat fibres. [C] Branched fibres. [D] Split fibres [24].

Sometimes, beaded fibres can also be formed. Furthermore, depending on the spinning conditions, the morphology of beads changes from spherical to spindle-like shape to finally uniform fibres (Figure 2.3).

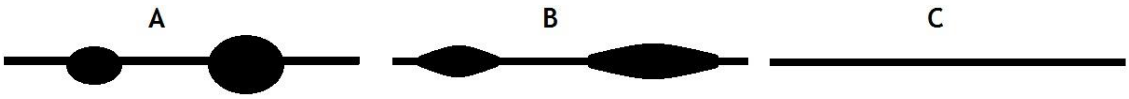

Figure 2.3. Schematic image of: [A] Fibre with spherical like beads; [B] Fibre with spindle like beads; [C] Bead-free fibre (uniform fibre). Adapted from [25].

2.3. Electrospinning

Electrospinning is an old method of electrostatic fibre production technique. Its first observation is dated 1897 by Rayleigh. The method was studied in detail by Zeleny (1914) on electrospraying and it was patented by Formhals in 1934 [26].

Electrospinning has evidenced great versatility and potential for generating thin and ultrathin fibres from different materials such as polymers, composites and ceramics, with potential applications in several technological and scientific fields. This method had gained particular attention in the last decade, not only due to its capacity in spinning a wide variety of polymers, but also due to its ability to produce fibres in the submicron range. Easily, fibres ranging from 2 nm to several micrometers are obtained with this method (whereas it is a difficult task to achieve it with other standard mechanical fibre-spinning techniques) [26]. Moreover, electrospun fibres offer several advantages, such as an extremely high surface-to-volume ratio, tunable porosity, malleability to conform to a wide variety of sizes and shapes and the ability to control the nanofibre composition [26].

Figure 2.4 shows schematic diagrams of the two standard electrospinning setups, vertical and horizontal. Three major components are fundamental to fulfill the process: a high-voltage power supply, a spinneret (a metallic needle) and a collector (a grounded conductor).

In terms of the voltage supplier, a direct current (DC) is usually used. Nevertheless, the use of alternating current (AC) is also possible and feasible. A spinneret is connected to the syringe where the polymer solution (or melt) is hosted. Using a syringe pump, the solution is fed through the spinneret at a controllable rate. As a result, a pendent drop of the solution is formed at the nozzle of the spinneret. Due to the high voltage (usually between 1 and 30 kV), an electrically charged jet of solution is thus ejected and after an evaporation phenomenon, the solution is collected as an interconnected web of small fibres [27]. Although it seems to be an extremely simple process, this mechanism is rather complicated. So, it is important to understand in greater detail the electro-fluid-mechanical issues behind the electrospinning technique.

As shown in the Figure 2.4, one electrode is placed into the spinning solution/melt and the other at the collector level. When high voltage is applied, the pendent drop becomes electrified and the induced charges are distributed over the surface. Subsequently, the drop experiences electrostatic repulsion between the surface charges and also the Coulombic force exerted by the external electric field [23, 27]. As a result of these electrostatic actions, the spherical shape of the drop is distorted into a conical configuration, commonly known as the Taylor cone (see in Figure 2.4 [A]). As soon as the electrical field attains a critical voltage, V_c, the repulsive electrostatic forces overcome the surface tension of the polymer solution, forcing the ejection of the fluid from the tip of the spinneret. Meanwhile, the solvent evaporates and attracted by the grounded collector, the charged fibre is deposited as a randomly oriented mesh.

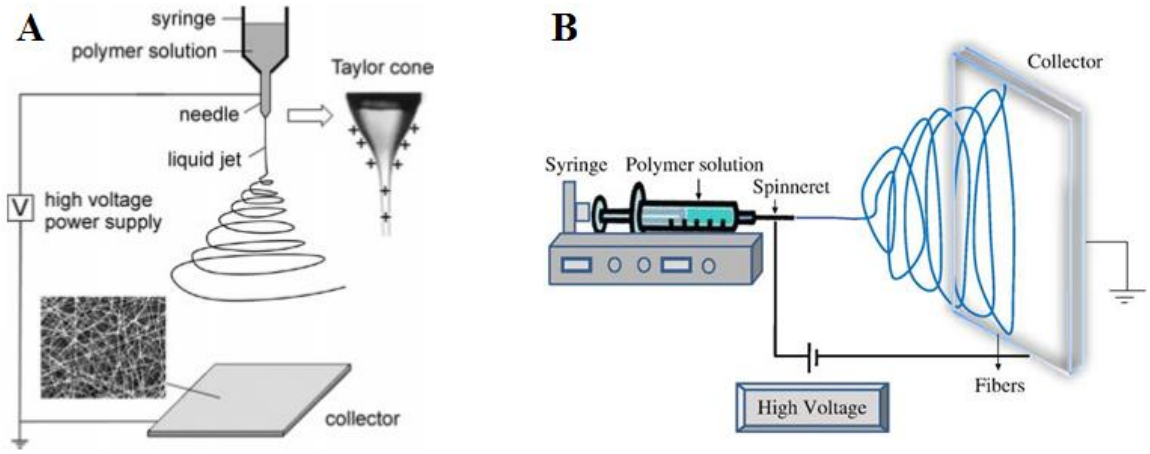

Figure 2.4. Schematic illustration of the basic setup for electrospinning – [A] and [B] show, respectively, the typical vertical and horizontal setup. The Taylor cone formed in the nozzle of the spinneret is also illustrated [26, 27].

2.3.1. Effects of Various Parameters on Electrospinning

The polymer transformation into nanofibres through electrospinning is dependent on many parameters, generally classified into solution parameters, process parameters and ambient parameters [22, 26]. Viscosity (or concentration), conductivity, surface tension and molecular weight encompass the solution parameters. The processing parameters include the electric field (voltage and the distance between the tip and the collector) and the feeding/flow rate [26]. Both kinds of parameters will affect the fibres morphology. In addition to these variables, the humidity, temperature and pressure of the surroundings are the ambient parameters which may also play an important role in determining the morphology and diameter of the electrospun fibres [26, 27]. Varying the aforementioned parameters, it is possible to come out with different setups to fabricate fibrous structures of diverse arrangements and morphologies.

2.3.1.1. Solution Parameters

2.3.1.1.1. Concentration and Viscosity

The solution viscosity is strongly related to its concentration. The solution viscosity is proportional to the polymer concentration, so, these parameters are herein discussed together.

The concentration of the solution is a crucial variable in the electrospinning process, since a minimum solution concentration is required. Previous studies showed that there should be found the optimum concentration to obtain good results [22]. Low solution concentration leads to a mixture of beads and fibres. On the other hand, at high concentrations it is almost impossible the formation of continuous fibres, due to the inability to control and maintain the flow of the polymer solution at the tip of the needle, due to the cohesive nature of the high viscosity solutions. Therefore, increasing the solution concentration or viscosity it is possible to create larger fibres [26]. In fact, there is in the

literature a power law relationship that depicts the increase on the fibre diameter with increasing polymer concentration [28].

Viscosity plays a crucial role in determining the fibre size and morphology. At a lower viscosity, there is no continuous fibre formation and certain concentration drops will form instead of smooth fibres. This is the consequence of the higher amount of solvent molecules and fewer polymer chain entanglements, which will mean that surface tension has a dominant influence along the electrospinning jet, causing beads to form along the fibre [22]. Using high solution viscosities, the fibre processing will be prohibited by the difficulty in the ejection of jets from the solution. As a result, there is less stretching of the solution, resulting in larger fibre diameter and needle clogging. In the literature are pointed out maximum spinning viscosities ranging from 1 to 215 poise [26]. Furthermore, other researchers that focused their work in the polyethylene oxide (PEO) fibres described the production of uniform electrospun fibres using a range of viscosity between 1 and 20 poise [29]. It was also reported that as the viscosity of the solution is increased, beads and beaded fibres are less likely to be formed. However, beads do not completely disappear and if there is any, for the more viscous solutions, its diameters become bigger and the average distance between the beads on the fibres longer. Meanwhile, as the viscosity increases, the shape of the beads gradually changes from spherical to spindle-like [29]. Figure 2.5 shows the different fibre morphologies according to different viscosities for PEO.

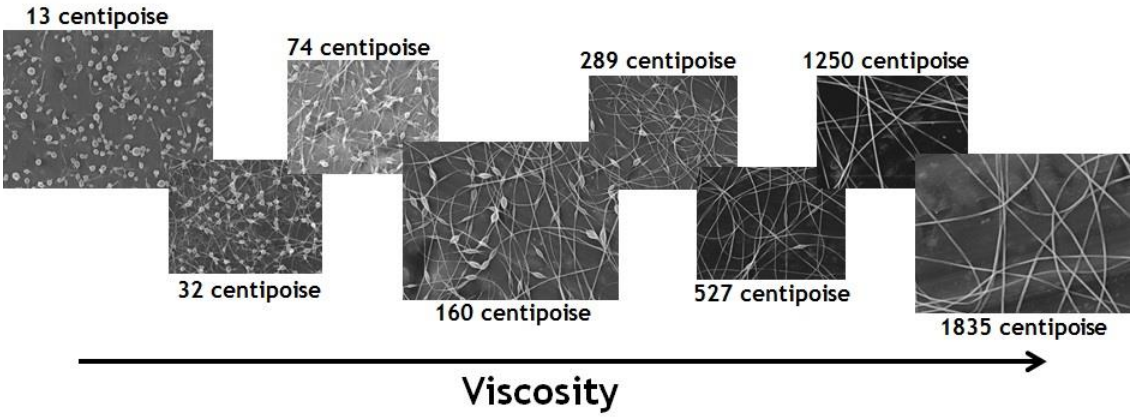

Figure 2.5. SEM photographs of the morphology of PEO beaded fibres, obtained by electrospinning, versus solution viscosity. The horizontal edge of each image represents 20 microns long. Adapted from [29].

2.3.1.1.2. Molecular Weight

As discussed before, the polymer concentration affects the solution viscosity. Nevertheless, the molecular weight of the polymer which represents the length of the polymer chain, also have a significant effect on the viscosity of the solution since the polymer length determines the amount of entanglements of the polymer chains in the solvent [22]. Besides, the molecular weight can influence other variables, such as the surface tension, conductivity and dielectric strength [26].

Molecular weight will affect the morphology of electrospun fibres and usually high molecular weight polymer solutions are preferred, as they provide the desired viscosity for

fibre fabrication. Considering the dissolution of different polymers in the same solvent, in the majority of cases, polymers with higher molecular weight lead to higher solution viscosity than polymers with lower molecular weight [22]. Bearing in mind the effect of the molecular weight on the solution viscosity, the fibre morphology according to the molecular weight is already predictable. So, low molecular weight solution contributes to form beads rather than smooth fibres, whereas high molecular weights tend to form fibres with larger diameters.

Molecular weight reflects the number of entanglements of polymer chains in a solution, which are in turn fundamental to the electrospinning process. During the stretching of the polymer solution, it is the entanglement of the molecule chains that prevents the electrically driven jet from breaking up, thus maintaining a continuous solution jet [22, 26]. Even when the polymer concentration is too low, the entanglements of the polymer chains may be capable of ensuring an acceptable viscosity to produce uniform jets during the electrospinning, and thus inhibiting, in a certain way, the effect of the surface tension that would lead to beads formation on the fibres [26].

2.3.1.1.3. Surface Tension

Surface tension is considered the primary force opposing the Coulomb repulsion, thus the electrospinning process is initiated only when the repulsion forces overcome the surface tension of the charged solution [22, 30].

Surface tension provokes a decreasing in the surface area per unit mass of a fluid. Hence, for low viscosity (high concentration of free solvent molecules), the solvent molecules tend to congregate and adopt a spherical shape due to the surface tension (Figure 2.6 [A]) [22]. On the other hand, with higher viscosity, the tendency of the solvent molecules to come together by the action of the surface tension is minimized, since there is a greater interaction between the solvent and polymer molecules [22]. Consequently, solvent molecules will spread over the entangled polymer molecules as soon as the solution is stretched along the electrospinning process (Figure 2.6 [B]).

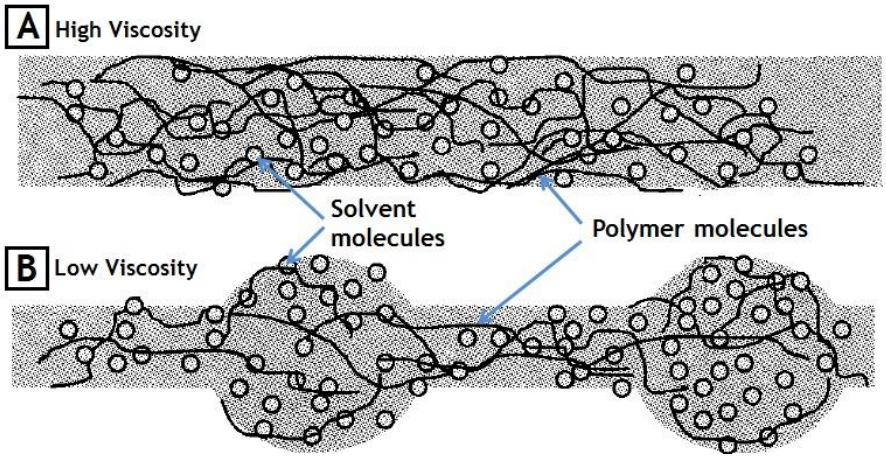

Figure 2.6. Effect of the surface tension on the solvent distribution. [A] High viscosity solution – the solvent molecules are completely distributed over the entangled polymer molecules. [B] Low viscosity solution - the solvent molecules have the tendency to congregate and adopt a spherical shape. Adapted from [22].

Reducing the surface tension of the polymer solution, fibres without beads can be obtained. Bearing in mind that surface tension is function of the solvent composition in the solution, beaded fibres may be converted into smooth ones, using for that solvents with low surface tensions [22]. Nonetheless, it is important to clarify that the low surface tension of a particular solvent does not mean that it is suitable for electrospinning. Basically, the surface tension only determines the upper and lower boundaries of the electrospinning window if all other parameters are fixed.

Yang and Wang [31] tested the influence of solvents with different surface tensions on the formation of electrospun ultrathin PVP nanofibres. Using different solvents (ethanol, dimethylformamide (DMF) and dichloromethane (MC)) but identical concentration, voltage and tip-to-collector distance, they proved that in fact, reducing the surface tension of the solution makes possible to convert beaded fibres into smooth ones. Figure 2.7 illustrates the obtained fibres. The same researchers also demonstrated that the surface tension and solution viscosity can been adjusted by changing the mass ratio of solvents mix [31].

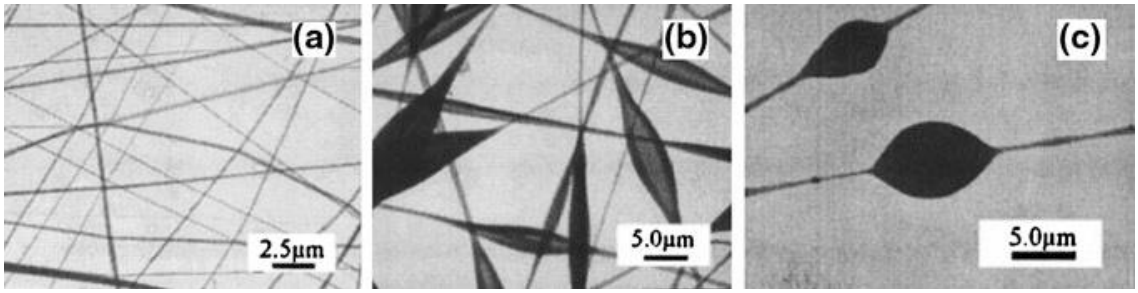

Figure 2.7. TEM images of PVP electrospun nanofibres from [a] ethanol, [b] MC, and [c] DMF (PVP: 4 wt.%). The surface tension (in centipoise) of each one of the systems is (a) 29.3, (b) 38.7, (c) 47.1. Nanofibres from ethanol present a largely smooth distribution (100-625 nm). A lot of spindle-like beads are seen on the nanofibres from MC solution. Sphere-like beads are shown on the nanofibres from DMF solution [31].

2.3.1.1.4. Conductivity

Solution conductivity is mainly determined by the polymer type, solvent sort and the salt. Considering that, during the electrospinning process, repulsion of the charges at its surface causes the stretching of the solution, with an increased conductivity, more charges will be carried by the electrospinning jet. The conductivity of the solution can be increased by the addition of ions [22]. Thus, when any polyelectrolyte or salt is added to the solution, the larger amount of charges will cause an increased stretching of the solution, leading to the formation of smooth fibres. Otherwise, a low conductivity may be responsible by the production of beaded fibres. Besides, the electrical conductivity of the solution has a direct influence with respect to the fibre diameter. If the conductivity of a solution is increased, the diameters of the resultant fibres can be significantly reduced. This increase in charges also results in a greater bending instability, leading to an increase in deposition area of the fibres [22].

As understandable, high solution conductivities also has the benefit of lowering the critical voltage required to initiate the electrospinning process [22].

It is referenced in the literature that the size of the ions has an important impact on the resulting fibre diameter [32]. Electrospun fibres were obtained from 30 wt% PDLA solution with

different ion compositions: 1 wt% NaCl or 1 wt% KH_2PO_4 or 1 wt% NaH_2PO_4. The fibres electrospun from the solution with NaCl exhibited the smallest average diameter. Fibres electrospun from solution with NaH_2PO_4 had the largest diameter and fibres electrospun from solution with KH_2PO_4 presented an intermediate diameter [32]. This means that ions with smaller atomic radius have a higher charge density and thus a higher mobility under an external electrostatic field. As sodium and chloride ions have smaller radius than potassium and phosphate ions, the elongational forces imposed on the jet with NaCl were higher, producing fibres with smaller diameters [22, 32].

The solution conductivity can still be increased by changing the pH of the solution. As said before, ions addition will increase the solution conductivity. However, that addition can also lead to an increase in the solution viscosity, which in turn will cause an increase in the fibre diameter. In spite of increasing conductivity, the viscoelastic force becomes stronger than the Coulombic one, preventing the jet formation [22].

2.3.1.2. Processing Parameters

2.3.1.2.1. Electric Field

The electric field is expressed in terms of voltage/distance, where the distance in the specific case of electrospinning represents the gap between the tip of the needle and the collector [33].

The application of a high voltage is crucial to initiate the electrospinning. Whilst the critical voltage is not achieved, there is no fibre formation [27]. In other words, this critical voltage will induce the necessary charges on the solution, which is required for the electrostatic force in the solution to overcome its surface tension.

Usually, a voltage of more than 6 kV (negative or positive) is sufficient to the spherical shape of the solution drop at the spinneret tip to distort into the conical configuration (Taylor cone), followed by the jet initiation [22].

The voltage effect in the fibres morphology is not yet completely understood and there are controversial ideas about it. In the specific case of polyethylene oxide, Reneker and Chun [26] developed an experiment where they showed that there is no significant influence of the electric field on the fibre diameter. Still, Zhang *et al.* demonstrated that when higher voltages are used, there is more polymer ejection, leading to the formation of larger fibres [34]. On the other hand, other authors referred that in most cases, a higher voltage will lead to greater stretching of the solution caused by the greater Coulombic forces in the jet, as well as the stronger electric field. As a result, there will be a reduction of the fibres diameter [22]. It was also found that high voltages can be responsible for beads formation which may be the result of increased instability of the jet as the Taylor Cone recedes into the syringe spinneret [22].

The flight time of the electrospinning jet may influence the fibre diameter and this aspect can be correlated with the voltage. For example, at a lower voltage, there is reduced jet acceleration and thus the weaker electric field increases the flight time. As a result, before the fibres reach the collector, they have more time to stretch and elongate, favoring the production of finer fibres.

The high voltage may also have an important impact in the crystallinity of the polymer fibre. The electrostatic field promotes the ordering of the polymer molecules, inducing a greater crystallinity in the fibre [22]. However, this is not always as linear as expected, since above a certain voltage, the crystallinity of the fibre may be reduced. Once again, the flight time is related with it. For a higher voltage, the acceleration of the fibres will increase, meaning less flight time of the electrospinning jet. This has a repercussion in the fibre crystallinity, bearing in mind that fibres will be deposited on the collector before the polymer molecules have enough time to align itself [22].

The distance between the tip and the collector will directly influence the flight time and the electric field which in turn have important roles to control the fibre diameters and morphology [22]. This distance should be optimized in order to give enough time to evaporation of solvent from the nanofibres [26].

At short distances between the tip and the collector, the jet has a short travel before reaching the collector. Moreover, this causes an increase in the electric field strength, increasing therefore the jet acceleration. Solvents may not have sufficient time to evaporate, thus creating an interconnected fibre mesh (Figure 2.8 [B])[35]. Although this is far way to be desirable in the electrospinning, the merged fibres result in inter and intra layer bonding with improved strength.

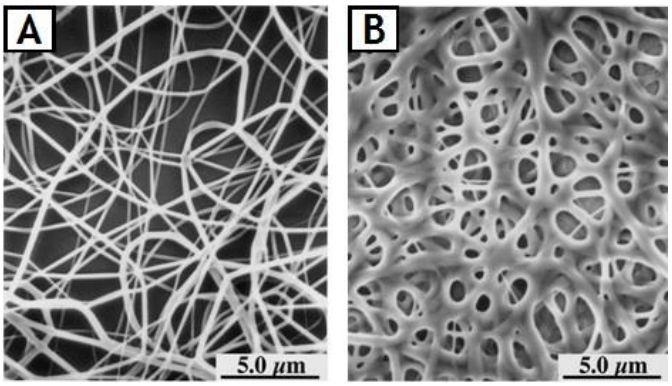

Figure 2.8. Electrospun nylon using different distances between the tip and the collector. [A] Deposited at 2.0 cm, resulting in round fibres. [B] Deposited at 0.5 cm, resulting in flat fibres [35].

The tip to collector distance does not have always a significant effect on the fibre morphology. This is dependent on the solution properties that we deal with. However, in general, beads formation is reported when the distance is either too close or too far [26].

In terms of fibre diameter, it was shown different conclusions. There are circumstances where longer distances result in a decrease in the average of fibre diameter and others where the opposite happens (longer distance lead to an increase of the fibre diameter) [22]. The first event may be interpreted by the longer flight time, which allows the jet to stretch before reaching the collector. The increase of the diameter for long distances is due to a decrease in the electrostatic field strength, which means that there is less stretching action.

2.3.1.2.2. Flow Rate/ Feed Rate

The flow rate is an important process parameter since it will determine the amount of solution available for electrospinning. Jet velocity and the material transfer rate depend on

the flow rate. Generally, it is recommended a lower feed rate as the solvent will have enough time for evaporation [36]. Nevertheless, a minimum flow rate of the spinning solution is demanded. On the contrary, high flow rates result in beaded fibres owing to insufficient drying time. If the feed rate is even increased, there is a proportional increase in the fibre diameter or beads size (Figure 2.9).

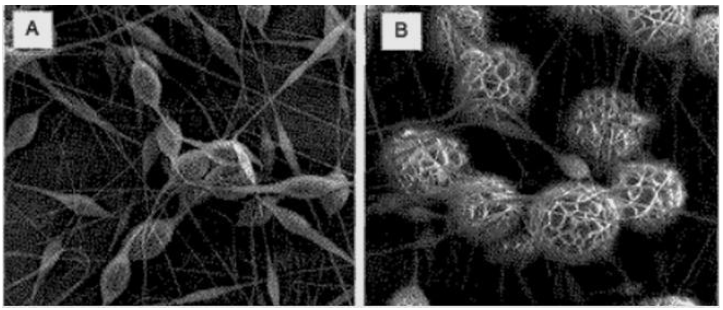

Figure 2.9. Polycaprolactone fibres with increasing beads size with increasing feed rate: [A] 0.5 mL/hour and [B] 2 mL/hour [22].

2.3.1.3. Ambient Parameters

In this section, ambient parameters like humidity, temperature and pressure will be discussed. There is lack of investigation about the effect of the electrospinning jet surrounding but, some aspects regarding the pointed out parameters were already reviewed in the literature [22].

2.3.1.3.1. Humidity

The humidity of the environment may have different impacts during the electrospinning process. The variation in humidity was assessed during the spinning of polystyrene solutions. It was shown that by increasing the humidity, small circular pores are formed on the fibre surfaces. The size of pores increases with increasing humidity until they coalesce to form thereby large and non-uniform shaped structures [22]. S. Ribeiro *et al*. also reported that the texture of electrospun materials is indeed affected by humidity - larger pores are formed with increasing humidity [37].

The humidity of the surroundings will also determine the evaporation rate of the solvent in solution. A volatile solvent will dry rapidly in the presence of very low humidity. So, the solvent evaporation rate is faster than the removal of the solvent from the tip of the needle. Therefore, the electrospinning process stops within few minutes because the needle tip will clog [38].

2.3.1.3.2. Pressure

The electrospinning process should be run at atmospheric pressure. Otherwise, when the pressure is below the atmospheric pressure, the polymer solution held in the syringe will tend to flow out of the spinneret, causing unstable jet initiation. Besides, at a very low pressure

the electrospinning is simply impossible. Herein, there is a direct discharge of the electrical charges [22].

2.3.1.3.3. Temperature

The temperature effect on electrospinning is strictly related to the viscosity of the polymer. There is an inverse relationship between the temperature and the viscosity. Hence, when a polymer is electrospun at high temperatures, there is a yield of fibres with decreased fibre diameter. This is due to the consequent decrease in the fibre viscosity, in which the Coulombic forces exert a greater stretching force on the solution, thus resulting in the narrowing of the fibres [22].

Summing up and as understandable, the electrospinning process may be influenced by a large variety of parameters. These variables are not independent of each other, thus it is important to make a judicious and balanced decision about it, so that the important features that optimize the technique are met. Table 2.1 summarizes the principal effects of the aforementioned parameters in the electrospun fibre morphology.

Table 2.1 — Electrospinning parameters and their respective effect on fibre morphology. Adapted from [26].

PARAMETERS	EFFECT ON FIBRE MORPHOLOGY
Solution parameters	
Viscosity	Low-beads generation, high-increase in fibre diameter, disappearance of beads.
Polymer concentration	Increase polymer concentrations lead to increased fibre diameter.
Molecular weight of polymer	Higher molecular weight of polymer leads to less number of beads and droplets.
Conductivity	Decrease in fibre diameter with increase in conductivity.
Surface Tension	Reducing the surface tension of the polymer solution, fibres without beads can be obtained. No other conclusive link between the surface tension and fibre diameter.
Processing parameters	
Voltage	Generally, there is a decrease in fibre diameter with increase in voltage (not consensual)
Tip to collector distance	Generation of beads with too small and too large distance, minimum distance required for uniform fibres.
Feed/flow rate	Low flow rate leads to thinner fibres. If flow rate is too high, generation of beads occurs.
Ambient parameters	
Humidity	Circular pores are generated on the fibre in cases of high humidity.
Temperature	Increase in temperature results in decrease in fibre diameter.
Pressure	Atmospheric pressure is preferential. No conclusive link with fibre morphology.

A suitable solvent should be used for dissolving the polymer. Its vapor pressure has to be suitable too, allowing a quick solvent evaporation before the polymer reaches the collector. Regarding the viscosity and surface tension of the solvent, they must neither be too large to prevent the jet from forming, nor be too small, which would cause the free drain of the polymer solution from the pipette. The power supply should fulfill two objectives: overcome the viscosity and the surface tension of the polymer solution. Finally, the gap between the tip of the spinneret and the grounded collector has to be large enough for the solvent evaporation [22].

2.3.2. Fibre Alignment

As noticed, there is a certain control over the fibre morphology with the electrospinning process. However, a basic setup of electrospinning can only yield randomly aligned nanofibres. This restricts the areas where fibre mats can be used. This is easily understood with the following examples: Aligned fibres are characteristic of some tissues extracellular matrix (ECM) [4]. It is also reported that aligned polymer fibre-based constructs present topographical cues that facilitate the regeneration of peripheral nerves across long nerve gaps [39]. In order to fully explore all the capacities of the electrospinning and thus solving the aforementioned problems, different approaches were already explored to obtain aligned fibre membranes. Here, it is discussed two main approaches which involve a different design of the collector in the electrospinning setup.

2.3.2.1. Cylinder Collector and Thin Wheel with Sharp Edge

The most basic form of getting aligned fibres is through the use of a rotating mandrel (Figure 2.10 [A]). By rotating the cylinder collector at a very high speed up to thousands of rpm (round per minute), aligned fibres are obtained along the circumference of the mandrel [22, 23]. This method has been successful in obtaining aligned fibres [22]. Nonetheless, the degree of alignment is only possible to some extent.

Since the jet during the electrospinning is traveling at a very high speed, it is necessary that the mandrel is rotating at a very high speed so that fibres can be taken up on the surface of the mandrel and wounded around it [22]. Such a speed can be called as an alignment speed and if the surface speed of the cylinder in slower than the alignment one, randomly fibres will be collected [23]. On the other hand, there is too a limit rotating speed, otherwise an overfast speed may break the fibre jet.

Using a similar approach but with the configuration of a thin wheel/collector with sharp edge, there is significant advancement in collecting aligned electrospun fibres. Nanofibres are positioned and aligned on a tapered and grounded wheel-like bobbin (Figure 2.10 [B]). This is advantageous when compared to the previous methodology since the tip-like edge substantially concentrates the electrical field [23]. As a result, electrospun fibres are almost all attracted by it and are therefore continuously wound on the bobbin edge of the rotating wheel. It is important to refer that nanofibres retain a certain residual charges and as soon as they reach the collector, repulsive forces are exerted on the next fibre to be attracted. It results in separation between the deposited nanofibres.

2.3.2.2. Parallel Conducting Collector

In this method, the alignment of the electrospun fibres is obtained purely trough a different behavior of the electrospinning jet in the electrostatic field. Xia and Li [27] demonstrated that by using a collector consisting of two conductive strips separated by a void gap (Figure 2.10 [C]), electrospun fibres could be uniaxially aligned. Introducing a gap between the collectors will alter the configuration of electrostatic forces acting on the fibres (Figure 2.10 [C]). Since the electrospinning jet is influenced by the electrostatic field profile, the charged fibres are stretched to align themselves perpendicular to each edge of the gap [22, 27]. Moreover, the electrostatic repulsions between the deposited nanofibres will enhance the parallel and relatively even distribution of the fibres.

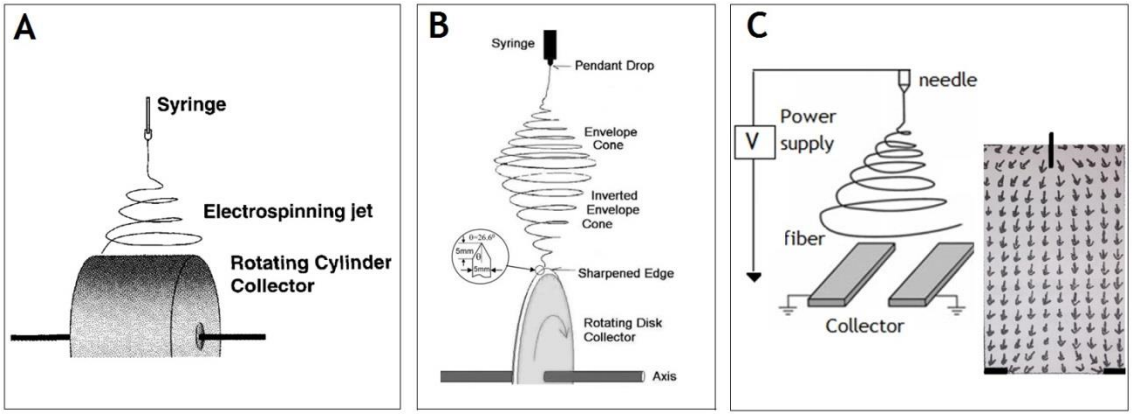

Figure 2.10. Schematic electrospinning setups to obtain aligned fibres. [A] Cylinder collector [22]. [B] Thin wheel with sharp edge collector [23]. [C] Two parallel conducting collector and the profile of the electric field (adapted from [22, 27]).

2.3.3. Polymers and Solvents Used in Electrospinning

So far, a wide range of polymers have been successfully used in electrospinning and are able to form fine nanofibres within the submicron range [23, 26]. Electrospun nanofibres can be either originated from synthetic polymers, from natural polymers or even from a blend of both including proteins [26].

Natural polymers can be advantageous over the synthetic considering their capability for binding cells since they carry specific protein sequences, such Arginylglycylaspartic Acid (RGD). However, natural polymers already reported to cause some problems in terms of their partial denaturation [26]. Herein, the synthetic polymers are preferred as they can be tailored to give specific mechanical properties (strength and viscoelasticity) or desired degradation rate.

In the field of natural polymers, collagen, chitosan, gelatin, casein, cellulose acetate, silk protein, chitin, fibrinogen were already used with electrospinning. The fabrication of electrospun fibres was also performed with numerous synthectic polymers such as, poly (ε-caprolactone) (PCL), poly (lactic acid) (PLA), poly (glycolic acid) PGA, polyurethane (PU), poly (lactide-co-glycolide) (PLGA) and poly (L-lactide-co-ε-caprolactone) [P(LLA-CL)] [26].

It is possible to perform the electrospinning technique using a polymer melt instead of a polymer solution. Nevertheless, most of the polymers are electrospun using polymer solutions. For that reason, polymers are dissolved in solvents before electrospinning.

As discussed before, morphology and size of electrospun nanofibres are strongly influenced by the solution properties like the surface tension. Since different solvents will interfere in the surface tension solution (generally, the decrease in surface tension leads to thinner fibres), a judicious choice of what solvent should be used is demanded. Besides, solvent vapour pressure plays an important role in determining the evaporation rate and drying time of the electrospinning jet. Different solvents were already used and tested in the electrospinning process, where their effect in the fibres morphology was assessed [26]. Table 2.2 shows some solvents that may be used in the electrospinning and their respective properties that should be taken in consideration during it. Since in this work PLA polymer will be used, it is important to perceive what solvent should be used to prepare the polymeric solution. Fang *et al*. dissolved PLLA into dichloromethane/ dimethylformamide (70:30) [40], which is the solvent mixture that will be used to prepare our polymeric solution.

Table 2.2 — Properties of different solvents used in electrospinning [26].

Solvents	Surface Tension (mN/m)	Dielectric constant	Boiling point (°C)	Density (g/mL)
Chloroform	26.5	4.8	61.6	1.498
Dimethylformamide	37.1	38.3	153	0.994
Hexafluoro isopropanol	16.1	16.7	58.2	1.596
Tetrahydrofuran	26.4	7.5	66	0.886
Trifluoro ethanol	21.1	27	78	1.393
Acetone	25.2	21	56.1	0.786
Water	72.8	80	100	1.000
Methanol	22.3	33	64.5	0.791
Acetic acid	26.9	6.2	118.1	1.049
Formic acid	37	58	100	1.21
Dichloromethane	27.2	9.1	40	1.326
Ethanol	21.9	24	78.3	0.789
Tri fluoro acetic acid	13.5	8.4	72.4	1.525

2.3.4. Electrospinning Applications

As it could be noticeable, electrospun fibres provide several advantages, such as high surface to volume ratio, very high porosity and enhanced physico-mechanical properties. These characteristics, aligned with the relatively high production rate and simplicity of the setup, make electrospinning highly attractive to a wide range of applications [26, 41]. Figure 2.11 summarizes the application areas of electrospun fibres. However, attending in Figure 2.12, which depicts the main fields targeted by US patents on electrospun fibres, it is easily realized that some of the applications presented in Figure 2.11 did not reach the industry level yet [23]. Nevertheless, they have being more and more a target of researches due to their potentialities.

Bearing in mind the context of this work, the biomedical applications of the electrospun fibres will be discussed from now on. In the biomedical area, electrospun fibres are broadly applied as tissue engineering scaffolds, as prostheses, in wound healing , in drug delivery, among others [26]. In a biological approach, considering that almost the human tissues and

organs are deposited in nanofibrous forms and structures, it seems logic the use of electrospun fibres in contact with bone, dentin, cartilage or even with the skin. There are also reports that in fact cell-matrix and cell-cell interactions are enhanced and promoted by electrospun fibres [26].

With respect to medical prostheses or/and tissue engineering, nanofibrous scaffolds produced with electrospinning technique have been considered for dermal tissue engineering, bone and cartilage, arterial blood vessels, heart, nerves [23, 26].

Polymers nanofibres can also be used for the treatment of wounds or burns of a human skin, where an action directed to the formation of normal skin growth instead of the formation of scar tissue, is pretended. Drug delivery with polymer nanofibres is based on the principle that the dissolution rate of a given particulate drug increases with increasing surface area which would be the drug and the nanofibrous carrier [26].

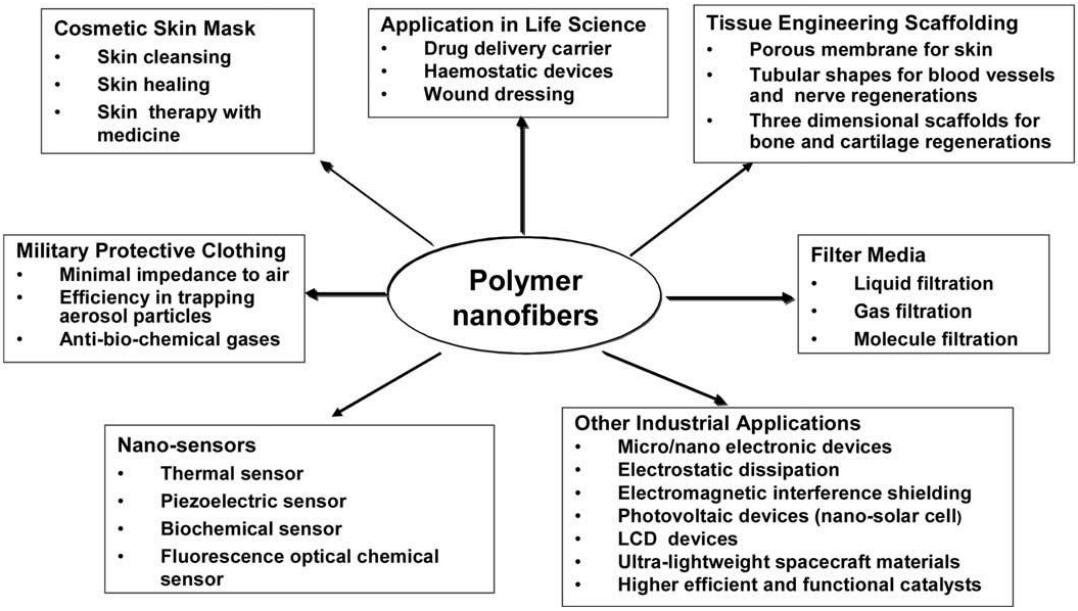

Figure 2.11. Current and potential applications of electrospun polymer nanofibres [23].

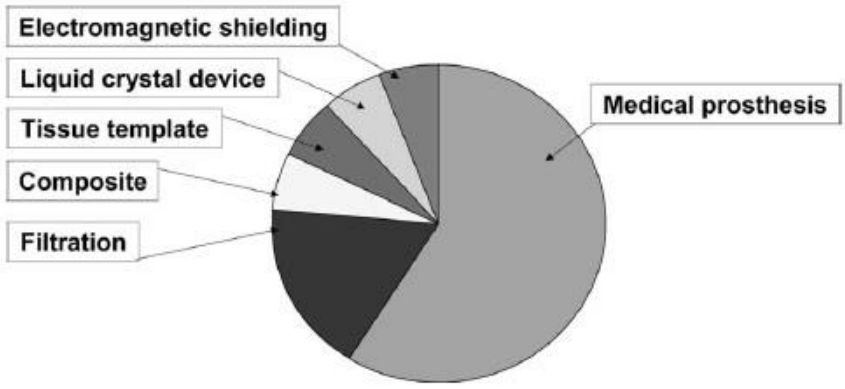

Figure 2.12. Main application fields targeted by US patents on electrospun nanofibres [23].

2.4. Poly (lactic acid) (PLA)

Polymers consist of long chain molecules with repeating units called monomers that are mostly covalently bonded. The monomer must either have reactive functional groups or have double bonds, which may react under suitable conditions to provide the covalent linkage between the repeating units [22].

Polymer products are largely required for a large variety of application in diverse fields. With respect to the biomedical applications, biodegradable polymers have gained more and more interest [14].

Among the family of biodegradable aliphatic polyesters, PLA is one of the most promising polymers since it gathers important requirements, such as its thermoplastic processability and its biological biocompatibility [14]. Moreover, the degradation products of polylactides are also nontoxic and PLA has high mechanical performance when compared to those of commercial polymers such as polyethylene and polystyrene [14, 42].

The chemistry of PLA comprises two main steps, namely the processing and polymerization of its building block - lactic acid monomer [14]. Lactic acid (2-hydroxy proprionic acid) is a simple chiral molecule which can exists as two enantiomers, L- and D-lactic acid (Figure 2.13).

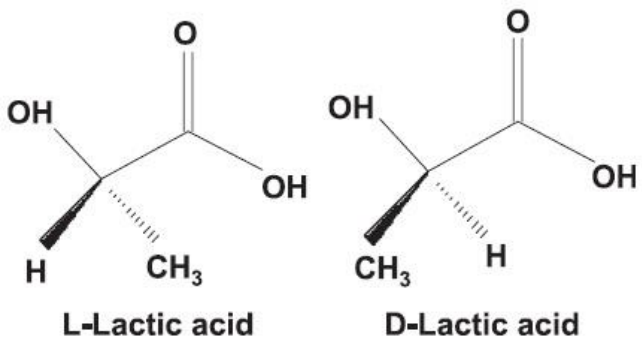

Figure 2.13. Optical isomers of lactic acid [14].

Depending on the proportion of the enantiomers, different PLA properties can be obtained [43]. The L-isomer [i.e., poly-(L-lactic acid) (PLLA)] has been attracting much attention because it is producible from renewable resources such as starch [42].

Generally, the lactic acid is produced by fermentation in which corn starch is converted into lactic acid by bacterial action of *Lactobacillus*. Regarding the polymerization of the lactic acid to high molecular weight PLA, there are two main processes: (1) direct condensation (solvents under high vacuum) and (2) formation of the cyclic dimer intermediate lactide (solvent free) [14].

Commercial PLA are copolymers of poly(L-lactic acid) (PLLA) and poly(D,L-lactic acid) (PDLLA). PLA physical properties can be tailored by material modifications [14]. For example, the melting temperature (T_m), glass transition temperature (T_g) and crystallinity decrease with decreasing L-isomer content [43].

In this work, 100/0 (L/D, L)-PLA will be used (PURASORB® PL 18, PLLA). Table 2.3 summarizes some of the physical characteristics of PLLA.

Table 2.3 — Properties of PLLA [14, 44, 45].

PROPERTIES	UNITS	CONDITION	VALUE
Degree of crystallinity (X_c)	%	---	0-37
Heat of fusion (ΔH_f)	KJ/mol	L-PLA complete crystalline L-PLA fibre (as extruded) L-PLA fibre (after hot draing)	146 2.5 6.4
Heat capacity (C_p)	J/K/g	L-PLA with Mv=(0.2-6.91)x10^5	0.54
Glass transition temperature (T_g)	K	---	326-337
Melting point (T_m)	K	---	418-459
Decomposition temperature	K	---	500-528
Inherent viscosity	dl/g	$CHCl_3$, 25ºC, 0.1g/dl	1.5-2.0
Molecular weight (Mw)	g/mol	---	217.000-225.000

Since the degradation of electrospun scaffolds of PLA will be also studied, it is important to have in consideration that when PLA is exposed to elevated temperatures, thermal degradation is expected, leading to the formation of lactide monomers. This is an important feature of recycle PLA. However, there is a tendency for the lactide monomer to undergo racemization, thus forming meso-lactide which in its turn may have impact in the resulting PLA properties [43].

2.4.1. PLA Applications

PLA is currently being commercialized for a wide spectrum of applications. This is largely due to the ability of a single polymer proving useful in diverse fields by a simple modification of its physico-chemical structure. In addition, and as previously noted, PLA is biodegradable and nontoxic to both humans and the environment [14, 46]. As a result, PLA and its copolymers have been extensively used in different fields such as polymer engineering, tissue engineering, drug delivery systems and in various medical applications (sutures, implants for bone regeneration, implantable matrices and organ reconstruction) [14, 46]. PLA was firstly reported as a bio-absorbable surgical device by Kulkarni *et al.* [47] and in 2010, it was regarded as the world's second most important bioplastic [46].

The purpose of this work falls in the context of implants or tissue engineering, where some PLA (and its copolymers) applications have already been pointed out. Herein, a fibrous membrane may have advantages over polymer films in terms of high porosity, which will be crucial for cell growth, vascularization and nutrients diffusion [14]. Three-dimensional porous scaffolds of PLA have been created for culturing different cell types in the therapy of cardiovascular diseases, muscle tissues, bone and cartilage regeneration [48].

Since materials for bone fixation require high strength, similar to bone characteristics, PLA is tremendously useful in this field [48]. In fact, PLA composites constitute effective scaffolds that stimulate cells/tissue for both proliferation and osteogenic differentiation in bone tissue engineering [46]. Hence, PLA has already shown favorable results in the fixation of fractures [14]. Sanders *et al.* [49] evaluated tissue response upon PLA microfibres implanted in rats. Herein, different fibre diameters ranging from 4 to 15 μm were used and it was observed the lowest capsule thickness formation for the thin fibre. Kellomãki *et al.* [50]

studied self-reinforced PLLA rods as scaffolds for bone formation in muscle by free tibial periosteal grafts. Bhattarai *et al.* [51] developed a electrospun membrane of poly(p-dioxanone-co-L-lactide)—block–poly(ethylene glycol) as a scaffold for tissue engineering. Currently, PLA is also being used in orthognathic surgery and as fixation material in cranio-maxillofacial surgery.

PLA and its composites have applicability as ureteral stents for the treatment of ureteral injury [52]. Filamentous carbon and PLA polymer composite have also been used for repairing tendon and ligament injuries [46]. Moreover, PLA filaments have been developed experimentally for regeneration of nerves in paralyzed patients [53].

2.5. Piezoelectricity

As introduced in Chapter 1, the piezoelectricity is an important characteristic of some materials that should be considered for tissue regeneration or other biomedical applications. A smart material is the designation for a material that changes systematically one or more of its properties in response to an external stimulus [12]. Herein, piezoelectric materials may be considered as smart materials since they generate transient surface charges by tiny mechanical deformations under mechanical solicitation. Besides, piezoelectric materials also display the reverse phenomena as the application of electrical charge or signal results in mechanical deformation [12].

Early in 1950s, Fukada found piezoelectricity in various kinds of biopolymers [13], where shear piezoelectricity was observed in the uniaxially oriented systems of crystallites of cellulose and collagen, as well as in a number of uniaxially elongated films of optically active synthetic and biological polymers [13]. In 1953, Yasuda *et al.* [13] discovered that bone produces electricity by bending deformation, where the compressed and the elongated regions are respectively, negatively and positively polarized, being the callus formed in the negatively polarized regions.

Recently, several artificial biocompatibility, bioactivity and osteoconductivity biomaterials have been developed and used as bone substitutes. Substitutes with piezoelectric properties have been reported to be capable of stimulating osteocyte growth and bone formation *in vivo* [11]. This mechanism is not fully understood, even though piezoelectric effects on bone crystal or matrix might affect bone cells and consequently alter their activity [54]. As a result, the clinical significance and motivation into the piezoelectric behaviour of bone have been gaining more and more interest since a better bone regeneration may be achieved.

A quantitative verification of the shear piezoelectric effects in bone was first demonstrated by Fukada in 1957 [55], where the shear piezoelectric constant for dry bone was pointed out as -0.2 pC/N. Halperin *et al.* [15] reported that the piezoelectric coefficient for the human bone can go up to 7 pC/N. The piezoelectric activity of bone was attributed to the collagen biopolymer and it is dependent on the direction of applied load, frequency and moisture [56].

As above stated, piezoelectricity in uniaxially oriented polymers was observed. Therefore, piezoelectricity may be found in fibrous form of polymers in which the uniaxial symmetry exists [13]. Regarding the sign of shear piezoelectric constant, it is dependent upon the chirality of asymmetric carbon atoms. In fact, shear piezoelectricity is originated from the internal rotation of polar atomic groups associated with an asymmetric carbon atom [13].

The magnitude of the piezoelectric constant is proportional to the degree of orientation and the degree of crystallinity. Figure 2.14 shows the piezoelectric constant for three optically active polymers. Between them, PLA presented the highest piezoelectric constant (10 pC/N) [13]. PLA is consequently a promising material for bio applications due to its stress induced electroactivity, making it advantageous for bone growth and regeneration [56].

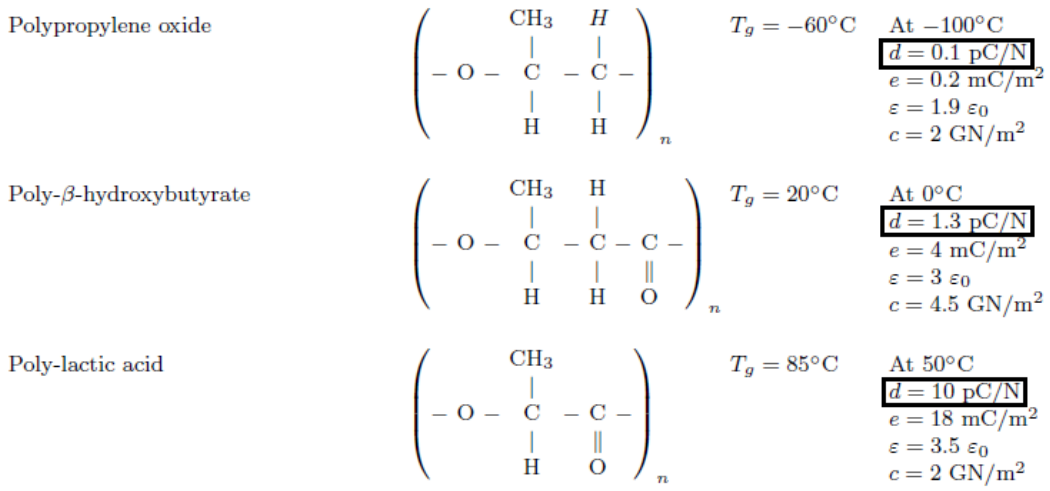

Figure 2.14. Piezoelectric constant, d, of three optically active polymers [13].

2.6. Bonelike®

Ceramics are inorganic materials made from metallic and non-metallic components. The respective atomic bonding is either ionic and/or covalent. Ceramics have found uses as biomaterials such as calcium carbonate-based ceramics and hydroxyapatite ceramics [22].

HA ($Ca_{10}(PO_4)_6(OH)_2$) is the major mineral constituent of the bone matrix. Synthetic HA has already demonstrated its excellent biocompatibility with bones and teeth due to its similar structure to the bone's mineral phase, bioactivity, osteoconductivity [18, 19].

However, HA compromises in a certain way the bone remodeling, since it is a fragile compound and has a low reabsorption rate by the organism (5-15% per year). Therefore, the bone remains brittle and easily prone to fractures [19]. These limitations led to the development of alternative materials and thus much attention is being directed towards an innovational solution - Bonelike®. Bonelike® is a patented product developed by Santos *et al.* [19, 57]. Herein, a production method consisting in the incorporation of a glass, based on P_2O_5-CaO-Na_2O system, into a HA matrix is described.

Bonelike® is a synthetic bone substitute, consisting of a three-phase material: HA, α and β-Tricalcium Phosphates (α-TCP and β-TCP) [58]. The α- and β-TCP phases are homogeneously dispersed in the HA matrix, resulting in a material with improved mechanical properties and enhanced bioactivity, compared to the usual commercial HA [19]. Bonelike® compressive strength and reabsorption rate are dependent on the sintering temperature, glass quantity and fraction of its constituents. Moreover, the inclusion of ions into Bonelike® composition, such as fluoride and sodium, among others, makes it possible to achieve a chemical composition closer to the mineral phase of bone [58].

As an osteconductive material, it is expected that Bonelike® provides an appropriate framework for bone to grow in eventual damaged areas, namely it should function as a

scaffold on which locally osteoblasts can attach [59]. In this context, a suitable porosity (pores with diameters equal to or greater than 100 μm) is fundamental, since the presence of pores, macropores, micropores and interconnected pores allows blood vessels and cells invasion and an appropriate flow of proteins, nutrients and metabolic waste [19, 60]. The micro and macroporosity and the rate of interconnectivity of Bonelike® pores make it ideal for osteoconduction and osteointegration as a bone substitute.

2.6.1. Bonelike® Applications

As noted, Bonelike® is a synthetic bone graft material specially designed for clinical applications of bone regeneration. It can be applied in different cases ranging from trauma, old age or bone diseases, in the fields of maxillofacial surgery, implantology and othopaedics.

Until now, Bonelike® has been revealed great success in its applications [59]. R. Sousa *et al*. [59] evaluated the osteoconductivity and bioactivity of the Bonelike® graft in repairing surgical maxillary cystic bone defects and their results indicated perfect bone bonding between new bone formed and Bonelike® granules. M. Gutierres *et al*. [61] evaluated the biological behavior of Bonelike® implanted in the lateral aspect of the tibia, during osteotomy surgery for the treatment of medial compartment osteoarthritis of the knee. Herein, Bonelike® allowed effective vascularization and bone ingrowth throughout the defected site. In addition, M. Gutierres *et al*. [62] tested Bonelike® in porous edge shape in the treatment of medial compartment osteoarthritis of varus knees. It was also reported the fast osteointegration of Bonelike® after implantation (after 4 months, signs of fusion at the osteotomy site and good integration of the implanted Bonelike® were observed). In the dental area, some promising results were also obtained. G. Pavan Kumar *et al*. [63] demonstrated the guided bone regeneration procedure using a glass-reinforced HA (Bonelike®) and collagen membrane in the treatment of peri-implantitis. J. Lobato *et al*. [64] evaluated the biological response of pure titanium dental implants coated with Bonelike® placed in human maxilla and mandible. These implants proved to be highly bioactive with extensive new bone formation and attachment.

In order to expand the range of Bonelike® applications, it can be interesting to associate it with resorbable matrices, which is exactly what we intend to do in this work. In this context, animal studies already showed that the use of resorbable matrices does not interfere in the Bonelike® bioactivity [65].

2.7. MG-63 Cell Line

Upon implantation of any biomaterial in bone, mesenchymal stem cells (MSCs) are recruited from the bone marrow to the implant site, where they bind to the material surface and then differentiate in bone-forming osteoblasts [66]. The osteoblast-material interaction depends on the surface characteristics, such as its topography, chemistry and surface energy [67]. These aspects influence molecular adsorption, which in turn plays a major role in the osteoblast attachment/adhesion and subsequent proliferation and differentiation (osteogenic cells typically bind to biomaterials through integrin-mediated mechanisms; integrins are glycoproteins composed by noncovalently-associated α and β subunits [66]).

In several *in vitro* studies of cell-material interactions, most authors prefer using immortalized cell lines over primary cells like MSCs or bone-derived osteoblasts. This is due

to the fact that immortalized cell lines (including cells derived from osteosarcomas) are easier to acquire than primary cells and grow *in vitro* for an indefinite number of passages [66]. MG-63 is one of those osteosarcoma cell lines which has been well characterized and validated as a model to test biocompatibility of various materials. In response to osteogenic chemical cues, they are capable of undergoing osteoblastic differentiation [66, 68].

The $p75^{NTR}$ is an important neuronal signaling molecule that interacts with numerous lingands and coreceptors [69]. In addition, it was demonstrated that exogenous $p75^{NTR}$ enhances the potential for cell proliferation and osteogenic differentiation in pre-osteoblast cell lines [69].

MG-63 cells produce collagen type I and express alkaline phosphatase (ALP) activity, which are further enhanced by dihydroxyvitamin D3. Osteocalcin is also synthesized in response to all markers of osteoblastic function. MG-63 differentiation into mineralized state is induced by the interaction between dihydroxyvitamin D3 and TGF-β (local growth and differentiating agent) [70]. This mineralization occurs without continued differentiation into the mineralization state.

Regarding the morphology, attached osteosarcoma cells (MG-63) are oval to spindle-shaped, without branching cell processes. Besides, their cell size is independent on cell density, which is uncommon among the normal human osteoblasts [71].

Chapter 3

Materials and Methods

3.1. Materials Fabrication

3.1.1. Bonelike®

Bonelike® production comprises the preparation of a suspension composed of hydroxyapatite, bioglass (P_2O_5-CaO), microcrystalline cellulose and polyvinyl alcohol (PVA), and subsequent combustion of the microcrystalline cellulose and sintering at 1300 ºC.

Regarding HA, its preparation required the precipitation between calcium hydroxide [$Ca(OH)_2$] and ortophosphoric acid 85 wt%, (H_3PO_4), according to the following chemical route [72]:

$$10Ca(OH)_2 + 6H_3(PO)_4 \rightarrow Ca_{10}(PO_4)_6(OH)_2 + 18H_2O$$

The resulting HA precipitate was filtered through a vacuum system and dried in an oven at 60 ºC for two days. Then, HA was ground into a fine powder with a granulometry smaller than 75 µm.

The P_2O_5-CaO based glass with the chemical composition of $65P_2O_5$-$15CaO$-$10CaF_2$-$10Na_2O$ [73] (mol %) was prepared by mixing the appropriate quantities of high purity (>98%) grade reagents (sodium carbonate (Na_2CO_3), calcium hydrogenphosphate ($CaHPO_4$), calcium fluoride (CaF_2) and di-phosphorus penta-oxide (P_2O_5)) in a platinum crucible, and then heating it at 1450 ºC for 90 min in a furnace. The prepared glass was crushed in an agate mortar and sieved to a granule size below 50 µm.

Summarizing, Bonelike® was obtained by adding 2.5% of glass to the prepared HA. The Bonelike® powder was first mixed with the microcrystalline cellulose and PVA, which are agents responsible for the formation of porosity and PVA, as an organic ligand, also enables the solid components to be kept together in the suspension, avoiding their deposition [74].

The resulting suspension was poured into Alumina (Al_2O_3) plates, the wet homogeneous mixture was dried in an oven at 60 ºC for two days and then the samples were sintered at 1300 ºC using a heating rate of 4 ºC.min^{-1}, followed by natural cooling inside the furnace.

Finally, using standard milling and sieving techniques, Bonelike® granules with particle size ≤150 µm were obtained.

3.1.2. PLLA and PLLA/Bonelike® Solutions

Purasorb PL18 PLLA, with an average molecular weight of 217.000-225.000 g.mol^{-1}, was purchased from Purac and dissolved in a 3/7 (vol/vol) mixture of N,N-dimethylformamide (DMF, from Merck) and dichloromethane (MC, from Sigma-Aldrich) in order to achieve a polymer concentration of 10 wt% in the solution. The process was conducted at room temperature using a magnetic stirrer until complete polymer dissolution. Following a similar approach to the previous one, Bonelike® particles (diameter ≤150 μm) were dissolved in a PLLA solution obtaining, therefore, a polymeric/ceramic (20/80) concentration of 10 wt% in the solution.

3.1.3. Electrospun PLLA and PLLA/Bonelike® Membranes

PLLA or PLLA/Bonelike® solutions were placed in a commercial plastic syringe fitted with a steel needle (0.5 mm of inner diameter) connected to a high-voltage supply (PS/FC30P04 from Glassman). An electric field of 1.5 kV.cm^{-1} was applied to the polymer solution, and a syringe pump (from Syringepump) was used to feed the polymer solution into the needle tip at a rate of 0.5 mL.h^{-1}. The random electrospun fibres were collected on a grounded collecting plate placed 15 cm away from the needle.

3.2. Fibre Membranes Characterization

3.2.1. Morphology

Electrospun fibre membranes were coated with a thin gold layer using a sputter coater (Polaron, SC502) and their morphology was analyzed using a scanning electron microscope (SEM, JSM-6300, JEOL) at an accelerating voltage of 15 kV. Fibres average diameter was calculated over 50 fibres using the SEM images (10000X magnification for the PLLA membrane and 5000X magnification for the PLLA/Bonelike® membrane) and the Image J software [75].

3.2.2. Porosity

The porosity of PLLA and PLLA/Bonelike® membranes was measured using the pycnometer method. First, a pycnometer filled with ethanol was weighted and labeled as W_1. Then, the sample (with a weight of W_{sample}) was immersed in ethanol and, when it was saturated by the ethanol, additional ethanol was added to complete the volume of the pycnometer. The weight of this system was labeled as W_2. Finally, the sample saturated with the ethanol was taken out of the pycnometer and the residual weight of the ethanol and the pycnometer was labeled as W_3. The porosity of each membrane was calculated according equation 1. The porosity of each membrane was obtained as the mean value of the porosity determined in three samples.

$$\text{Ɛ}\,(\%) = \frac{W_2 - W_3 - W_{sample}}{W_1 - W_3} \cdot 100 \qquad \text{(Eq.1)}$$

3.2.3. Wettability

Static contact angles were measured at room temperature using a DataPhysics OCA-20 drop shape analysis system (DataPhysics Instruments GmbH, Filderstadt, Germany) controlled by SCA20 software. A sessile drop (3 µL) of ultrapure water (Milli-Q) was deposited on the PLLA and PLLA/Bonelike® membranes and the contact angle was measured using a DataPhysics OCA 35 goniometer and SCA20 software. For the same sample, contact angles were measured on 8 different spots and the result is expressed as their average and standard deviation.

3.2.4. Fourier Transform Infrared (FTIR) Spectroscopy

Infrared spectra analysis was performed with a FTIR system from Shimadzu IRAffinity-1S apparatus in the attenuated total reflectance (ATR) mode from 4000 to 600 cm^{-1}. FTIR spectra were collected after 32 scans with a resolution of 2 cm^{-1}.

3.2.5. X-Ray Diffraction

XRD analysis was performed on a powder sample of Bonelike® and on PLLA/Bonelike® fibre membranes using a Phillips Analytical X-Ray model PW 1710, employing Cu Kα monochromatic radiation (40 kV, 30 mA, Kα=1.541838 Å). Data were collected at room temperature, for 2θ values ranging from 5 to 70º in increments of 0.02º and a counting time of 2s/step.

3.2.6. Thermal Analysis

3.2.6.1. Differential Scanning Calorimetry (DSC)

Thermal behavior of the electrospun fibre membranes was analyzed by differential scanning calorimetry with a Mettler Toledo 823e apparatus using a heating rate of 10 ºC.min^{-1} under nitrogen purge. Samples were cut into small pieces from the middle region of the electrospun membranes, placed into 40 µL aluminum pans and heated between 30 and 200 ºC. The glass transition temperature (T_g), cold-crystallization temperature (T_{cc}), melting temperature (T_m), and melting enthalpy (ΔH_m) of electrospun samples were obtained.

3.2.6.2. Thermogravimetry

The thermal degradation kinetics of PLLA and PLLA/Bonelike® membranes was characterized by thermogravimetric analysis (TGA) in Perkin-Elmer Pyris-1 TGA (USA) apparatus. In this study, the thermal degradation behavior of the samples was recorded heating them from 30 to 600 ºC at different heating rate scans (10 ºC.min^{-1}; 20 ºC.min^{-1}; 30 ºC.min^{-1} and 40 ºC.min^{-1}). All measurements were performed under a nitrogen atmosphere.

For the TGA data analysis, important thermodynamic considerations were taken into account. In theory, the expression for the thermal decomposition of a homogeneous system has its general form given by equation 2 [76, 77].

$$\frac{\partial \alpha(t)}{dt} = k(T) f[\alpha(t)] \quad \text{(Eq.2)}$$

α represents the reaction extent of the component of the sample being degraded, defined by the equation 3:

$$\alpha(t) = \frac{w_0 - w(t)}{w_0 - w_\infty} \quad \text{(Eq.3)}$$

where w_0, w(t)and $w_\infty$are the weights of the sample before degradation, at a given time t and after complete degradation, respectively. k(T), the rate coefficient, changes with the absolute temperature according to the Arrhenius equation (Eq.4) [78]:

$$k(T) = A \exp\left(\frac{-E_{act}}{R\,T}\right) \quad \text{(Eq.4)}$$

where A is the pre-exponential factor (min^{-1}), E_{act} is the apparent activation energy ($kJ.mol^{-1}$), R is the gas constant (8.314 $J.K^{-1}.mol^{-1}$) and T is the absolute temperature (K).

The differential conversion function, $f(\alpha)$, may be described by various functional forms, nevertheless its most common form, which represents a solid-state reaction, is given by the equation 5 [76, 77].

$$f(\alpha) = (1 - \alpha)^n \quad \text{(Eq.5)}$$

In the previous equation (Eq.5), n is the reaction order, assumed to remain constant during the entire degradation process.

The combination of equations 2 and 4 gives the following relationship (Eq.6):

$$\frac{\partial \alpha(t)}{\partial t} = A \exp\left(\frac{-E_{act}}{R\,T}\right) f[\alpha(t)] \quad \text{(Eq.6)}$$

For a dynamic TGA process, introducing heating rate (β, given by the equation 7) into equation 6, equation 8 is obtained [78].

$$\beta = \frac{\partial T}{\partial t} \quad \text{(Eq.7)}$$

$$\frac{\partial \alpha}{\partial T} = \left(\frac{A}{\beta}\right) \exp\left(\frac{-E_{act}}{R\,T}\right) f(\alpha) \quad \text{(Eq.8)}$$

Equations 6 and 8 are the fundamental expressions of analytical methods to calculate kinetic parameters on the basis of TGA data [78]. In this study, TGA results were interpreted using the Kissinger's method.

- Kissinger's method

The Kissinger's method is one of the most accurate and popular approaches [79, 80] for determining kinetic parameters by thermal analysis and takes the form of equation 9 [76]:

$$\ln\left(\frac{\beta}{T_p^2}\right) = \frac{\ln(A\,E_{act})}{\mathrm{R}} + \ln\left[\mathrm{n}\left(1-\alpha_p\right)^{1-n}\right] - \frac{E_{act}}{R.T_p} \qquad \text{(Eq.9)}$$

where T_p and α_p are the absolute temperature and the conversion at the maximum weight loss rate, respectively. $\ln\left(\frac{\beta}{T_p^2}\right)$ is plotted against $1/T_p$ for a series of experiments at different heating rates with the peak temperature, T_p, being taken from the differential thermogravimetric (DTG) curve [78]. Hence, the slope of the function ($-E_{act}/R$) is obtained and the activation energy can be then calculated without a precise knowledge of the reaction mechanism.

3.3. *In Vitro* Cell Studies

3.3.1. Cell Culture and Seeding

MG-63 cells were cultured in minimum essential medium (MEM) Eagle, alpha modification (α-MEM), supplemented with 10% fetal bovine serum (FBS), 1% Fungizone and 1% Penicillin. Culture flasks were maintained in a humidified atmosphere of 95% air and 5% carbon dioxide (CO_2) at 37 ºC.

Cells were passaged every 3-4 days, when cell density reached 80-90% of confluence. During this passaging procedure, cells were washed twice with phosphate buffered saline (PBS; Gibco, UK) and detached from the cultures flasks with trypsin solution at 37 ºC for 5 min. Cell content was then subjected to centrifugation at 1200 rpm for 5 min. The supernatant was removed and cell pellet was mixed with fresh cell culture medium, followed by resuspension in two/three new T75 flasks.

PLLA and PLLA/Bonelike® membranes were cut in small round pieces (diameter around 1.3 cm), sterilized for 30 min, each side, under ultraviolet (UV) radiation and pre-incubated with the α-MEM for 2 h at 37 ºC in a humidified atmosphere of 95% air and 5% CO_2. Then, cells (passage 10) were seeded on these samples and on tissue culture polystyrene (TCPS, controls) at a density of $1.5x10^4$ cells/well. It is important to point out that fibre membranes were kept in the bottom of the cell culture wells using cylindrical inserts (inner diameter=1.05 cm; cell growth area=0.865 cm^2), as Figure 3.1 illustrates.

Cultured fibre membranes were observed by SEM at days 1, 3 and 7. In vitro osteoblast proliferation was assessed by MTT and Resazurin assays (days 1, 3, and 7). Alkaline phosphatase activity and total protein content (days 3 and 7) were also evaluated.

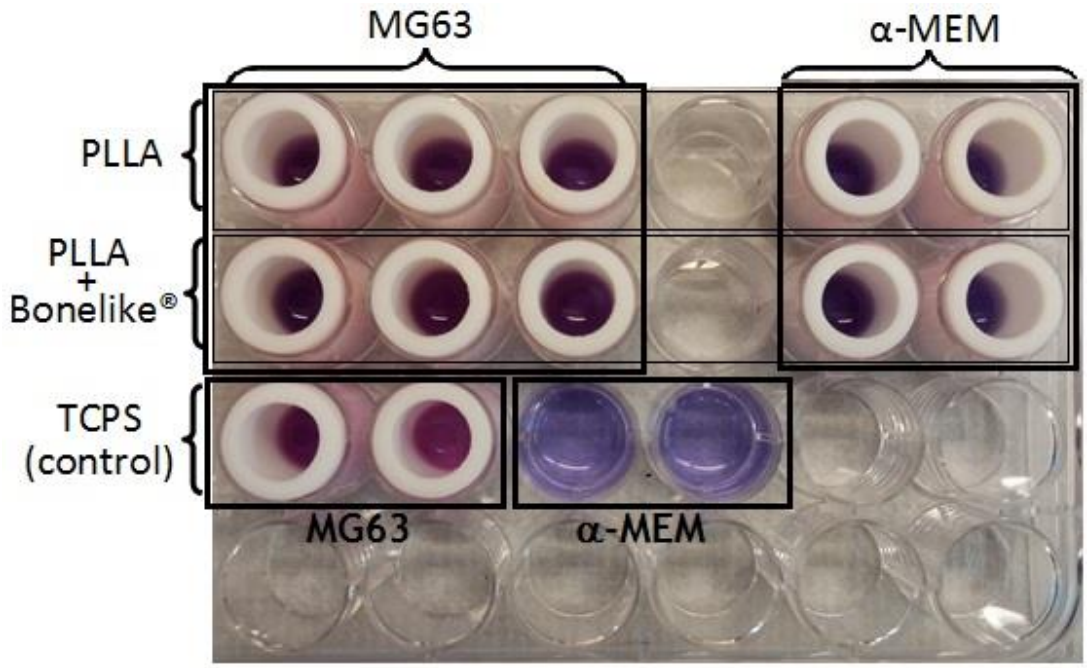

Figure 3.1. Illustration of the samples display (the inserts mentioned above are the white tubes) 7 days after cell seeding. Different colors are due to the resazurin solution where a change from blue to pink is observed in each of the growing cultures.

3.3.2. SEM

Before SEM observation, cells were fixed with 1.5% glutaraldehyde in PBS for 10 min. Then, samples were washed three times with water, and dehydrated in graded series of ethanol solutions (70%, 80% and 90% for 10, 10 and 20 minutes, respectively). Until SEM analysis, samples were kept in ethanol 100% at 4 ºC. SEM was performed using the same equipment and method aforementioned in the fibre membranes characterization.

3.3.3. MTT Assay

Cell viability was analyzed by performing an MTT assay 1, 3 and 7 days after seeding the cells in the fibre membranes (PLLA (n=3), PLLA/Bonelike® (n=3) and control (n=3)). In this test, the mitochondrial dehydrogenase activity of the MG-63 cells is determined by using the substrate 3-(4,5-Di-methylthiazol-2-yl)-2,5-diphenyl tetrazolium bromide (MTT; Sigma) which is reduced to formazan that accumulates in the cytoplasm of viable cells [81]. For this purpose, the medium was removed from the wells to eliminate any dead cells and, was substituted by fresh one. Then, 50 µL of MTT solution (5 $mg.mL^{-1}$) was added to each of the culture wells (24-well plate) containing 500 µL of α-MEM and the samples were incubated at 37 ºC in humidified atmosphere of 95% air and 5% CO_2 for 3 h. After the incubation period, the medium with the MTT solution was discarded and the samples were observed under the microscope. Finally, the formazan salts were dissolved with 150 µL of dimethylsulphoxide (DMSO). 100 µL of the supernatant were transferred to a 96-well plate and the absorbance was measured at 550 nm on a plate reader (Power Wave XS2 spectrophotometer, Biotek).

3.3.4. Resazurin Assay

Cell viability was also quantified by performing a resazurin assay after 1, 3 and 7 days after seeding the cells in the fibre membranes (PLLA (n=3), PLLA/Bonelike® (n=3) and control (n=3)). Herein, a nontoxic alamar blue dye (resazurin) is reduced by intracellular enzyme activity to resofin, a fluorescent form of alamar blue [81]. The medium was removed from the wells and 50 µL of 10% (v/v) of resazurin solution was added to each well previously filled with fresh medium (step performed in dark). Samples were incubated at 37 ºC in humidified atmosphere of 95% air and 5% CO_2 for 3.5 h and after it, 100 µL of this solution were transferred to a 96-well plate. The fluorescence intensity was measured in a Power Wave XS2 spectrophotometer (Biotek) at 530 and 590 nm for excitation and emission wavelength, respectively.

3.3.5. Alkaline Phosphatase (ALP) Activity and Total Protein Content

ALP is a membrane enzyme that acts as a nucleation agent in the initiation of mineralization process by cell differentiation [82]. ALP hydrolyzes phosphate esters which causes an increase of phosphate concentration, and thus the mineralization of extracellular matrix (ECM). The expression of this enzyme is associated with the appearance of bone cells phenotype and the maturation of the extracellular matrix, before mineral deposition (Figure 3.2) [83]. Since ALP is regarded to be an important phenotype of bone-forming cells [82, 84], it is one of the most widely used biochemical marker of osteoblasts differentiation.

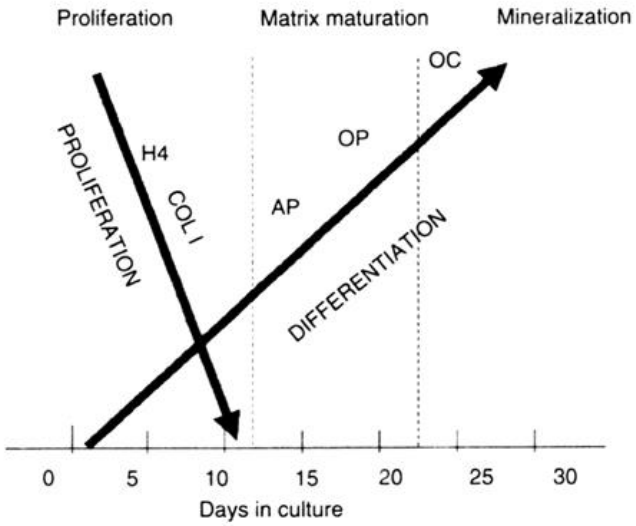

Figure 3.2. Principal stages of the osteoblast development in culture and respective temporal expression of genes characteristic of this process. H4, histone; COL I, type I collagen; ALP, alkaline phosphatase; OPN, osteopontin; OC, osteocalcin [83].

Here, cell cultured membranes and controls (PLLA (n=3), PLLA/Bonelike® (n=3) and control (n=3)) were washed with PBS and with a cell lysis buffer containing 0.1% Triton X-100. Samples were frozen and stored at -20 ºC until ALP and total protein measurements. In order to perform the measurements, samples were thawed at 37 ºC for 5 min, and the ALP

secretion of the osteoblasts cultured on the fibre membranes for 3 and 7 days was determined quantitatively using p-nitrophenyl phosphate (pNPP) solution as the reaction substrate. For this purpose, the lysis solution (100 µL) was incubated in 80 µL of pNPP in alkaline buffer solution (bicarbonate 0.15 M in $MgCl_2$ 2.5 mM, pH=10). After incubation 1h at 37 ºC, the reaction was stopped adding NaOH (5 M) and the absorbance of the hydrolysis product (p-nitrophenol) was immediately measured at 400 nm using a plate reader (Power Wave XS2 spectrophotometer, Biotek).

ALP activity results were normalized by total protein content, quantified by Lowry's method. The content of each stored cell lysate sample was homogenized, and 30 µL of each were transferred to a 96-well plate and 150 µL of solution made from Reagent A and Reagent B (50:1) were added for 10 min (Reagent A: 2% Na_2CO_3 in NaOH 0.1 M. Reagent B: 0.5% $CuSO_4 \cdot 5H_2O$, in 1% $Na_2C_4H_4O_6$ (sodium tartrate) and a droplet of H_2SO_4). Then, 15 µL of Folin & Ciocalteu's Phenol reagent (Sigma-Aldrich) were added, the plate was placed in the orbital shaker for 30 seconds, and incubated for 1hour at 37 ºC in the dark. After the incubation period, absorbance was measured at 750 nm using a plate reader (Power Wave XS2 spectrophotometer, Biotek).

3.4. Statistical Analysis

All quantitative data are presented as mean± standard deviation. Significant differences in statistical analysis were determined using one-way ANOVA test with Tukey's HSD post hoc analysis. Statistical differences are found when $p<0.05$.

Chapter 4

Results and Discussion

4.1. Bonelike® Morphology and Porosity

Bonelike® porosity and morphology were analyzed by SEM (Figure 4.1). An interconnected porosity with macro and micropores is observed. Nevertheless, due to the reduced size of Bonelike® granules, the porous structure is mainly composed by micropores. Macroporosity is mostly observed in the Bonelike® surface since these particles were obtained from bigger fragments of higher macroporosity. This porous feature allows the growth of a capillary vascular network and the establishment of cell-cell contact between the bone graft [74], making it ideal for osteoconduction and osteointegration.

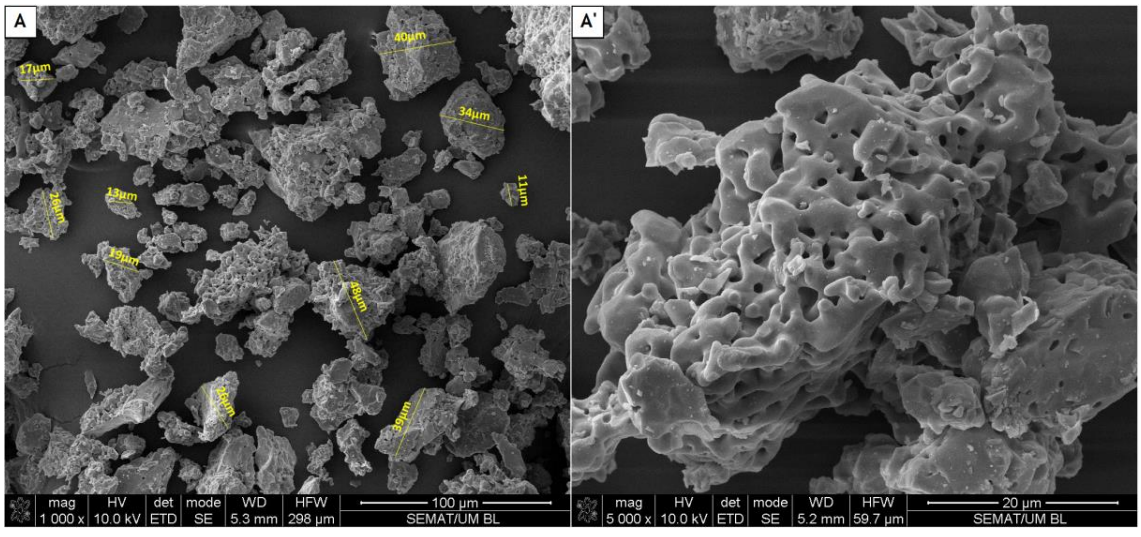

Figure 4.1. SEM images showing Bonelike® granules. The scale bar corresponds to 100 µm and 20 µm in [A] and [A'], respectively.

As it is shown in Figure 4.1-A, Bonelike® granules have a wide range of sizes. Nevertheless, particle size is always ≤150 µm, as was intended during their fabrication. It is worth noting that Bonelike® particles of larger granulometry were also tested. However, due

to their size and also its high speed during electrospinning, it was observed that these granules pierced the PLLA mats rather than being incorporated therein. Thus, decreasing particle sizes were tested until there was no apparent perforation of the membranes.

4.2. Fibre Membranes Characterization

4.2.1. Morphology

As discussed in Chapter 2, there are many parameters which have direct influence in determining the morphology and diameter of the electrospun fibres. Both fibres (PLLA and PLLA/Bonelike®) were electrospun in the same conditions since the main goal of this work encompasses the study of the biological response of each type of fibre membrane rather than the study of the influence of such parameters on their respective morphology. In such a way, the solvent choice became fundamental to obtain proper fibres. PLLA or PLLA/Bonelike® was dissolved in a mixture of MC and DMF has detailed in Chapter 3. The high polarity of DMF facilitates fibre formation and MC allows a quick evaporation due to its high volatility (see Table 2.2). This combined action permits the fibre to maintain its integrity during the travel from the tip of the needle to the collector, ending up on a polymer matrix without traces of the solvent in the membranes [76].

The surface morphology and structure of the neat PLLA and PLLA/Bonelike® electrospun fibre membranes were observed by SEM. In a first observation, it is possible to notice the random distribution of the PLLA fibres and also the well spread arrangement of the Bonelike® granules (Figure 4.2). Besides, compared to the smooth morphology of PLLA fibres, rough surfaces are formed for the composite membrane (PLLA/Bonelike®).

Regarding Bonelike® distribution, due to the higher ceramic concentration and high particle size, Bonelike® is mainly present in the pores between fibres and some particles are present inside or even at the fibre surface, especially the smaller particles (Figure 4.2-B' (inset)). Bonelike® particles are spread over the PLLA membrane, but it is unclear that it is in a homogeneous away due to their different sizes.

Figure 4.3 shows size distribution of the fibre diameters. PLLA membranes presented a diameter distribution ranging from 0.2 to 0.9 μm, with an average size of 0.51±0.15 μm. PLLA/Bonelike® samples exhibited a broader size distribution (0.1 to 1.1 μm) but with a lower average size, 0.44±0.17 μm (Table 4.1). Both fibre sizes fall in the range of bone's collagen fibres (0.1-2 μm) [85] which confers these membranes a structural similarity.

Table 4.1 — Physical properties (fibre diameter; porosity and water contact angle) of PLLA and PLLA/Bonelike® fibre membranes.

Material	Fibre Diameter (μm)	Membrane porosity (%)	Water Contact Angle (deg)
PLLA	0.51±0.15	79±3	131±2
PLLA/Bonelike®	0.44±0.17	89±5	132±3

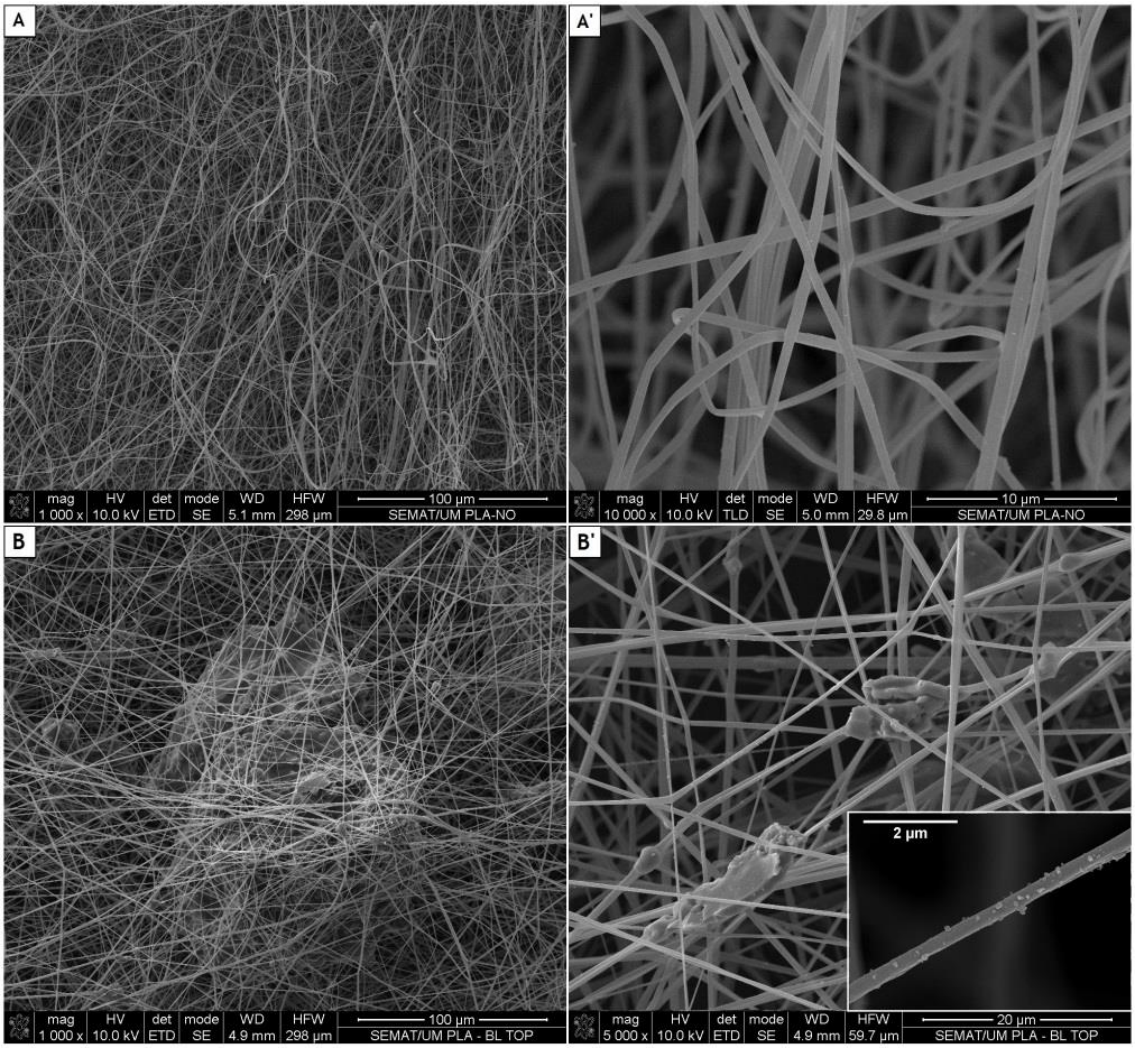

Figure 4.2. SEM images showing the PLLA ([A] and [A']) and PLLA/Bonelike® ([B] and [B']) microfibres electrospun at a traveling distance of 15 cm, a needle diameter of 0.5 mm, an electric field of 1.5 $kV.cm^{-1}$ and flow rate of 0.5 $mL.h^{-1}$. The scale bar corresponds to 100 µm in ([A]; [B]) and to 10 µm and 20 µm in [A'] and [B'], respectively. Inset in [B'] shows a higher magnification of a single fibre (scale bar corresponds to 2 µm).

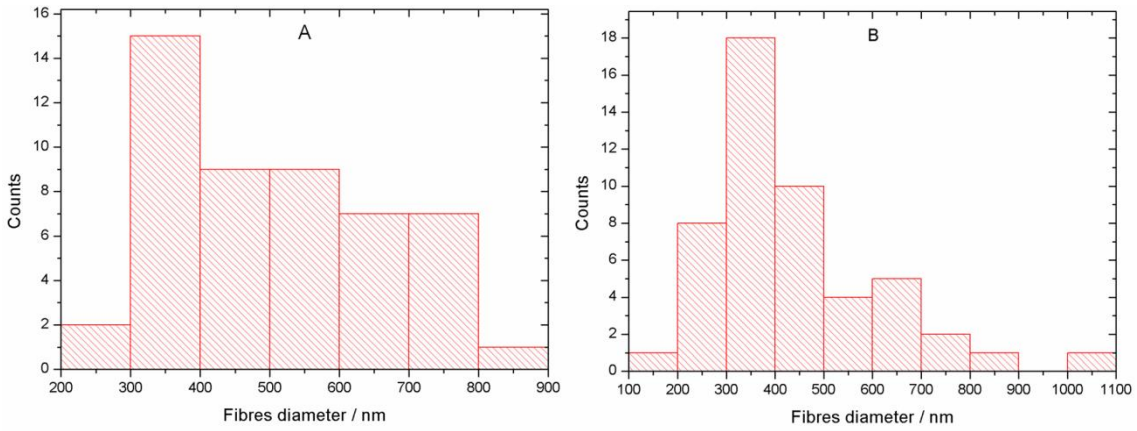

Figure 4.3. Size distribution of fibres in SEM photographs of Figure 4.1 [A'] and Figure 4.1 [B']. Graph A corresponds to PLLA microfibres and graph B corresponds to PLLA/Bonelike® microfibres. Average diameter of the fibres was 0.51±0.15 µm in the PLLA membranes and 0.44±0.17 µm in the PLLA/Bonelike® membranes (data is expressed as mean ± standard deviation of 50 measurements).

4.1.1. Porosity

Regarding membrane porosity, a 3-D porous structure is crucial to guide cell attachment, proliferation and tissue regeneration. Taking into account the porous nature of PLLA and PLLA/Bonelike® membranes, the pycnometer procedure revealed to be a suitable method to estimate their porosity (data in Table 4.1). Thus, PLLA membrane exhibited a porosity of 79±3%. The Bonelike® granules added to the PLLA membranes led to an increase on porosity up to 89±5%. This increase does not corroborate the results of another study [86] where a similar ceramic filler provoked a decrease on the polymeric membranes porosity. The authors referred that the ceramic nanoparticles might tend to occupy the free spaces available in the pores thereby reducing the porosity of the scaffolds. However, in this particular study, there was the opposite effect due to the fabrication process of the fibre membranes. Herein, the Bonelike® particles induced a certain deformation in the PLLA mats. Besides, due to the size of the Bonelike® granules, the PLLA fibres are held more far apart from each other, leading to a higher porosity, as indeed it is noticed in the SEM Images of Figure 4.2 and particularly in detail with the SEM image of Figure 4.4.

Figure 4.4. SEM image showing the Bonelike® effect on maintaining a higher distance between the PLLA fibres. The scale bar corresponds to 20 µm.

4.1.2. Water Contact Angles

In relation to the water contact angles measurements, no significant differences were found between the two studied fibre membranes. The water contact angle of PLLA electrospun membrane was 131±2º and that of PLLA/Bonelike® was 132±3º (Table 4.1/Figure 4.5), indicating thereby their hydrophobic characteristic.

Similar PLLA water contact angles are reported in the literature [87, 88]. In respect to PLLA/Bonelike® contact angles, no data was found in the literature for comparison. However, membranes with similar composition (PLLA/HA) were already reported with identical hydrophobic behavior [89].

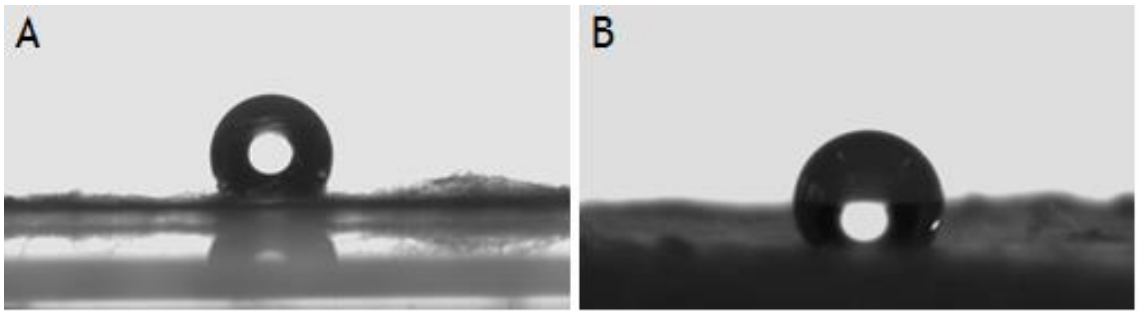

Figure 4.5. Water sessile drop on [A] PLLA and [B] PLLA/Bonelike® membranes.

4.1.3. Fourier Transform Infrared Spectroscopy

FTIR has been widely used as a powerful analysis technique in chemistry, physics and engineering [90]. A FTIR spectrum represents the molecular absorption/transmission profile, creating thereby a fingerprint of the sample.

In what concerns PLLA, previous studies have reported infrared absorption bands which are characteristic of the vibrations of the molecular groups which form this polymer (Table 4.2). Comparing such literature findings with the PLLA spectrum obtained in this study (Figure 4.6, and in more detail in Figure 4.7-A), some information regarding the crystallinity of this polymer can be discussed.

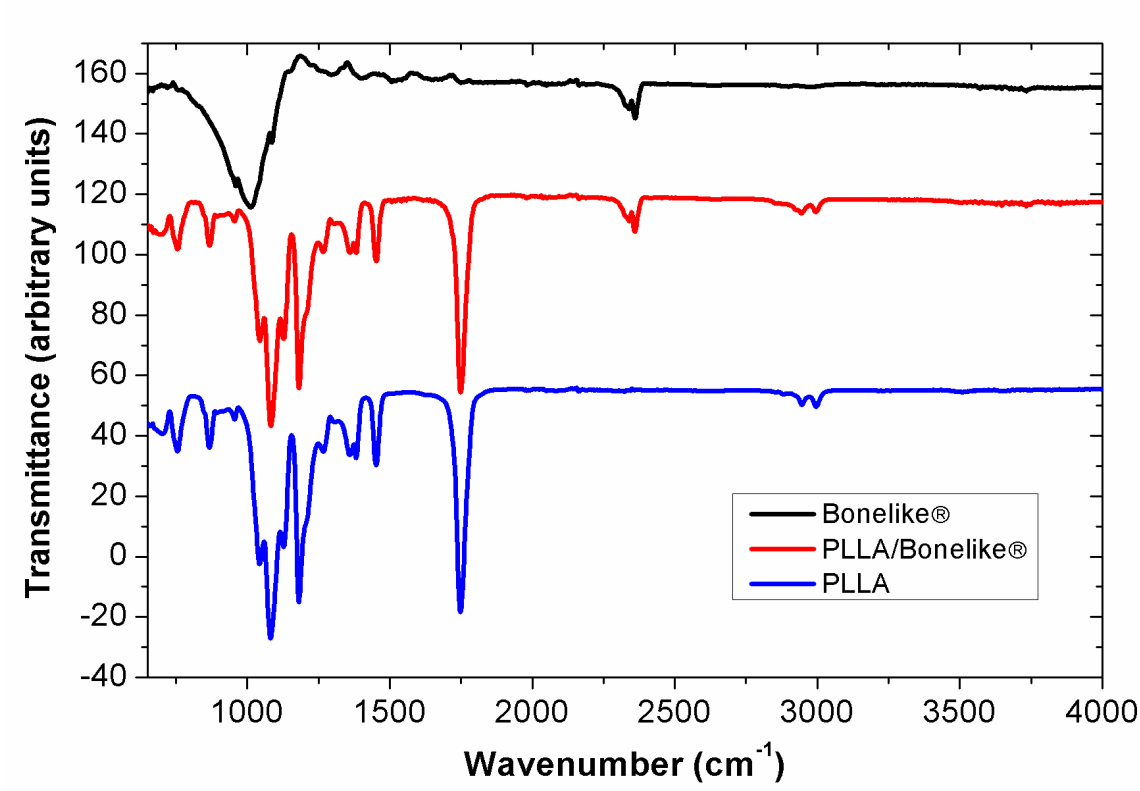

Figure 4.6. FTIR transmission spectra of Bonelike®, PLLA and PLLA/Bonelike® electrospun fibres.

Table 4.2 — Wavenumbers (cm^{-1}) and vibrational assignments associated with different phases of PLLA [91].

IR Frequency (cm^{-1})	Phase Form	Assignment
860	Amorphous	
871	α	
908	β	
921	α	Coupling of the C-C backbone stretching with the CH_3 rocking mode
955	Amorphous	
1044	Amorphous α′ and α	$\nu(C–CH_3)$
1053	α	$\nu(C–CH_3)$
1092	α′ and α	$\nu_s(C–O–C)$
1107	α′ and α	
1134	Amorphous α′ and α	$r_s(CH_3)$
1183	Amorphous α′ and α	$\nu_{as}(C–O–C) + r_{as}(CH_3)$
1213	a′ and α	$\nu_{as}(C–O–C) + r_{as}(CH_3)$
1222	α	$\nu_{as}(C–O–C) + r_{as}(CH_3)$
1268	Amorphous + semicrystalline	$\nu(CH) + \nu(COC)$
1302	Amorphous	C–H stretching
1360	Semicrystalline	δ (CH), CH wagging (bending)
1363	Amorphous	δ (CH), CH wagging (bending)
1368	Semicrystalline	δ (CH), CH wagging (bending)
1382	α	$\delta_s (CH_3)$
1386	α′ and α	$\delta_s (CH_3)$
1387	Amorphous	$\delta_s (CH_3)$
1444	α	$\delta_{as} (CH_3)$
1454	Amorphous	$\delta_{as} (CH_3)$
1457	α′ and α	$\delta_{as} (CH_3)$
1749	α	$\nu(C=O)$
1757	Amorphous	$\nu(C=O)$
1759	α	$\nu(C=O)$
1761	α′	$\nu(C=O)$
2945	Amorphous	$\nu_s(CH_3)$
2946	α′ and α	$\nu_s(CH_3)$
2964	α	$\nu_s(CH_3)$
2995	Amorphous	$\nu_s(CH_3)$
2997	α′ and α	$\nu_{as}(CH_3)$
3006	α	$\nu_{as}(CH_3)$

In Figure 4.7-A is possible to highlight, right away, the absence of the absorption band at 921 cm^{-1}, which is assigned to the coupling of the C-C backbone stretching with the CH_3 rocking mode and sensitive to the 10_3 helix chain conformation of PLLA α-crystals [92]. Moreover, the lack of the characteristic band of PLLA β crystal at 908 cm^{-1} indicates that there is no β crystal in the PLLA sample [92]. Regarding the absorption band between 840 and 880 cm^{-1}, two main peaks are reported in the literature [91], at 860 and 871 cm^{-1}, ascribed to the skeletal stretching and CH_3 rocking of amorphous and crystalline (α) phases. In this range,

the PLLA spectrum of Figure 4.7-A only shows an absorption peak at 867 cm^{-1}. Bearing in mind the absence of crystalline (α) peak at 871 cm^{-1}, it is possible to conclude that PLLA membranes are essentially amorphous. In fact, the jet deformation with rapid solidification during the electrospinning results in a metastable phase [91], resulting in PLLA electrospun membranes nearly amorphous and high nucleated. As soon as the membranes are heated, there is a rapid growth of the crystals taking into account that α form of PLLA is believed to grow upon melt or cold crystallization [92].

Other peaks can be observed in the PLLA spectrum, namely representative stretching frequencies for C=O, -CH_3 asymmetric, -CH_3 symmetric and C-O-C, at 1748, 2996, 2946 and 1082 cm^{-1}, respectively. The adsorption peaks at 1360 and 1452 cm^{-1} are attributed to the vibration of C-H bend and –CH_3 asymmetric, respectively.

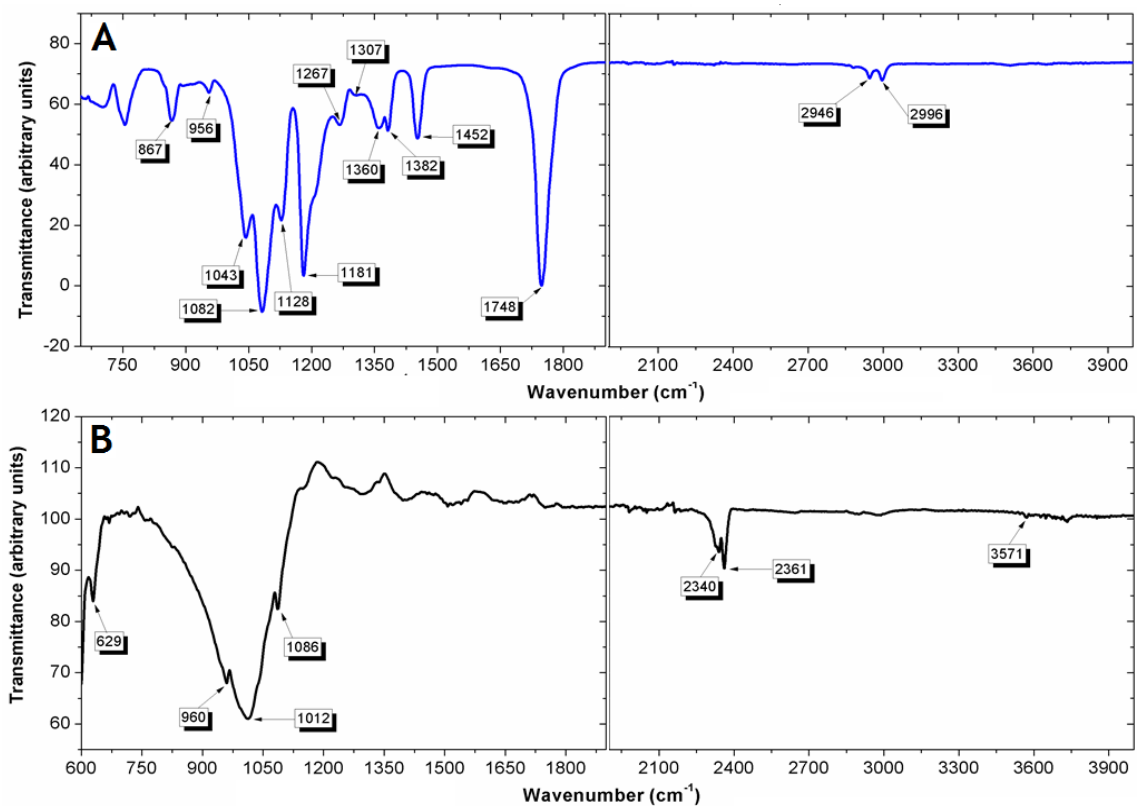

Figure 4.7. FTIR transmission spectra of [A] PLLA and [B] Bonelike® with identified absorption bands.

Regarding the Bonelike® infrared spectrum (Figure 4.6 and in more detail in Figure 4.7-B), some characteristic peaks were found. Similarly to literature, the obtained FTIR data have revealed peaks of functional groups OH^- and PO_4^{3-} [73]. A sharp and dominant band at 960 cm^{-1} was observed, which indicates the presence of PO_4^{3-}groups in the Bonelike® composition [93]. Besides, another characteristic phosphate (PO_4^{3-}) peak [72] was detected at 1086 cm^{-1}, due to the PO_4^{3-} symmetric stretching mode [93]. The PO_4^{3-} antisymetric stretching mode is reported in the literature at 1040 cm^{-1} [93], but in such frequency there is no absorption band. Nevertheless, a peak at 1012 cm^{-1} is noticed.

Hydroxyl groups (OH^-) were detected at 3571 and 630 cm^{-1}, which is in agreement with the bibliography [72], even though the 3571 cm^{-1} peak is almost invisible in the spectrum (Figure 4.7-B). OH^- can hardly be detected in the Bonelike® spectrum taking into account that the Tricalcium Phosphates (α and β-TCP, $Ca_3(PO_4)_2$), present in the Bonelike® constitution,

are not composed by OH^- . In fact, during Bonelike® fabrication, HA reacts with the glass over the sintering process and therefore part of HA is decomposed into β-TCP and this last one inverted to α -TCP [73].

Figure 4.7-B also shows two peaks at 2340 and 2361 cm^{-1} that are not described as characteristic bands of the Bonelike®. Such range bands are interpreted as a consequence of residual CO_2 present in the atmosphere.

The spectrum of electrospun PLLA/Bonelike® fibres is also presented in Figure 4.6. This spectrum is characterized by absorption bands arising from Bonelike® and PLLA. It should be noticed that there are no detectable changes in terms of peaks' morphology and intensity, proving that there is no chemical interaction between PLLA and Bonelike® components [94].

4.1.4. X-Ray Diffraction

Figure 4.8 shows the XRD pattern of Bonelike® which depicts the presence of three phases (HA, β-TCP and α-TCP), supporting the Bonelike® composition. Additionally, this XRD profile is in agreement with the ones found in the literature [73, 93].

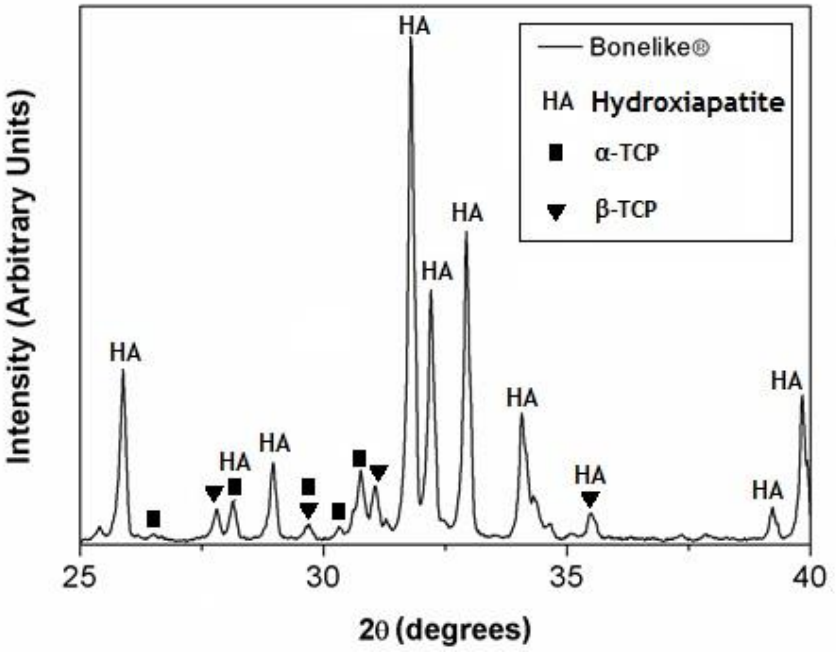

Figure 4.8. XRD pattern of Bonelike®.

Figure 4.9 presents the diffraction profiles of the Bonelike® and the PLLA/Bonelike® fibre membrane. As can be seen, the diffraction pattern of the PLLA/Bonelike® membrane follows a very similar trend to that of Bonelike® powder, where there is almost a perfect match for all the peaks. This result proves that there was an effective incorporation of the ceramic filler in the polymeric membrane, and the composite membrane was mainly made of ceramic particles.

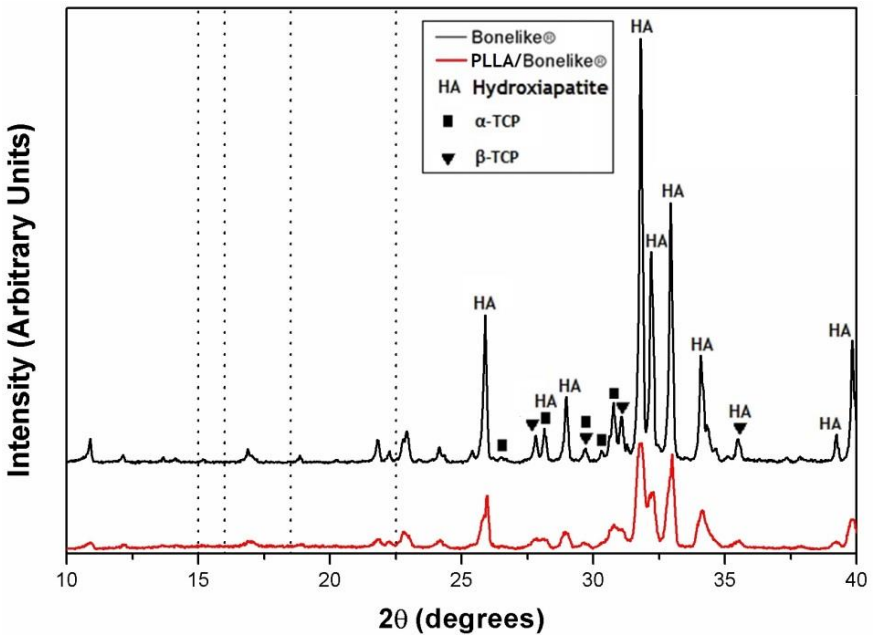

Figure 4.9. XRD pattern of Bonelike® and PLLA/Bonelike® composite fibre membranes.

The internal molecular structure of the polymers may also be investigated using XRD data [95]. According to previous studies, the XRD profile of neat PLLA shows characteristic peaks at 15, 16, 18.5 and 22.5° [96] (marked in the Figure 4.9 with the dotted lines) as a result of its crystalline structure. However, PLLA/Bonelike® XRD pattern does not present different peaks aside the Bonelike® pattern, exhibiting therefore the absence of those PLLA characteristic peaks. Thereby, this PLLA/Bonelike® XRD diagram supports the idea explained along the FTIR discussion, where it was referred that these fibre membranes are characterized by an amorphous structure as soon as they are obtained with the electrospinning process. Moreover, this result is corroborated by another study where XRD pattern of electrospun PLLA fibres do not present any crystalline peak diffraction [95].

4.1.5. Thermal Properties

4.1.5.1. Differential Scanning Calorimetry

Figure 4.10 depicts DSC normalized thermograms (heat flow divided by the sample mass and the heating rate) of the neat PLLA fibres and PLLA/Bonelike® fibres. Focusing on the PLLA thermogram, three main steps may be observed including the step of glass transition temperature around 59 ºC followed by an exothermic peak of cold crystallization around 81 ºC and the melting temperature peak at 149 ºC. Cold crystallization is a transition that occurs at low temperatures due to enhanced primary nucleation as a result of the energy provided during the heating scan of DSC. When polymer chains have enough energy to become mobile, they settle back in a more stable conformation via an exothermic reaction [97, 98]. This cold crystallization event in the PLLA fibres was already reported in the literature [99]. Regarding the PLLA/Bonelike® DSC profile, the curve appears shifted towards lower temperatures when compared to the PLLA one. This can be ascribed by the defects introduced in the fibre membranes by the addition of the Bonelike® particles and also due to the amount of

interfaces between the polymer chains and the ceramic particles, which gives origin to high energy regions and consequently the thermal events occur at lower temperatures. Therefore, the glass transition peak is observed at 51 ºC and the exothermic peak of the cold crystallization at 73 ºC. The melting takes place in the region between 135 and 165 ºC with a minimum at 151 ºC. However, the melting curve also presents a shoulder around 147 ºC. This double melting peak is somewhat expected taking into account the existence of PLLA crystals with different imperfections or sizes and also due to the polymer crystallization in the ceramic boundary region. So, the lower temperature melting peak is the result of imperfect crystals formed in the course of heat-treatment while the higher temperature one is the melting peak of more well organized polymer crystallites [100, 101].

Melting enthalpies of the electrospun membranes were also assessed, calculating the area under the curve of such thermal event (the baseline for this integration is shown in Figure 4.10-B and Figure 4.10-C). The obtained ΔH_m values of PLLA and PLLA/Bonelike® membranes were quite similar, being 28.0 and 27.5 $J.g^{-1}$, respectively. These results show the amorphous state of the membranes as soon they are electrospun, taking into account that the enthalpy of melting for a 100% crystalline PLA sample is 93 $J.g^{-1}$ [102].

The thermal properties of electrospun PLLA and PLLA/Bonelike® fibre membranes are tabulated in Table 4.3.

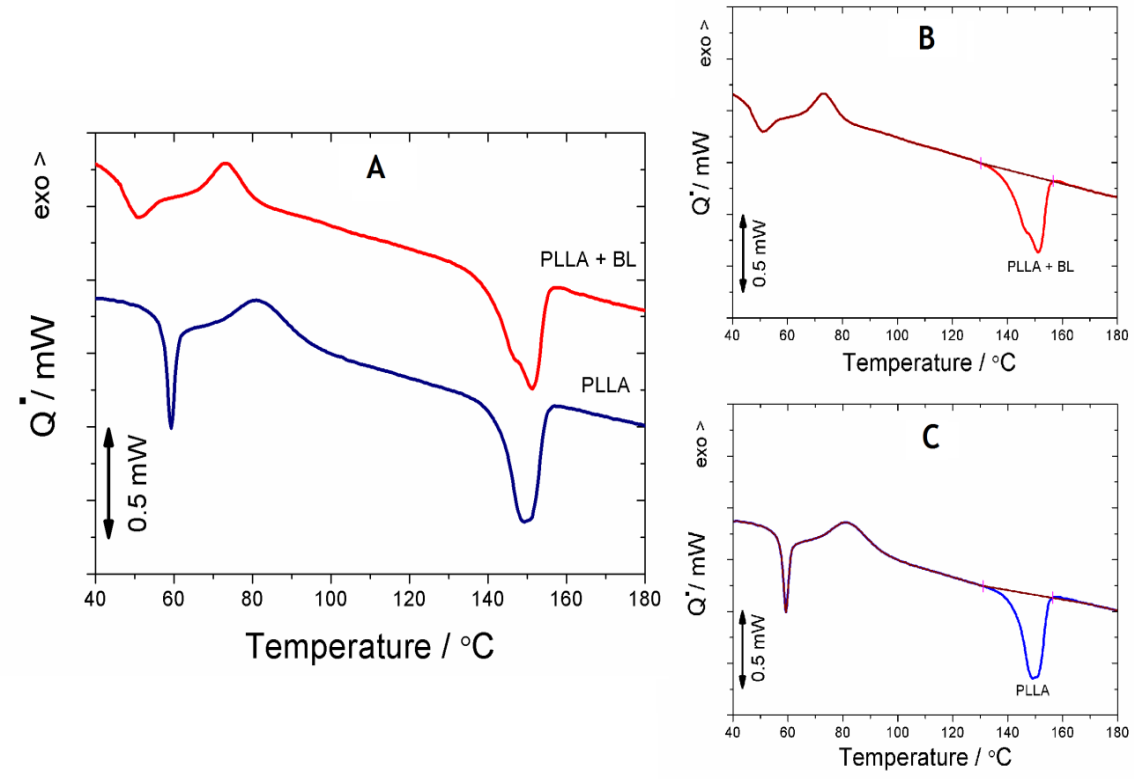

Figure 4.10. [A] DSC normalized thermograms of electrospun PLLA (blue curve) and PLLA/Bonelike® (red curve) membranes. Both thermograms were recorded after heating the samples from 30 to 200 ºC at a heating rate of 10 ºC.min^{-1}. [B] PLLA/Bonelike® thermogram represented in detail with the used baseline (brown) for integration in ΔH_m calculation. [C] PLLA thermogram represented in detail with the used baseline (brown) for integration in ΔH_m calculation.

Table 4.3 — Thermal parameters of the fibres of neat PLLA and PLLA/Bonelike® composite.

MATERIAL	T_g (°C)	T_{cc} (°C)	T_m (°C)	ΔH_m (J/g)
PLLA	59	81	149	28,0
PLLA/Bonelike®	51	73	151	27,5

4.1.5.2. Thermogravimetric Analysis

TGA has been widely used to study the thermal stability and decomposition of PLA and PLA based materials, as well as to determine the amount of inorganic filler in such polymeric materials [103]. Figure 4.11 shows TGA data obtained for the PLLA fibres at various heating rates, and their respective differential degradation curves (DTG). Corresponding data for PLLA/Bonelike® fibres are represented in Figure 4.12. In a first analysis, it is worth noting that TGA and DTGA curves shifted towards higher temperatures as the heating rate was increased from 10 to 40 °C.min^{-1}.

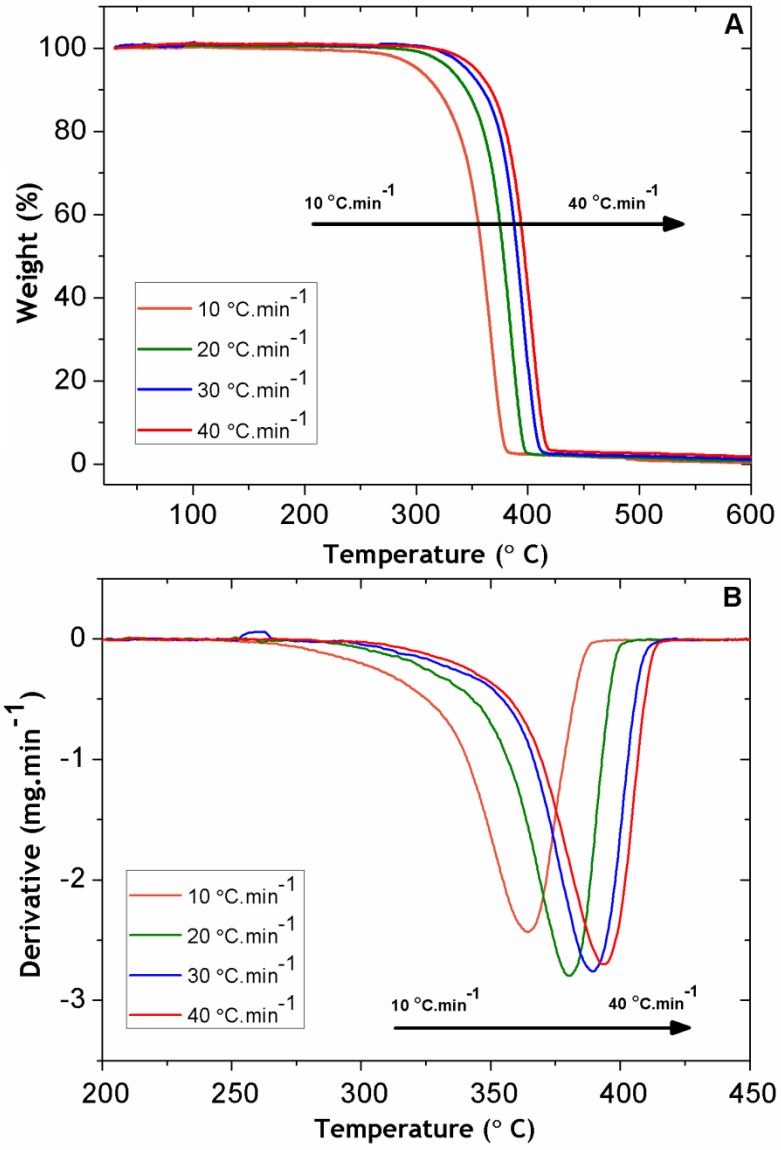

Figure 4.11. [A] TGA and [B] DTG results for PLLA electrospun mats at different heating rates.

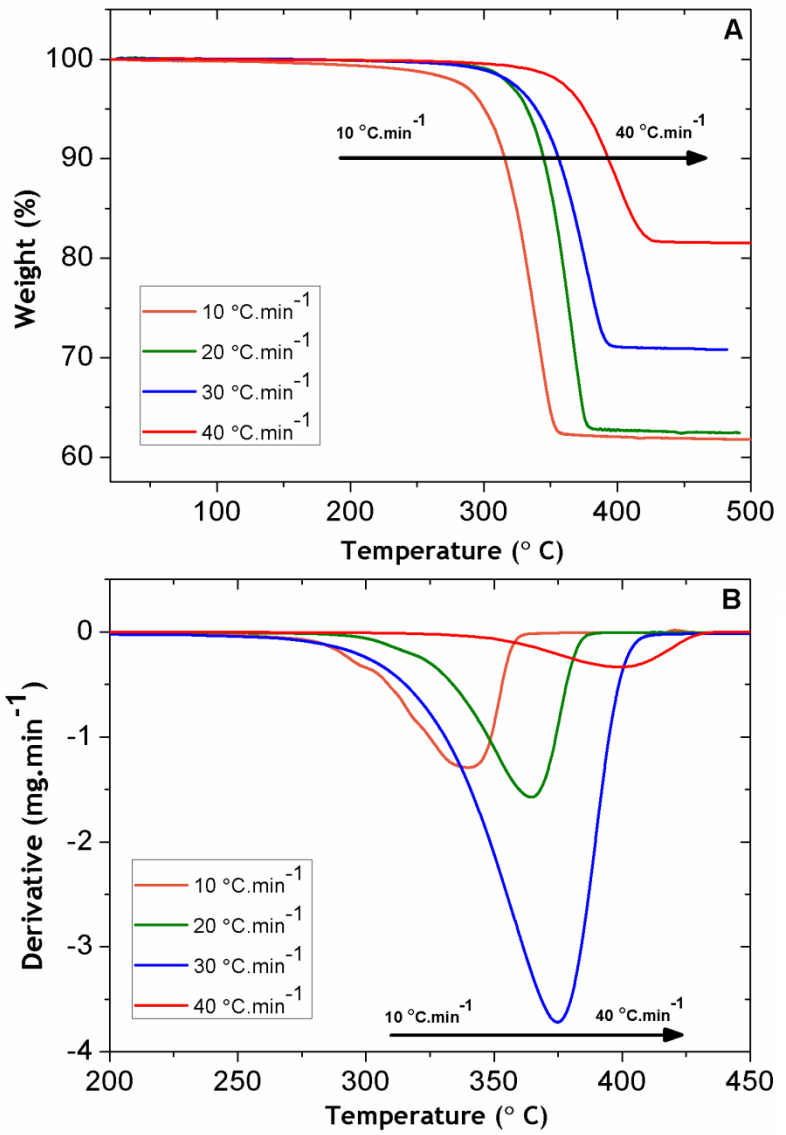

Figure 4.12. [A] TGA and [B] DTG results for PLLA/Bonelike® electrospun composite membranes. In [A], when temperature exceeded 450 °C, approximately 82, 71, 63 and 62% of the original weight remained for 40, 30, 20 and 10 °C.min^{-1} heating rates, respectively.

As it is shown, the weight of the PLLA fibres decreased dramatically when temperature rose from approximately 300 °C to 450 °C, which is due to the PLLA decomposition. In the case of PLLA/Bonelike® membranes, PLLA was also decomposed, but Bonelike® is not degradable in such range of temperatures. Hence, for the neat PLLA fibres, when temperature exceeded 450 °C, only a trace amount of undecomposed components was observed, while approximately 62-82% relative to the original weight (100%) remained for PLLA/Bonelike® fibres, which represents the ceramic component that was not degraded in the range of temperatures investigated. However, if we take into account that PLLA/Bonelike® fibres were produced with 80% of ceramic component, the maximum value of this range, 82%, is ascribed by 80% of ceramic and 2% due to the weight of the trace amount of the degraded PLLA. Thus, it is possible to conclude that there is indeed 62-80% of the ceramic filler incorporated in the PLLA membranes. Therefore, when the weight showed in the TGA data is lower than 80%, two main reasons can justify such result. Some Bonelike® weight loss could happen during the electrospinning process. Moreover, it was reported in the literature that

the residual value obtained during the TGA is dependent on ceramic particle size [104]. In fact, higher residual values were found for composites with the smallest size, indicating, therefore, a larger interaction of the smaller ceramic particles with the polymer due to their larger effective interaction area [104].

Figure 4.13 shows TGA and DTG data obtained for the PLLA and PLLA/Bonelike® fibres, at a single heating rate (30 ºC.min^{-1}). We can observe in detail the almost complete degradation of neat PLLA membranes (with just a trace amount remaining) while around 71% of the weight remains in the PLLA/Bonelike® membrane due to the presence of non-degraded ceramic component. Besides, DTG results show the point at which weight loss is most apparent. Hence, we observe that PLLA/Bonelike® membranes experienced a maximum degradation at a lower temperature.

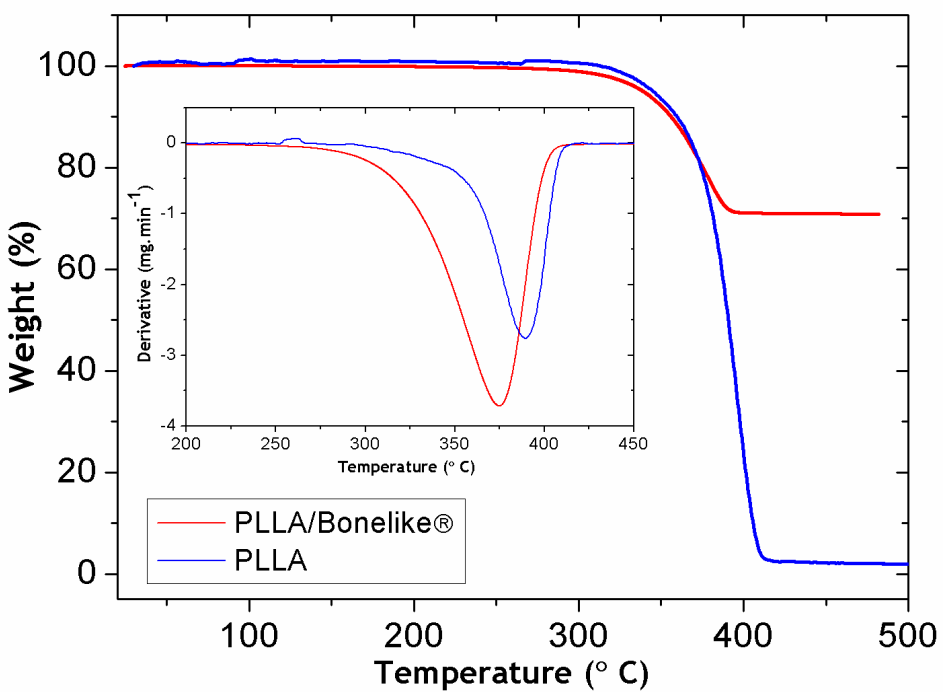

Figure 4.13. TGA and DTG (inset) results for PLLA and PLLA/Bonelike® electrospun membranes at a heating rate of 30 ºC.min^{-1}.

Still regarding all TGA curves (Figure 4.11 and Figure 4.12), it is noted that no dehydration is found around 100 ºC, which supports the hydrophobic nature of the polymer matrix and ceramic filler exhibited with the water contact angle results [104].

Two main temperatures were determined from the TGA curves: the initial temperature, $T_{initial}$ (temperature at which the experimental curve deviates from the tangent line that the mass evolution follows before degradation [76]) and the onset temperature, T_{onset} (temperature that is calculated by extending the pre-degradation portion of the curve to the point of interception with a line drawn as a tangent to the steepest portion of the mass curve occurring during degradation [76]). From the DTG curves, T_p (temperature measured on the inflection point of the thermograms) was also pointed out. $T_{initial}$, T_{onset} and T_p results are listed in Table 4.4.

Table 4.4 — Thermogravimetric characteristic temperatures ($T_{initial}$, T_{onset} and T_p) for PLLA and PLLA/Bonelike® membranes.

Heating rate (°C.min^{-1})	PLLA			PLLA/Bonelike®		
	$T_{initial}$ (°C)	T_{onset} (°C)	T_p (°C)	$T_{initial}$ (°C)	T_{onset} (°C)	T_p (°C)
10	207	336	364	170	304	340
20	242	354	380	218	333	364
30	255	370	389	226	341	378
40	265	377	393	256	363	396

Comparing the onset temperatures measured for each membrane, it is shown that they experienced a decrease after adding the inorganic filler. This result may be ascribed as an improvement of the thermal stability of the fibres caused by the interfacial interactions between the organic and inorganic phases [87].

A further analysis on the degradation kinetics was performed through Kissinger's method. Herein, $\ln\left(\frac{\beta}{T_p^2}\right)$ was plotted against $1000/T_p$ (Figure 4.14) at different heating rates with the peak temperature (inflection point of the thermogram), T_p, obtained from the DTG curves (Figure 4.11-B and Figure 4.12-B). The activation energies of the samples were then calculated from the linear fitting slopes, being 153 and 76 kJ.mol^{-1} (correlation coefficient>0.99) for neat PLLA and PLLA/Bonelike® electrospun membranes, respectively. The thermal degradation activation energy of the composite sample revealed to be lower than that of neat PLLA, which may be attributed to the incorporation of Bonelike® that induces distortions on polymer chain rearrangement during crystallization. Such results are in accordance to the ones observed previously by DSC in Figure 4.10. It should also be noted that the Kissinger's method led to values of activation energies close to the ones reported in other studies for PLA and PLA with similar composite ceramic filler [76, 105-107].

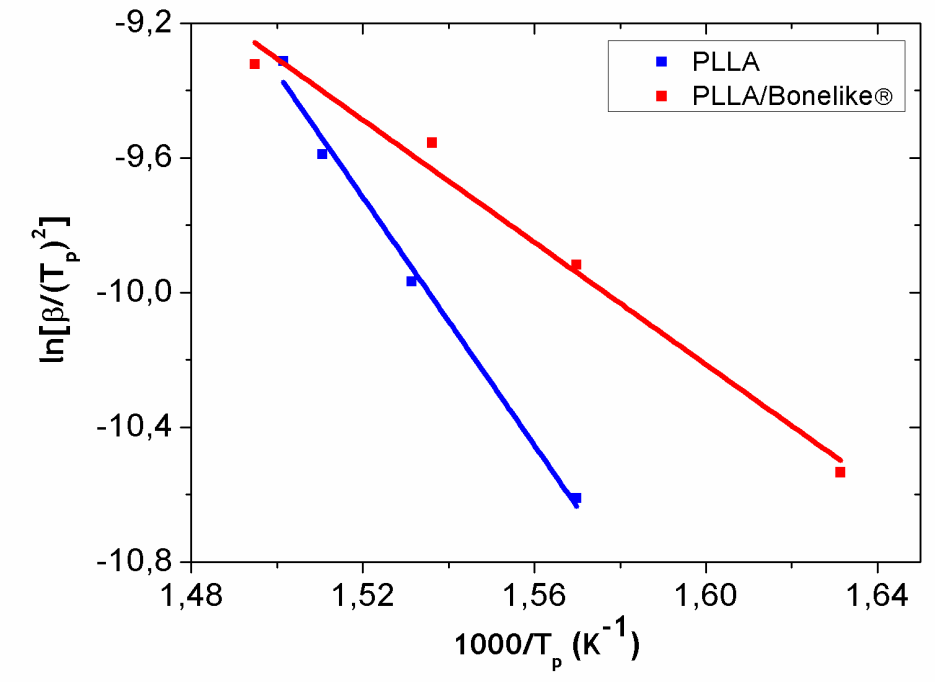

Figure 4.14. Linear fittings obtained with Kissinger's method for PLLA and PLLA/Bonelike® membranes.

4.2. *In Vitro* Cell Studies

4.2.1. MTT Assay

MTT is a precise method used to assess cell viability through their metabolic activity and short-term proliferation on biomaterials [108]. For that purpose, MTT assay was performed on PLLA and PLLA/Bonelike® fibre membranes after 1, 3 and 7 days of incubation with MG-63 cells. Cell proliferation profile of MG-63 cells cultured on PLLA and PLLA/Bonelike® membranes and cell distribution across the membranes is depicted in Figure 4.15 and in Table 4.5, respectively. Cell metabolic activity increased over the time up to 7 days, indicating cell proliferation on the tested membranes. After 1 and 3 days, no significant differences ($p>0.05$) were found between PLLA and PLLA/Bonelike® membranes, with respect to cell proliferation. However, after 3 days, a tendency is noticeable on the PLLA/Bonelike® result, where this composite membrane seems to be preferred by the cells than the PLLA membranes. After 7 days, that tendency was confirmed by the statistical differences ($p<0.05$) between the PLLA/Bonelike® and PLLA membranes. The ceramic-polymer composite fibre membrane herein proved to have improved biological properties in terms of humam osteoblastic cell response, in comparison with the PLLA fibres. Those results were confirmed by microscope observation of the insoluble formazan crystals prior to dissolution, as depicted in Table 4.5. By these images it was possible to observe that the membranes did not degrade during the seven days of culture, since they present the same aspect since day 1. Moreover, MG-63 cells (purple dots) were homogeneously dispersed throughout the membranes and it is easily observed that cell density increased with the time in culture. It is also possible to note that after 7 days, cells are almost completely spread over the entire membrane.

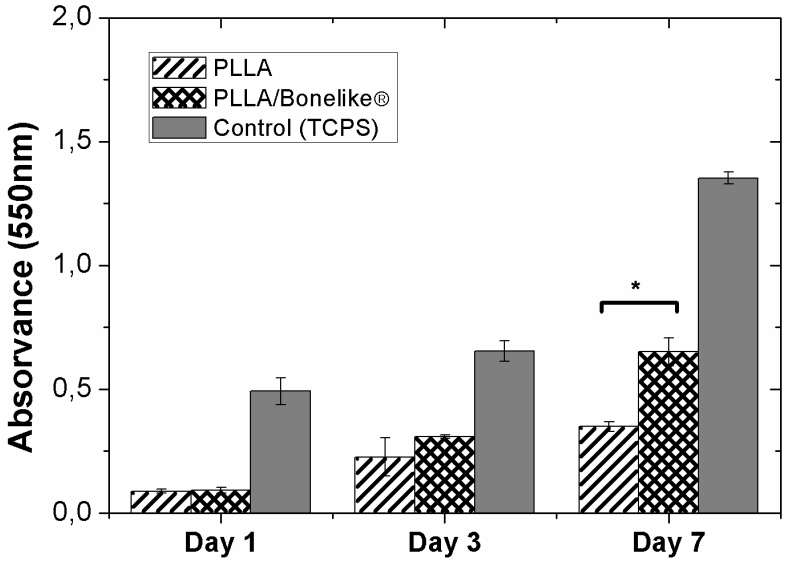

Figure 4.15. Cell proliferation of MG-63 cells cultured on PLLA (n=3) and PLLA/Bonelike® membranes (n=3) for 1, 3 and 7 days, estimated by MTT assay. Controls were performed on TCPS. Data plotted as mean ± standard. Statistical analysis was only performed between PLLA and PLLA/Bonelike® results; *$p<0.05$.

Table 4.5 — Microscopic photographs of PLLA and PLLA/Bonelike® membranes taken before the addition of the DMSO during the MTT assay. Purple dots indicate the presence of cells. The scale bar corresponds to 0.5 cm.

SAMPLE	DAY 1	DAY 3	DAY 7
PLLA+ αMEM (control)	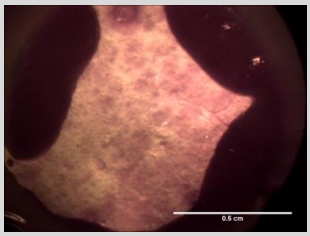	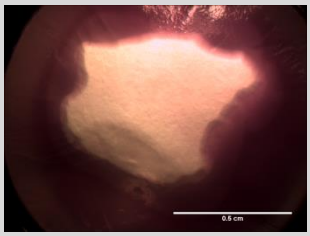	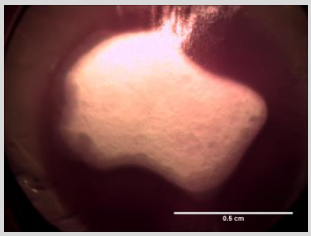
PLLA+ MG63	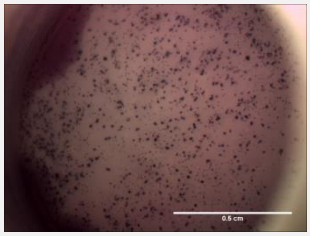	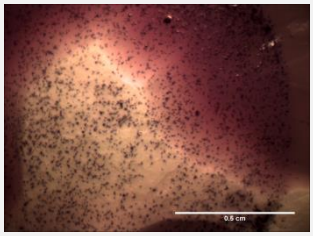	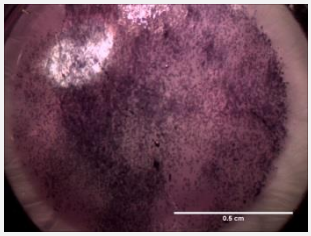
PLLA/ Bonelike® + αMEM (control)	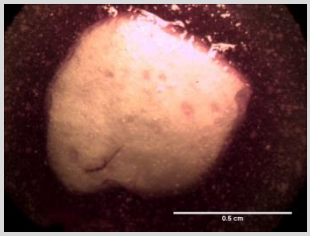	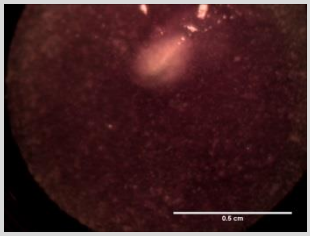	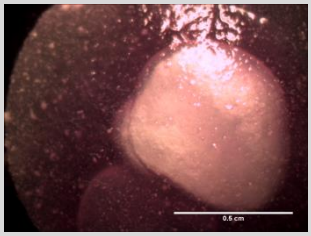
PLLA/ Bonelike® + MG63	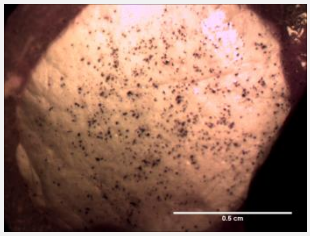	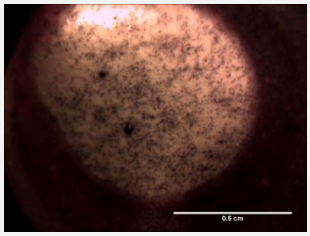	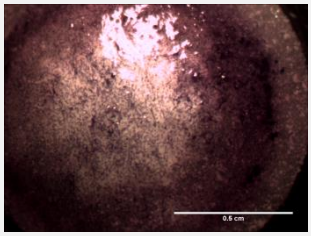

4.2.2. Resazurin Assay

Parallel to MTT, a resazurin assay was performed in which the oxidized blue, non-fluorescent alamar blue is reduced to pink fluorescent dye in the medium by cell activity [109].

Despite being another methodology to assess cell viability, results obtained herein are not in complete agreement with those of MTT. Once again, cell density increased with time in culture, as expected (Figure 4.16). However, there are no significant differences between the two types of membranes for any time points. There was indeed a slightly higher fluorescence in the PLLA/Bonelike® membrane after 3 days in culture. Nevertheless, after 7 days, PLLA/Bonelike® exhibited a similar cell density to that of PLLA, which goes against what was observed in the MTT data, where significant differences were obtained at this time point. These resazurin results may be ascribed by the higher entropy that cell cultures are subjected during the process. In MTT, different cell plates are needed for each time point (cells die during the test) while in the resazurin assay the same culture plate is used during the whole experiment. So, as it involves too many changes of medium during the entire

experiment, some cells could detach from the membranes influencing, therefore, the results. Moreover, in spite of being considered a nontoxic assay, it was reported in literature that some problems may arise during resazurin assay when exposure times are extended to longer-term cultures on the order of days [110].

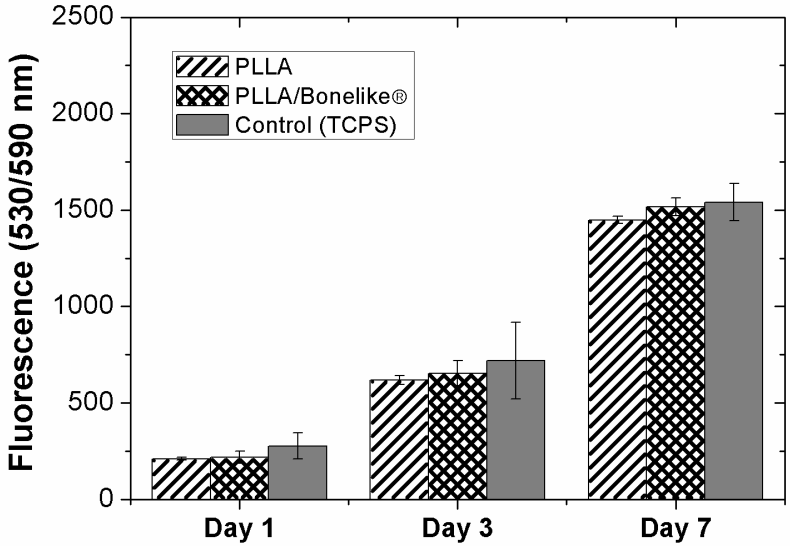

Figure 4.16. Cell proliferation of MG-63 cells cultured on PLLA (n=3) and PLLA/Bonelike® membranes (n=3) for 1, 3 and 7 days, estimated by Resazurin assay. Controls were performed on TCPS. Data plotted as mean ± standard. Statistical analysis was only performed between PLLA and PLLA/Bonelike® results (no significant differences were found).

4.2.3. SEM

Biological performance of PLLA and PLLA/Bonelike® membranes was evaluated through MG-63 osteoblast-like cell culturing. For this purpose, scanning electron micrographs (Figure 4.17) were used to observe the cellular morphology on these materials. As it can be seen, both types of membranes allowed cell attachment and spreading, and there is an increase in cell number with increasing days in culture, as expected. Besides, a typical flat configuration of the cells is noticeable [81]. After 3, and especially after 7 days in culture, MG-63 cells exhibited that flat morphology with extended cytoplasm in different directions, appearing to interact and associate with surrounding fibres. In fact, at day 7, cells with more lamellopodia connecting to neighboring cells were observed, starting to form a continuous cell layer. Moreover, an increase in cells presenting cytoplasmatic extensions was observed at day 7 on PLLA/Bonelike® membranes, when compared to the PLLA one, corroborating the proliferation studies. Bonelike® seems, therefore, to have an important role during cell adhesion and proliferation. It is worth noting in the Figure 4.17-F, the interaction among the fibres, cells and Bonelike® granules.

4.2.4. ALP

In this work, ALP activity normalized by total protein content was assessed on PLLA and PLLA/Bonelike® fibre membranes after 3 and 7 days of incubation with MG-63 cells. Figure 4.18 shows that ALP increased with culture time in both materials and control. Moreover, a

statistically significant difference ($p<0.05$) was found after 7 days, where a higher ALP activity was observed on PLLA/Bonelike® membranes when compared to PLLA ones. This result confirms the crucial role of Bonelike® component in the stimulation of bone cell response, namely in what concerns cell differentiation.

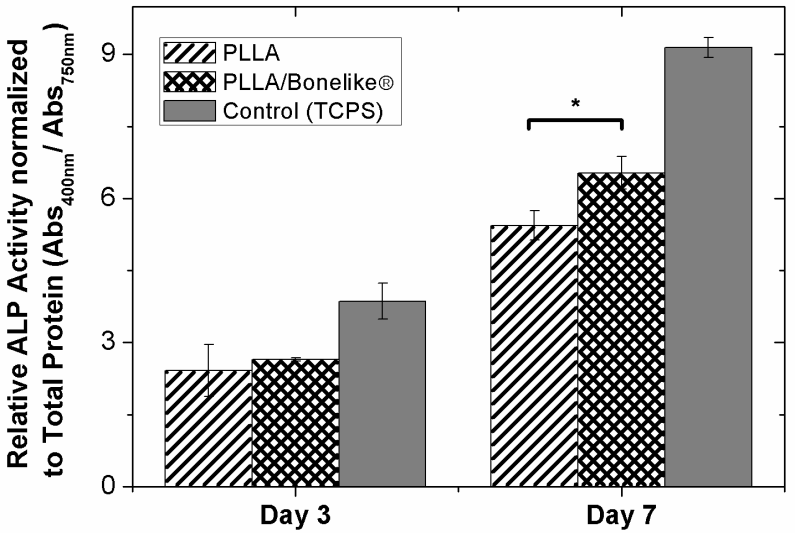

Figure 4.18. ALP activity of MG-63 cells cultured on PLLA (n=3) and PLLA/Bonelike® membranes (n=3) for 3 and 7 days. Controls were performed on TCPS. Data plotted as mean ± standard. Statistical analysis was only performed between PLLA and PLLA/Bonelike® results; *p<0.05.

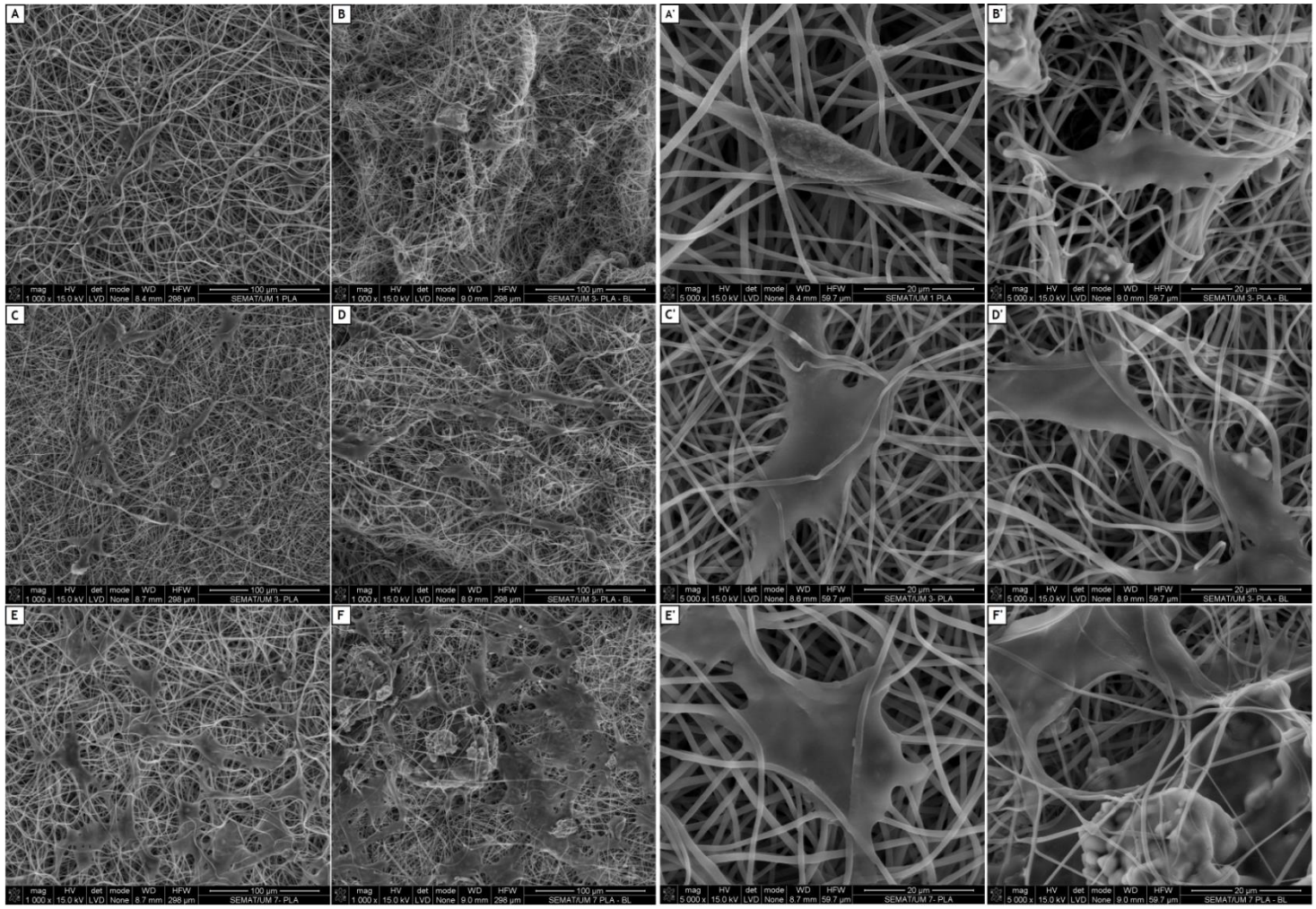

Figure 4.17. SEM images of MG-63 cells cultured on PLLA ([A], [C] and [E] represent samples at day 1, 3 and 7, respectively] and on PLLA/Bonelike® ([B], [D] and [F] represent samples at day 1, 3 and 7, respectively]. [A'], [B'], [C'], [D'], [E'] and [F'] (scale bar corresponds to 20 μm) are higher magnifications images of [A], [B], [C], [D], [E] and [F] (scale bar corresponds to 100 μm).

Chapter 5

Conclusions

This work aimed at developing a bone regenerative matrix with improved biological, electrical, mechanical and electromechanical properties based on PLLA and Bonelike®.

For this purpose, polymeric (PLLA) and composite (PLLA/Bonelike®) fibre membranes were produced using the electrospinning technique, which is known as a simple and versatile technology capable of generating fibres in the submicron range. In fact, it was obtained an average fibre diameter of 0.51±0.15 μm and 0.44±0.17 μm for PLLA and PLLA/Bonelike® membranes, respectively.

An exhaustive study of the membranes morphological, thermal and physico-chemical properties was performed using several techniques. Both membranes exhibited high porosity (79.3±2.9% and 88.9±4.8% for PLLA and PLLA/Bonelike®, respectively) and reported similar hydrophobic behavior due to the highly identical water contact angles.

FTIR spectra showed that PLLA/Bonelike® profile exhibited adsorption bands arising from Bonelike® and PLLA without any detectable changes in morphology and intensity, leading to the conclusion that there is no chemical interaction between the filler and the polymeric matrix.

X-Ray Diffraction results proved the effective incorporation of the ceramic filler in the polymeric membranes since the pattern of Bonelike® depicted the presence of its characteristic three different phases (HA, β-TCP and α-TCP). Additionally, it was demonstrated that the polymeric fibre membranes are characterized by an amorphous structure.

Thermal behavior was investigated through DSC, whereby PLLA membrane had well defined glass transition, cold crystallization and melting temperatures identified at 59, 81 and 149 ºC, respectively. In the composite membranes, due to defects introduced in the PLLA mats by Bonelike® particles, and also due to the amount of interfaces between the polymer chains and ceramic particles, there was a shift towards lower temperatures of the polymer glass transition and cold crystallization, and the melting temperature occurred at ~150 ºC.

Using thermogravimetry, a complete PLLA degradation was observed when temperature rose from approximately 300 ºC to 450 ºC. Regarding PLLA/Bonelike® fibres, 62-80% of its weight remained after the TGA process (smaller particles leave larger solid residuals after the polymer degradation), representing the real amount of the ceramic component present in the

PLLA mats. Kissinger's model was used to determine the activation energy of the degradation process. Herein, activation energy of the composite sample revealed to be lower than that of neat PLLA, attributed to distortions on polymer chain rearrangement during crystallization, caused by Bonelike®.

MG-63 cell viability was analyzed by performing MTT and Resazurin assays. MTT and respective SEM images showed that the ceramic-polymer composite fibre membrane demonstrated improved biological properties in terms of human osteoblastic cell response, since after 7 days, significant proliferation was detected, when compared to PLLA mats. Resazurin results did not go in complete agreement with MTT ones, which was attributed to the higher entropy that cell cultures are subjected during the process. Nevertheless, it would be important to repeat this test. ALP analysis also proved the crucial role of Bonelike® component in the stimulation of bone cell response taking into account that, after 7 days in culture, a significantly higher ALP activity was observed on PLLA/Bonelike® membranes when compared to PLLA ones.

In summary, PLLA/Bonelike® composite fibre membranes developed in this study proved to recruit favorable adhesion and growth of osteoblastic cells, as well as to stimulate them to exhibit functional activity of bone-associated cells. Despite being very difficult to extrapolate from *in vitro* to *in vivo* conditions, the *in vitro* studies led to promising results for a possible applicability of these fibre membranes associated to bone grafts (PLLA/Bonelike®) for bone regeneration. As a final remark, in a future work, it will be crucial to perform a semi quantitative inflammatory evaluation of these fibres implanted into living tissues.

References

[1] J. Venugopal, M. P. Prabhakaran, Y. Zhang *et al.*, "Biomimetic hydroxyapatite-containing composite nanofibrous substrates for bone tissue engineering," *Philos Trans A Math Phys Eng Sci,* vol. 368, no. 1917, pp. 2065-81, Apr 28, 2010.

[2] M. Navarro, A. Michiardi, O. Castano *et al.*, "Biomaterials in orthopaedics," *J R Soc Interface,* vol. 5, no. 27, pp. 1137-58, Oct 6, 2008.

[3] M. P. Prabhakaran, J. Venugopal, and S. Ramakrishna, "Electrospun nanostructured scaffolds for bone tissue engineering," *Acta Biomater,* vol. 5, no. 8, pp. 2884-93, Oct, 2009.

[4] S. Lyu, C. Huang, H. Yang *et al.*, "Electrospun fibers as a scaffolding platform for bone tissue repair," *J Orthop Res,* vol. 31, no. 9, pp. 1382-9, Sep, 2013.

[5] X. Wang, B. Ding, and B. Li, "Biomimetic electrospun nanofibrous structures for tissue engineering," *Mater Today (Kidlington),* vol. 16, no. 6, pp. 229-241, Jun 1, 2013.

[6] H. Liu, X. Ding, G. Zhou *et al.*, "Electrospinning of Nanofibers for Tissue Engineering Applications," *Journal of Nanomaterials,* vol. 2013, pp. 1-11, 2013.

[7] M. Wang, "Developing bioactive composite materials for tissue replacement," *Biomaterials,* vol. 24, no. 13, pp. 2133-2151, 6//, 2003.

[8] C. Ribeiro, D. M. Correia, S. Ribeiro *et al.*, "Piezoelectric poly(vinylidene fluoride) microstructure and poling state in active tissue engineering," *Engineering in Life Sciences*, pp. n/a-n/a, 2015.

[9] V. C. Costa, H. S. Costa, W. L. Vasconcelos *et al.*, "Preparation of hybrid biomaterials for bone tissue engineering," *Materials Research,* vol. 10, pp. 21-26, 2007.

[10] J. T. Seil, and T. J. Webster, "Electrically active nanomaterials as improved neural tissue regeneration scaffolds," *Wiley Interdiscip Rev Nanomed Nanobiotechnol,* vol. 2, no. 6, pp. 635-47, Nov-Dec, 2010.

[11] D. Fu, Z. Hou, Q. H. Qin *et al.*, "Influence of shear stress on behaviors of piezoelectric voltages in bone," *J Appl Biomech,* vol. 28, no. 4, pp. 387-93, Aug, 2012.

[12] J. S. Harrison, and Z. Ounaies, "Piezoelectric Polymers," *Encyclopedia of Polymer Science and Technology*: John Wiley & Sons, Inc., 2002.

[13] E. Fukada, "History and recent progress in piezoelectric polymers," *Ultrasonics, Ferroelectrics, and Frequency Control, IEEE Transactions on,* vol. 47, no. 6, pp. 1277-1290, 2000.

[14] B. Gupta, N. Revagade, and J. Hilborn, "Poly(lactic acid) fiber: An overview," *Progress in Polymer Science,* vol. 32, no. 4, pp. 455-482, 2007.

[15] C. Halperin, S. Mutchnik, A. Agronin *et al.*, "Piezoelectric Effect in Human Bones Studied in Nanometer Scale," *Nano Letters,* vol. 4, no. 7, pp. 1253-1256, 2004.

[16] N. Barroca, P. M. Vilarinho, A. L. Daniel-da-Silva *et al.*, "Protein adsorption on piezoelectric poly(L-lactic) acid thin films by scanning probe microscopy," *Applied Physics Letters,* vol. 98, no. 13, pp. 133705, 2011.

[17] J. C. Knowles, G. W. Hastings, and S. S. J. D. De, "Sintered hydroxyapatite compositions and method for the preparation thereof," Google Patents, 2000.

[18] H. W. Kim, H. H. Lee, and J. C. Knowles, “Electrospinning biomedical nanocomposite fibers of hydroxyapatite/poly(lactic acid) for bone regeneration,” *J Biomed Mater Res A,* vol. 79, no. 3, pp. 643-9, Dec 1, 2006.

[19] L. M. Atayde, P. P. Cortez, A. Afonso *et al.*, “Morphology effect of bioglass-reinforced hydroxyapatite (Bonelike) on osteoregeneration,” *J Biomed Mater Res B Appl Biomater,* May 13, 2014.

[20] J. H. Jang, O. Castano, and H. W. Kim, “Electrospun materials as potential platforms for bone tissue engineering,” *Adv Drug Deliv Rev,* vol. 61, no. 12, pp. 1065-83, Oct 5, 2009.

[21] A. Di Martino, L. Liverani, A. Rainer *et al.*, “Electrospun scaffolds for bone tissue engineering,” *Musculoskelet Surg,* vol. 95, no. 2, pp. 69-80, Aug, 2011.

[22] K. F. S. Ramakrishna, W.E. Teo, T.C. Lim, "An Introduction to Electrospinning and Nanofibres," pp. 15-143: Hackensack NJ : World Scientific, Singapore ,(2005).

[23] Z.-M. Huang, Y. Z. Zhang, M. Kotaki *et al.*, “A review on polymer nanofibers by electrospinning and their applications in nanocomposites,” *Composites Science and Technology,* vol. 63, no. 15, pp. 2223-2253, 2003.

[24] C.-M. Hsu, “Electrospinning of Poly(ε-Caprolactone). Master Thesis,” Materials Science and Engineering, WORCESTER POLYTECHNIC INSTITUTE, 2003.

[25] W. N. Chang, *Nanofibers: Fabrication, Performance, and Applications*: Nova Science, 2009.

[26] N. Bhardwaj, and S. C. Kundu, “Electrospinning: a fascinating fiber fabrication technique,” *Biotechnol Adv,* vol. 28, no. 3, pp. 325-47, May-Jun, 2010.

[27] D. Li, and Y. Xia, “Electrospinning of Nanofibers: Reinventing the Wheel?,” *Advanced Materials,* vol. 16, no. 14, pp. 1151-1170, 2004.

[28] J. M. Deitzel, J. Kleinmeyer, D. Harris *et al.*, “The effect of processing variables on the morphology of electrospun nanofibers and textiles,” *Polymer,* vol. 42, no. 1, pp. 261-272, 1//, 2001.

[29] H. Fong, I. Chun, and D. H. Reneker, “Beaded nanofibers formed during electrospinning,” *Polymer,* vol. 40, no. 16, pp. 4585-4592, 7//, 1999.

[30] N. Okutan, P. Terzi, and F. Altay, “Affecting parameters on electrospinning process and characterization of electrospun gelatin nanofibers,” *Food Hydrocolloids,* vol. 39, no. 0, pp. 19-26, 8//, 2014.

[31] Q. Yang, Z. Li, Y. Hong *et al.*, “Influence of solvents on the formation of ultrathin uniform poly(vinyl pyrrolidone) nanofibers with electrospinning,” *Journal of Polymer Science Part B: Polymer Physics,* vol. 42, no. 20, pp. 3721-3726, 2004.

[32] X. Zong, K. Kim, D. Fang *et al.*, “Structure and process relationship of electrospun bioabsorbable nanofiber membranes,” *Polymer,* vol. 43, no. 16, pp. 4403-4412, 7//, 2002.

[33] S. Sukigara, M. Gandhi, J. Ayutsede *et al.*, “Regeneration of Bombyx mori silk by electrospinning—part 1: processing parameters and geometric properties,” *Polymer,* vol. 44, no. 19, pp. 5721-5727, 9//, 2003.

[34] C. Zhang, X. Yuan, L. Wu *et al.*, “Study on morphology of electrospun poly(vinyl alcohol) mats,” *European Polymer Journal,* vol. 41, no. 3, pp. 423-432, 2005.

[35] C. J. Buchko, L. C. Chen, Y. Shen *et al.*, “Processing and microstructural characterization of porous biocompatible protein polymer thin films,” *Polymer,* vol. 40, no. 26, pp. 7397-7407, 12//, 1999.

[36] X. Yuan, Y. Zhang, C. Dong *et al.*, “Morphology of ultrafine polysulfone fibers prepared by electrospinning,” *Polymer International,* vol. 53, no. 11, pp. 1704-1710, 2004.

[37] S. Ribeiro, P. Costa, C. Ribeiro *et al.*, “Electrospun styrene–butadiene–styrene elastomer copolymers for tissue engineering applications: Effect of butadiene/styrene ratio, block structure, hydrogenation and carbon nanotube loading on physical properties and cytotoxicity,” *Composites Part B: Engineering,* vol. 67, no. 0, pp. 30-38, 12//, 2014.

[38] P. K. Baumgarten, “Electrostatic spinning of acrylic microfibers,” *Journal of Colloid and Interface Science,* vol. 36, no. 1, pp. 71-79, 5//, 1971.

[39] Y. T. Kim, V. K. Haftel, S. Kumar *et al.*, "The role of aligned polymer fiber-based constructs in the bridging of long peripheral nerve gaps," *Biomaterials,* vol. 29, no. 21, pp. 3117-27, Jul, 2008.

[40] F. Yang, C. Y. Xu, M. Kotaki *et al.*, "Characterization of neural stem cells on electrospun poly(L-lactic acid) nanofibrous scaffold," *J Biomater Sci Polym Ed,* vol. 15, no. 12, pp. 1483-97, 2004.

[41] S. Ramakrishna, K. Fujihara, W.-E. Teo *et al.*, "Electrospun nanofibers: solving global issues," *Materials Today,* vol. 9, no. 3, pp. 40-50, 2006.

[42] H. Tsuji, H. Daimon, and K. Fujie, "A New Strategy for Recycling and Preparation of Poly(l-lactic acid): Hydrolysis in the Melt," *Biomacromolecules,* vol. 4, no. 3, pp. 835-840, 2003/05/01, 2003.

[43] L. T. Lim, R. Auras, and M. Rubino, "Processing technologies for poly(lactic acid)," *Progress in Polymer Science,* vol. 33, no. 8, pp. 820-852, 2008.

[44] "Corbion.com, (2012). Product data sheet PURASORB® PL 18.," January, 2015; http://www.corbion.com/static/downloads/datasheets/45d/PURASORB%20PL%2018.pdf.

[45] C. Gomez-Sanchez, T. Kowalczyk, G. Ruiz De Eguino *et al.*, "Electrospinning of poly (lactic acid)/polyhedral oligomeric silsesquioxane nanocomposites and their potential in chondrogenic tissue regeneration," *Journal of Biomaterials Science, Polymer Edition,* vol. 25, no. 8, pp. 802-825, 2014.

[46] R. P. Pawar, S. U. Tekale, S. U. Shisodia *et al.*, "Biomedical Applications of Poly(Lactic Acid)," *Recent Patents on Regenerative Medicine,* vol. 4, no. 1, pp. 40-51, //, 2014.

[47] R. K. Kulkarni, E. G. Moore, A. F. Hegyeli *et al.*, "Biodegradable poly(lactic acid) polymers," *Journal of Biomedical Materials Research,* vol. 5, no. 3, pp. 169-181, 1971.

[48] A. J. Lasprilla, G. A. Martinez, B. H. Lunelli *et al.*, "Poly-lactic acid synthesis for application in biomedical devices—A review," *Biotechnology advances,* vol. 30, no. 1, pp. 321-328, 2012.

[49] J. E. Sanders, S. D. Bale, and T. Neumann, "Tissue response to microfibers of different polymers: Polyester, polyethylene, polylactic acid, and polyurethane," *Journal of Biomedical Materials Research,* vol. 62, no. 2, pp. 222-227, 2002.

[50] M. Kellomäki, H. Niiranen, K. Puumanen *et al.*, "Bioabsorbable scaffolds for guided bone regeneration and generation," *Biomaterials,* vol. 21, no. 24, pp. 2495-2505, 12/15/, 2000.

[51] S. R. Bhattarai, N. Bhattarai, H. K. Yi *et al.*, "Novel biodegradable electrospun membrane: scaffold for tissue engineering," *Biomaterials,* vol. 25, no. 13, pp. 2595-2602, 6//, 2004.

[52] J. LUMIAHO, A. HEINO, V. TUNNINEN *et al.*, "New bioabsorbable polylactide ureteral stent in the treatment of ureteral lesions: an experimental study," *Journal of endourology,* vol. 13, no. 2, pp. 107-112, 1999.

[53] H. Steuer, R. Fadale, E. Müller *et al.*, "Biohybride nerve guide for regeneration: degradable polylactide fibers coated with rat Schwann cells," *Neuroscience Letters,* vol. 277, no. 3, pp. 165-168, 12/31/, 1999.

[54] J. Behari, "Piezoelectricity in Bone," *Biophysical Bone Behavior*, pp. 53-102: John Wiley & Sons, Ltd, 2009.

[55] E. Fukada, and I. Yasuda, "On the Piezoelectric Effect of Bone," *Journal of the Physical Society of Japan,* vol. 12, no. 10, pp. 1158-1162, 1957/10/15, 1957.

[56] V. Sencadas, C. Ribeiro, A. Heredia *et al.*, "Local piezoelectric activity of single poly(L-lactic acid) (PLLA) microfibers," *Applied Physics A,* vol. 109, no. 1, pp. 51-55, 2012/10/01, 2012.

[57] J. Santos, L. Jha, and F. Monteiro, "In vitro calcium phosphate formation on SiO2-Na2O-CaO-P2O5 glass reinforced hydroxyapatite composite: a study by XPS analysis," *Journal of Materials Science: Materials in Medicine,* vol. 7, no. 3, pp. 181-185, 1996.

[58] "Biosckin.com, (2015). Bonelike - Technical Description | Biosckin.," January, 2015; http://www.biosckin.com/en/products-services/bonelike-technical-description/.

[59] R. C. Sousa, J. V. Lobato, A. C. Mauricio *et al.*, "A clinical report of bone regeneration in maxillofacial surgery using bonelike synthetic bone graft," *J Biomater Appl,* vol. 22, no. 4, pp. 373-85, Jan, 2008.

[60] "Biosckin.com, (2015). Bonelike - Porous Structure | Biosckin.," January, 2015; http://www.biosckin.com/en/products-services/bonelike-porous-structure/.

[61] M. Gutierres, M. A. Lopes, N. Sooraj Hussain *et al.*, "Bone ingrowth in macroporous Bonelike® for orthopaedic applications," *Acta Biomaterialia,* vol. 4, no. 2, pp. 370-377, 3//, 2008.

[62] M. Gutierres, A. G. Dias, M. A. Lopes *et al.*, "Opening wedge high tibial osteotomy using 3D biomodelling Bonelike® macroporous structures: case report," *Journal of Materials Science: Materials in Medicine,* vol. 18, no. 12, pp. 2377-2382, 2007/12/01, 2007.

[63] G. Pavan Kumar, B. Naga Sowmya, N. Sooraj Hussain *et al.*, "Guided Bone Regeneration using Glass-reinforced Hydroxyapatite and Collagen Membrane in the treatment of Peri-implantitis," *Solid State Phenomena,* vol. 207, pp. 109-119, 2014.

[64] J. Lobato, N. S. Hussain, M. Lopes *et al.*, "Clinical applications of Titanium dental implants coated with glass-reinforced Hydroxyapatite composite (Bonelike?)," *International Journal of Nanomanufacturing,* vol. 2, no. 1, pp. 135-148, 2008.

[65] J. V. Lobato, N. S. Hussain, C. M. Botelho *et al.*, "Assessment of Bonelike® graft with a resorbable matrix using an animal model," *Thin Solid Films,* vol. 515, no. 1, pp. 362-367, 9/25/, 2006.

[66] S. Vohra, K. M. Hennessy, A. A. Sawyer *et al.*, "Comparison of mesenchymal stem cell and osteosarcoma cell adhesion to hydroxyapatite," *J Mater Sci Mater Med,* vol. 19, no. 12, pp. 3567-74, Dec, 2008.

[67] K. Anselme, "Osteoblast adhesion on biomaterials," *Biomaterials,* vol. 21, no. 7, pp. 667-81, Apr, 2000.

[68] N. Price, S. P. Bendall, C. Frondoza *et al.*, "Human osteoblast-like cells (MG63) proliferate on a bioactive glass surface," *J Biomed Mater Res,* vol. 37, no. 3, pp. 394-400, Dec 5, 1997.

[69] Y. Akiyama, Y. Mikami, E. Watanabe *et al.*, "The P75 neurotrophin receptor regulates proliferation of the human MG63 osteoblast cell line," *Differentiation,* vol. 87, no. 3-4, pp. 111-8, Mar-Apr, 2014.

[70] G. Carmeliet, G. Nys, and R. Bouillon, "Microgravity reduces the differentiation of human osteoblastic MG-63 cells," *J Bone Miner Res,* vol. 12, no. 5, pp. 786-94, May, 1997.

[71] C. Pautke, M. Schieker, T. Tischer *et al.*, "Characterization of osteosarcoma cell lines MG-63, Saos-2 and U-2 OS in comparison to human osteoblasts," *Anticancer Res,* vol. 24, no. 6, pp. 3743-8, Nov-Dec, 2004.

[72] P. P. Cortez, L. M. Atayde, M. A. Silva *et al.*, "Characterization and preliminary in vivo evaluation of a novel modified hydroxyapatite produced by extrusion and spheronization techniques," *J Biomed Mater Res B Appl Biomater,* vol. 99, no. 1, pp. 170-9, Oct, 2011.

[73] M. S. Laranjeira, A. G. Dias, J. D. Santos *et al.*, "In vitro biological characterization of macroporous 3D Bonelike® structures prepared through a 3D machining technique," *Materials Science and Engineering: C,* vol. 29, no. 3, pp. 930-935, 4/30/, 2009.

[74] A. C. d. C. Lopes, "Bonelike® Associated to Stem Cells for the Regeneration of the Bone Tissue," FACULDADE DE ENGENHARIA DA UNIVERSIDADE DO PORTO, 2010.

[75] "Image J 2009 Image Processing and Analysis in Java," April, 2015; http://rsbweb.nih.gov/ij/index.html.

[76] V. Sencadas, C. M. Costa, G. Botelho *et al.*, "Thermal Properties of Electrospun Poly(Lactic Acid) Membranes," *Journal of Macromolecular Science, Part B,* vol. 51, no. 3, pp. 411-424, 2012/03/01, 2011.

[77] J. F. Mano, D. Koniarova, and R. L. Reis, "Thermal properties of thermoplastic starch/synthetic polymer blends with potential biomedical applicability," *J Mater Sci Mater Med,* vol. 14, no. 2, pp. 127-35, Feb, 2003.

[78] F. Yao, Q. Wu, Y. Lei *et al.*, "Thermal decomposition kinetics of natural fibers: Activation energy with dynamic thermogravimetric analysis," *Polymer Degradation and Stability,* vol. 93, no. 1, pp. 90-98, 1//, 2008.

[79] M. J. Starink, "A new method for the derivation of activation energies from experiments performed at constant heating rate," *Thermochimica Acta,* vol. 288, no. 1–2, pp. 97-104, 10/10/, 1996.

[80] R. L. Blaine, and H. E. Kissinger, "Homer Kissinger and the Kissinger equation," *Thermochimica Acta,* vol. 540, no. 0, pp. 1-6, 7/20/, 2012.

[81] M. S. Laranjeira, M. H. Fernandes, and F. J. Monteiro, "Innovative macroporous granules of nanostructured-hydroxyapatite agglomerates: Bioactivity and osteoblast-like cell behaviour," *Journal of Biomedical Materials Research Part A,* vol. 95A, no. 3, pp. 891-900, 2010.

[82] G.-J. Lai, K. Shalumon, and J.-P. Chen, "Response of human mesenchymal stem cells to intrafibrillar nanohydroxyapatite content and extrafibrillar nanohydroxyapatite in biomimetic chitosan/silk fibroin/nanohydroxyapatite nanofibrous membrane scaffolds," *International journal of nanomedicine,* vol. 10, pp. 567, 2015.

[83] G. S. Stein, and J. B. Lian, "Molecular mechanisms mediating developmental and hormone-regulated expression of genes in osteoblasts," *Cellular and molecular biology of bone*, pp. 48-95: Academic Press San Diego, 1993.

[84] G. Rodan, and S. Rodan, "Expression of the osteoblastic phenotype," *Bone and mineral research,* vol. 2, pp. 244-285, 1984.

[85] R. Murugan, and S. Ramakrishna, "Development of nanocomposites for bone grafting," *Composites Science and Technology,* vol. 65, no. 15–16, pp. 2385-2406, 12//, 2005.

[86] C. R. Kothapalli, M. T. Shaw, and M. Wei, "Biodegradable HA-PLA 3-D porous scaffolds: Effect of nano-sized filler content on scaffold properties," *Acta Biomaterialia,* vol. 1, no. 6, pp. 653-662, 11//, 2005.

[87] X. Zhao, J. Zhao, Z. Y. Lin *et al.*, "Self-coated interfacial layer at organic/inorganic phase for temporally controlling dual-drug delivery from electrospun fibers," *Colloids Surf B Biointerfaces,* vol. 130, pp. 1-9, Apr 3, 2015.

[88] S. Chen, Y. T. Hao, W. G. Cui *et al.*, "Biodegradable electrospun PLLA/chitosan membrane as guided tissue regeneration membrane for treating periodontitis," *Journal of Materials Science,* vol. 48, no. 19, pp. 6567-6577, Oct, 2013.

[89] D. Cao, Y.-P. Wu, Z.-F. Fu *et al.*, "Cell adhesive and growth behavior on electrospun nanofibrous scaffolds by designed multifunctional composites," *Colloids and Surfaces B: Biointerfaces,* vol. 84, no. 1, pp. 26-34, 5/1/, 2011.

[90] N. Ignjatović, V. Savić, S. Najman *et al.*, "A study of HAp/PLLA composite as a substitute for bone powder, using FT-IR spectroscopy," *Biomaterials,* vol. 22, no. 6, pp. 571-575, 3/15/, 2001.

[91] C. Ribeiro, V. Sencadas, C. M. Costa *et al.*, "Tailoring the morphology and crystallinity of poly (L-lactide acid) electrospun membranes," *Science and Technology of Advanced Materials,* vol. 12, no. 1, pp. 015001, 2011.

[92] J. Zhang, Y. Duan, H. Sato *et al.*, "Crystal Modifications and Thermal Behavior of Poly(l-lactic acid) Revealed by Infrared Spectroscopy," *Macromolecules,* vol. 38, no. 19, pp. 8012-8021, 2005/09/01, 2005.

[93] J. M. Oliveira, T. Miyazaki, M. A. Lopes *et al.*, "Bonelike®/PLGA hybrid materials for bone regeneration: Preparation route and physicochemical characterisation," *Journal of Materials Science: Materials in Medicine,* vol. 16, no. 3, pp. 253-259, 2005/03/01, 2005.

[94] J. Dong, and Y. Ozaki, "FTIR and FT-Raman Studies of Partially Miscible Poly(methyl methacrylate)/Poly(4-vinylphenol) Blends in Solid States," *Macromolecules,* vol. 30, no. 2, pp. 286-292, 1997/01/01, 1997.

[95] I. Ryuji, K. Masaya, and R. Seeram, "Structure and properties of electrospun PLLA single nanofibres," *Nanotechnology,* vol. 16, no. 2, pp. 208, 2005.

[96] Y. Ikada, K. Jamshidi, H. Tsuji *et al.*, "Stereocomplex formation between enantiomeric poly(lactides)," *Macromolecules,* vol. 20, no. 4, pp. 904-906, 1987/04/01, 1987.

[97] S. Solarski, M. Ferreira, and E. Devaux, “Characterization of the thermal properties of PLA fibers by modulated differential scanning calorimetry,” *Polymer,* vol. 46, no. 25, pp. 11187-11192, 2005.

[98] O. Ero-Phillips, M. Jenkins, and A. Stamboulis, “Tailoring crystallinity of electrospun PLLA fibres by control of electrospinning parameters,” *Polymers,* vol. 4, no. 3, pp. 1331-1348, 2012.

[99] R. Inai, M. Kotaki, and S. Ramakrishna, “Deformation behavior of electrospun poly(L-lactide-co-ε-caprolactone) nonwoven membranes under uniaxial tensile loading,” *Journal of Polymer Science Part B: Polymer Physics,* vol. 43, no. 22, pp. 3205-3212, 2005.

[100] Y. Tong-yin, B. Hai-shan, H. Jia-cong *et al.*, “The double melting peaks of polyethylene terephthalate,” *Acta Polymerica Sinica,* vol. 1, no. 6, pp. 461-467, 1981.

[101] L. Siqueira, F. R. Passador, M. M. Costa *et al.*, “Influence of the addition of β-TCP on the morphology, thermal properties and cell viability of poly (lactic acid) fibers obtained by electrospinning,” *Materials Science and Engineering: C,* vol. 52, no. 0, pp. 135-143, 7/1/, 2015.

[102] C. Migliaresi, D. Cohn, A. Delollis *et al.*, “DYNAMIC MECHANICAL AND CALORIMETRIC ANALYSIS OF COMPRESSION-MOLDED PLLA OF DIFFERENT MOLECULAR-WEIGHTS - EFFECT OF THERMAL TREATMENTS,” *Journal of Applied Polymer Science,* vol. 43, no. 1, pp. 83-95, Jul 5, 1991.

[103] X. Liu, T. Wang, L. C. Chow *et al.*, “Effects of Inorganic Fillers on the Thermal and Mechanical Properties of Poly(lactic acid),” *International Journal of Polymer Science,* vol. 2014, pp. 8, 2014.

[104] S. Mendes, C. Costa, V. Sencadas *et al.*, “Thermal degradation of Pb(Zr0.53Ti0.47)O3/poly(vinylidene fluoride) composites as a function of ceramic grain size and concentration,” *Journal of Thermal Analysis and Calorimetry,* vol. 114, no. 2, pp. 757-763, 2013/11/01, 2013.

[105] J. Li, W. Zheng, L. Li *et al.*, “Thermal degradation kinetics of g-HA/PLA composite,” *Thermochimica Acta,* vol. 493, no. 1–2, pp. 90-95, 9/10/, 2009.

[106] F. D. Kopinke, and K. Mackenzie, “Mechanistic aspects of the thermal degradation of poly(lactic acid) and poly(beta-hydroxybutyric acid),” *Journal of Analytical and Applied Pyrolysis,* vol. 40-1, pp. 43-53, May, 1997.

[107] M.-T. Run, X. Li, and C.-G. Yao, “Thermal degradation behavior and kinetic analysis of poly(L-lactide) in nitrogen and air atmosphere,” *Frontiers of Materials Science in China,* vol. 4, no. 1, pp. 78-83, 2010/03/01, 2010.

[108] T. Mosmann, “Rapid colorimetric assay for cellular growth and survival: Application to proliferation and cytotoxicity assays,” *Journal of Immunological Methods,* vol. 65, no. 1–2, pp. 55-63, 12/16/, 1983.

[109] J. O'Brien, I. Wilson, T. Orton *et al.*, “Investigation of the Alamar Blue (resazurin) fluorescent dye for the assessment of mammalian cell cytotoxicity,” *European Journal of Biochemistry,* vol. 267, no. 17, pp. 5421-5426, 2000.

[110] R. T. Pace, and K. J. L. Burg, “Toxic effects of resazurin on cell cultures,” *Cytotechnology,* vol. 67, no. 1, pp. 13-17, 2013.

Appendix A

- **General information about the VII INTERNATIONAL MATERIALS SYMPOSIUM | XVII CONFERENCE OF SOCIEDADE PORTUGUESA DOS MATERIAIS**

SCIENTIFIC COMMITTEE

Abel Dias dos Santos, P
Adélio Mendes, P
Albano Cavaleiro, P
Alberto Ferro, P
Altino Loureiro, P
Amélia Almeida, P
Ana Maria Pinto, P
Ana Maria Senos, P
Aníbal Guedes, P
Ascensão Lopes, P
Cândida Vilarinho, P
Carlos Fonseca, P
Carlos Silva Ribeiro, P
Carmén Rangel, P
Cláudio Schön, BR
Dalton Luis Razera, BR
Delfim Soares, P
Dulce de Meira Albach, BR
Eduardo Soares, P
Elvira Fortunato, P
Emília Rosa, P
Fernanda Margarido, P
Fernando Castro, P
Fernando Jorge Monteiro, P
Filipe Oliveira, P
Francisco Braz Fernandes, P
Hélder Puga, P
Helena Braga, P
Irene Cano, SP
Joana Espain, P
Joana Moreira Dias, P
Joana Sousa Coutinho, P
João Labrincha, P
João Moura Bordado, P
Joaquim Barbosa, P
Joaquim Vieira, P
Jon Sertucha, SP
Jorge Frade, P
José António Simões, P
José Covas, P
José Domingos Santos, P
José Luís Santos, P
Jose Manuel Torralba, SP
Josep Maria Guilemany, SP
Liliana Duarte, CH
Lucas Silva, P
Luís Gil, P
Luís Guerra Rosa, P
Luís Juvandes, P
Lurdes Lopes, P
Manuel Fernando Pereira, P
Maria Helena Fernandes, P
Maria Júlia Cristóbal Ortega, SP
Mário Ferreira, P
Núria Cinca (SP)
Patrícia Carvalho, P
Paula Vilarinho, P
Paulo Jorge Ferreira, USA
Paulo Tavares de Castro, P
Pedro Granja, P
Rogério Colaço, P
Rogério Simões, P
Rosa Miranda, P
Rui Jorge Silva, P
Rui Silva, P
Rui Vilar, P
Sergi Dosta, SP
Sónia Simões, P
Teresa Cidade, P
Teresa Duarte, P
Teresa Vieira, P
Valdemar Fernandes, P

17h30 – ORAL SESSIONS C

OS C3 | ROOM B002

29	FRICTION STIR TEXTURING	M. I. Costa, C. Leitão, A. Ramalho, D. M. Rodrigues
60	SPRAYING OF A WC-12Co CGS LAYER OVER A WC-Co HVOF COATING	M. Couto, S. Dosta, I. G. Cano, J. M. Guilemany
84	DEVELOPMENT OF FUNCTIONAL ADDITIVES BASED ON CORK FOR ANTI-CORROSION COATINGS	A. Caetano, F. Maia, L. Santos, J. Tedim, D. Evtyugin, M. G. S. Ferreira
103	CHARACTERIZATION OF NOBLE METALLIC THIN COATINGS ON LEAD GLASS SUBSTRATES	A. R. M. Sarabando, J. Mesquita-Guimarães, F. M. Santos, A. B. Lopes, A. P. Rodrigues, L. C. Alves, R. C. da Silva, A. Gil, A. Sá
172	STRUCTURAL STUDY AND AB-INITIO SIMULATION OF TaO_x COATINGS DEPOSITED BY MAGNETRON SPUTTERING	C.F. Almeida Alves, L. Marques, F. Paumier, T. Girardeau, D. Schneider, S. Carvalho

OS C4 | ROOM B003

95	USE OF PIG BONE IN VIVO FOR SIMULATION OF MASTICATORY PROCESS WITH DENTAL IMPLANTS	Moura, A. F. B. M., Sousa, J. A. L., Andrade, A. C., Aquino, G. dos S., Medeiros, J. T. N.
12	NEURO-MUSCULAR REGENERATION USING SCAFFOLDS WITH MESENCHYMAL STEM CELLS (MSCS) ISOLATED FROM HUMAN UMBILICAL CORD WHARTON'S JELLY	A. C. Maurício, A. R. Caseiro, Tiago Pereira, Jorge Ribeiro, J. D. Santos, A. L. Luís
17	BIOMATERIALS FOR SKELETAL MUSCLE REGENERATION - HOW CAN WE IMPROVE BIOCOMPATIBILITY AND CLINICAL OUTCOMES?	A. R. Caseiro, T. Pereira, P. J Bártolo, D. Santos, A.L. Luís, A. C. Maurício
27	DEVELOPMENT OF A HYALURONIC ACID-CHITOSAN-SILOXANE HYBRID HYDROGEL FOR UNDIFFERENTIATED MESENCHYMAL STEM CELLS PROLIFERATION	Joana M. Martins, Yuki Shirosaki, Dina M. Silva, A. R. Caseiro, A. C. Maurício, José D. Santos
30	MULTIFUNCTIONAL ELECTROSPUN FIBRE MEMBRANES ASSOCIATED TO BONE GRAFTS FOR BONE REGENERATION	Daniel Santos, Dina M. Silva, Cristina O. Correia, Pedro S. Gomes, Maria H. Fernandes, J. D. Santos and Vitor Sencadas
31	PREPARATION AND CHARACTERIZATION OF BIOACTIVE CALCIUM PHOSPHATE MACROPOROUS GRANULES FOR ORTHOPEDIC APPLICATIONS	Cristina O. Correia, Dina M. Silva, Pedro S. Gomes, Maria H. Fernandes, José D. Santos

- Abstract Submitted for the **VII INTERNATIONAL MATERIALS SYMPOSIUM | XVII CONFERENCE OF SOCIEDADE PORTUGUESA DOS MATERIAIS**

MATERIAIS 2015
Porto, 21-23 June, 2015

MULTIFUNCTIONAL ELECTROSPUN FIBRE MEMBRANES ASSOCIATED TO BONE GRAFTS FOR BONE REGENERATION

Daniel Santos[1,*], Dina M. Silva[2], Cristina O. Correia[1], Pedro S. Gomes[3], Maria H. Fernandes[3], J. D. Santos[1], Vitor Sencadas[4]

[1]CEMUC, Departamento de Engenharia Metalúrgica e Materiais, Faculdade de Engenharia, Universidade do Porto, Rua Dr Roberto Frias, 4200-465 Porto, Portugal.
[2]Biosckin, Molecular and Cell Therapies, SA. Parque Tecnológico da Maia – Tecmaia, Rua Eng.º Frederico Ulrich, 2650, 4470-605 Maia, Portugal.
[3]Faculdade de Medicina Dentária, Universidade do Porto (FMDUP), s/n, 4200-393 Porto, Portugal
[4]School of Mechanical, Materials and Mechatronics Engineering, University of Wollongong, Wollongong, NSW 2522, Australia.
[*]corresponding author: bio10056@fe.up.pt

Keywords: Biomaterial, Electroactive properties, Poly(lactic acid), Bonelike® bone graft, Electrospun fibres, Bone regeneration.

Abstract

The field of biomaterials has revealed a tremendous expansion over the last decade where they have been used in numerous *in vivo* purposes, ranging from ophthalmic, cardiovascular, orthopaedic and wound healing applications to drug delivery systems [1].

Different biomaterials, such as bioactive ceramics and degradable polymers have been developed to mimic the mechanical and biological properties required by the tissues. However, the electric properties of the materials, important to promote electrical stimulus to the cells, have been bleached in these advancements. More recently, conductive polymers have been used for tissue engineering applications, but some drawbacks exists concerning these materials such as the need of an external power source to promote electrical stimuli to the cells, their inability to biodegradation, which may induce chronic inflammation and required surgical removal [2]. Therefore, the next generation of biomaterials must combine biological, chemical, mechanical and electrical stimulatory cues, being the last one without wires.

In addition to conductive polymers, piezoelectric polymeric materials have also been considered for tissue and biomedical applications. Piezoelectric materials generate transient surface charges by tiny mechanical deformations of the material under mechanical solicitation and do not require additional energy sources or electrodes [2]. Piezoelectricity is a property of many non-centrosymmetric ceramics, polymers and other biological systems and seems to have therefore prospective utility to promote cell growth and proliferation by its electrical stimulation [2].

In 1953, *Yasuda et al.* [3] discovered that bone produces electricity by bending deformation, where the compressed and the elongated regions are respectively, negatively and positively polarized, being the callus formed in the negatively polarized regions. Since this work intends to achieve a better bone regeneration, it is crucial to have in mind the piezoelectric properties of the biomaterials.

This work aims at the development and characterization of multifunctional electrospun membranes for bone regeneration based on Poly(lactic acid) (PLA) and glass-reinforced hydroxyapatite - Bonelike®. PLA has generated great interest as one of the most promising biodegradable polymers due to its mechanical properties, thermoplastic processibility and biodegradability [4], becoming highly attractive for biological and medical applications. Furthermore, the degradation products of poly(lactides) are nontoxic, which is fundamental to its applications in biomedicine field. In addition, PLA is also known for the piezoelectric activity similar to the one found in human body.

Regarding Bonelike®, it is a synthetic hydroxyapatite (HA) which is sintered in the presence of $CaO\text{-}P_2O_5$ based glasses using a patented process (owned by Biosckin SA). Hydroxyapatite ($Ca_{10}(PO_4)_6(OH)_2$) is the major mineral constituent of the bone matrix. Synthetic HA has already demonstrated its excellent biocompatibility with bones and teeth due to its bioactivity and osteoconductivity [6]. However, its fragile characteristic and its low reabsorption rate by the organism compromise the recovery of bone's normal strength, causing the bone to remain brittle and easily prone to fractures [7]. These disadvantages led to the development of Bonelike®, a three-phase material consisting of HA, α and β-Tricalcium Phosphates (α-TCP and β-TCP). The α- and β-TCP phases are homogeneously dispersed in the HA matrix, resulting in a material with improved

mechanical properties and enhanced bioactivity, compared to the usual commercial HA [7]. Bonelike® reabsorption rate is dependent on the fraction of its constituents and the inclusion of ions into its composition, such as fluoride and sodium, among others, makes it possible to achieve a chemical composition closer to the mineral phase of bone. Bearing in mind the previous ideas, it is possible produce Bonelike® particles with a highly controlled micro and macroporous structure, making it ideal for osteoconduction and osteointegration as a bone substitute.

Considering that bone is composed of organic-inorganic nanocomposites and taking in account the properties of the PLA and the Bonelike®, the ceramic-polymer approach of this work intends to achieve a bone regenerative matrix with improved biological, electrical, mechanical and electromechanical properties.

Electrospinning is an electrostatic fibre production technique which has evidenced great versatility and potential for generating thin and ultrathin fibres from different materials such as polymers, composites and ceramics, with potential applications in several technological and scientific fields. Electrospun fibres offer several advantages such as, an extremely high surface-to-volume ratio, tunable porosity, malleability to conform to a wide variety of sizes and shapes and the ability to control the nanofibre composition [2,6].

In the present work, electrospun fibres with a highly concentration of ceramic filler was prepared in order to obtain a porous structure of PLA and Bonelike® with a particles size of ≤ 150 μm. It was observed that due to the higher ceramic concentration and high particle size, the Bonelike® is mainly present in the porous between fibres and some particles were present inside or even in the fibre surface, especially the smaller particles (figure 1). Water contact angle showed that the polymer presents a wettability behavior similar to neat electrospun PLA mats, around 121 ± 4º. The real amount of Bonelike® present in the membranes will be assessed by thermogravimetric analysis and the influence of the filler concentration on fibre morphology and mean diameter distribution and polymer crystallinity will be characterized. Further, cytocompatibility and cell proliferation studies will be made through the MTT assay as well as the mineralization degree by alizarin red, in a MG-63 osteoblastic cell line.

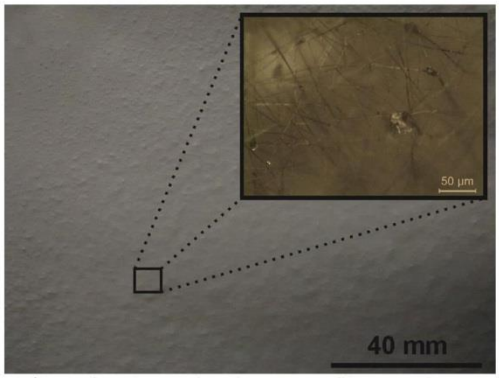

Figure 1 – Composite electrospun fibre membrane.

Acknowledgements

V. Sencadas thank support from the COST Action MP1206: "Electrospun nano-fibres for bio inspired composite materials and innovative industrial applications" and MP1301: "New Generation Biomimetic and Customized Implants for Bone Engineering".

References

[1] Davis, J. (2003). Handbook of materials for medical devices. Materials Park, OH: ASM International.
[2] C. Ribeiro et al. Engineering in Life Sciences, 2015, DOI: 10.1002/elsc.201400144
[3] Fukada, E. (2000). "History and recent progress in piezoelectric polymers." Ultrasonics, Ferroelectrics, and Frequency Control, IEEE Transactions on 47(6): 1277-1290.
[4] Gupta, B., et al. (2007). "Poly(lactic acid) fiber: An overview." Progress in Polymer Science 32(4): 455-482.
[5] Middleton, J. C. and A. J. Tipton (2000). "Synthetic biodegradable polymers as orthopedic devices." Biomaterials 21(23): 2335-2346.
[6] Kim, H.-W., et al. (2006). "Electrospinning biomedical nanocomposite fibers of hydroxyapatite/poly(lactic acid) for bone regeneration." Journal of Biomedical Materials Research Part A 79A(3): 643-649.
[7] Atayde, L. M., et al. (2014). "Morphology effect of bioglass-reinforced hydroxyapatite (Bonelike®) on osteoregeneration." Journal of Biomedical Materials Research Part B: Applied Biomaterials: n/a-n/a.